

# POLITECNICO DI TORINO

In collaboration with

École Polytechnique Fédérale de Lausanne (EPFL)

Corso di Laurea Magistrale in Ingegneria Civile - Geotecnica

Master's Degree Thesis



**EPFL**

## **Numerical approaches for the design and optimization of energy geostructures: assessment of the thermal resistance of energy piles**

### **Supervisors:**

Prof. Daniele Costanzo, Politecnico di Torino

Prof. Lyesse Laloui, EPFL

### **Co-Supervisors:**

Prof.ssa Alice Di Donna, Université Grenoble Alpes

Dott. Aldo Madaschi, EPFL

### **Candidate:**

Silvestro Massaro

A.A. 2019/2020

*Ai miei genitori  
che mi hanno sempre sostenuto,  
appoggiando ogni mia decisione.  
Con infinito affetto.*

# Acknowledgments

Le prime persone che vorrei ringraziare sono i Professori Gioacchino Viggiani e Alice Di Donna, per avermi dato l'opportunità di lavorare alla mia tesi di laurea in una importante università, come l'École Polytechnique Fédérale de Lausanne (EPFL). Desidero ringraziarli per avermi seguito durante il mio intero progetto.

I also wish to thank Professor Lyesse Laloui for making me work on a very interesting project, and for providing me with the necessary knowledge to carry on the work. I would also to thank him for the important professional opportunity he offered me.

Vorrei ringraziare il Professor Daniele Costanzo per essersi reso disponibile a seguirmi per il lavoro di tesi dal Politecnico di Torino, e per aver permesso la collaborazione tra il Politecnico di Torino e l'EPFL.

Inoltre, ringrazio il Dott. Aldo Madaschi (Laboratory of Soil Mechanics, EPFL) per avermi aiutato nell'apprendimento dei software e degli strumenti necessari al lavoro, e per avermi seguito costantemente durante tutto il lavoro.

Un ringraziamento in generale al Politecnico di Torino, per gli insegnamenti forniti in questi anni e per le importanti opportunità che mi ha dato, per la mia crescita professionale.

Infine, un sincero ringraziamento va ai miei genitori, che in tutto il percorso di studi mi sono sempre stati vicino e mi hanno sempre sostenuto in ogni mia decisione.

# Abstract

The shallow geothermal energy is a renewable source, which in recent years has found widespread use in the energy requirements of buildings. Using the natural thermal energy present in the soil, structural foundation elements, as piles, walls, or tunnel linings, can be exploited as ground heat exchangers. It consists of a multifunctional technology which requires multidisciplinary approaches. In the design of energy geostructures, structural problems, heat and mass transfers, as well as coupled hydro-thermo-mechanical response of geomaterials, must be taken into account. Actually, as it is an innovative technology developed over the past 20 years, there is no unified codes and framework, for the analysis and design of energy geostructures. Therefore, the aim of this work is to provide a numerical approach for the design and optimization of energy piles. In particular, the energy efficiency of the piles has been analysed using the concept of the thermal resistance. The latter is an important parameter, which allows to understand and quantify the heat exchange capacity of a pile. At first, the governing equations and fundamentals of heat and mass transfer in the context of energy piles, have been studied. Then, 3D numerical models have been implemented in the FEM software Lagamine, and the time evolution of the thermo-hydraulic coupled phenomena, in the operation of energy piles, has been analysed. A number of simulations have been performed on a single energy pile, to understand the key controlling geometrical and thermo-hydraulic parameters of the pile thermal resistance. Afterwards, a groundwater flow has been applied to the models, to investigate the influence on the pile and on the temperature field around it. In conclusion, a more real case of an energy pile group has been defined, to analyse both the thermal interaction between the piles and the pile screen effect with a flow applied.

# TABLE OF CONTENTS

---

|          |  |           |
|----------|--|-----------|
| <b>1</b> | <b>Introduction.....</b>   | <b>1</b>  |
| 1.1      | Classification of geothermal systems .....                         | 4         |
| 1.2      | Energy geostructures.....  | 5         |
| 1.3      | Ground source heat pump system applied to the energy piles.....    | 8         |
| <b>2</b> | <b>Theoretical background .....</b>                                | <b>11</b> |
| 2.1      | Principles of heat transfer in the energy piles .....              | 12        |
| 2.2      | Energy conservation equations in energy piles.....                 | 16        |
| 2.3      | Mass conservation equations in porous media .....                  | 18        |
| 2.4      | Convective heat exchange in the pipes .....                        | 20        |
| <b>3</b> | <b>Thermal resistance concept.....</b>                             | <b>24</b> |
| 3.1      | Thermal resistance components.....                                 | 25        |
| 3.2      | Calculation approaches.....  | 26        |
| 3.3      | Objective and outline of the project .....                         | 30        |
| <b>4</b> | <b>Equivalent single-phase analysis .....</b>                      | <b>32</b> |
| 4.1      | Model description and geometrical characterization .....           | 32        |
| 4.2      | Coupled constitutive laws and boundary conditions .....            | 34        |
| 4.3      | Model application .....  | 37        |
| 4.4      | Comparison with 2D analytical and numerical solutions.....         | 40        |
| 4.5      | Model validation – Reproduction of TRT field data.....             | 43        |
| <b>5</b> | <b>Multiphase analysis.....</b>                                    | <b>49</b> |
| 5.1      | TH coupled constitutive law for multiphase analyses.....           | 49        |
| 5.2      | Application of the multiphase model to the single energy pile..... | 54        |

|            |   |           |
|------------|---|-----------|
| <b>5.3</b> | <b>Application of the multiphase model to a 2xN energy piling .....</b> | <b>59</b> |
| <b>5.4</b> | <b>Application of the multiphase model to a 3xN energy piling .....</b> | <b>64</b> |
| <b>6</b>   | <b>Thermal resistance results .....</b>                                 | <b>68</b> |
| <b>7</b>   | <b>Conclusion .....</b>   | <b>72</b> |
| <b>8</b>   | <b>References .....</b>   | <b>75</b> |
| <b>9</b>   | <b>Appendices .....</b>   | <b>77</b> |

# List of Figures

|   |    |
|---|----|
| <b>Figure 1:</b> Energy consumptions related to the building area (Switzerland 2012). <i>Data from Kemmler et al., 2013.</i> .....  | 1  |
| <b>Figure 2:</b> Representative scheme of renewable and non-renewable energy sources. <i>Graph from the slides of the course of “Energy Geostructures – Prof. L. Laloui – 2019”</i> .....   | 2  |
| <b>Figure 3:</b> Temperature field with respect to depth in the shallow subsurface. <i>Sketch from the slides of the course of “Energy Geostructures – Prof. L. Laloui – 2019”</i> ....   | 3  |
| <b>Figure 4:</b> Examples of shallow and deep geothermal systems. <i>Picture from L. Laloui – A.F. Rotta Loria 2019.</i> .....  | 4  |
| <b>Figure 5:</b> Different ways in which the pipes are fixed to the steel cage, A) Energy piles B) Energy slab C) Energy tunnel D) Energy wall. <i>Photos from Courtesy BG Ingénieurs, BG Ingénieurs Conseils and Zublin Spezialtiefbau.</i> .....  | 6  |
| <b>Figure 6:</b> Pipe configurations: A) U-shaped pipe, B) W-shaped pipe C) parallel double U-shaped pipe D) spiral pipe E) Series double U-shaped pipe F) Multi U-shaped pipe. <i>Fadejev J., Simson R., Kurnitski J., Haghghat F., 2017. A review on energy piles design, sizing and modelling.</i> ..... | 7  |
| <b>Figure 7:</b> Operating scheme of a ground source heat pump, coupled with a geothermal heat exchanger. <i>Picture from L. Laloui – A.F. Rotta Loria 2019 – Modified after Agentur für Erneuerbare Energien</i> .....   | 8  |
| <b>Figure 8:</b> Typical orders of magnitude of thermal energy and temperature associated with energy piles. <i>Picture from the slides of the course of “Energy Geostructures – Prof. L. Laloui – 2019”</i> .....  | 10 |
| <b>Figure 9:</b> Extracted and injected energy rate for the energy piles installed in Zürich Airport. <i>Pahud D. Hubbuch M., 2007.</i> .....   | 10 |
| <b>Figure 10:</b> A) Multiphase model of a geomaterial B) REV, equivalent single-phase model. <i>Picture from L. Laloui – A.F. Rotta Loria 2019</i> .....   | 11 |
| <b>Figure 11:</b> Typical modes of heat transfer within the energy piles. <i>Picture from the slides of the course of “Energy Geostructures – Prof. L. Laloui – 2019” redrawn after Brandl 2006.</i> .....  | 15 |
| <b>Figure 12:</b> Radius of the soil affected from the thermal processes in an energy pile group. <i>Picture from L. Laloui – A.F. Rotta Loria 2019.</i> .....  | 21 |
| <b>Figure 13:</b> Characteristic regions of heat and mass transfer within the pipes. <i>Picture from Bergman T., Incropera F., Lavine A. 2011.</i> .....  | 22 |
| <b>Figure 14:</b> Qualitative trend of the temperature difference between the source and the sink. <i>Picture from L. Laloui – A.F. Rotta Loria 2019.</i> .....   | 24 |
| <b>Figure 15:</b> Thermal resistance components of a single energy pile. A) Top view B) Front view. <i>Picture from the slides of the course of “Energy Geostructures – Prof. L. Laloui – 2019” redrawn after Loveridge, 2012.</i> .....  | 25 |

|  |    |
|--|----|
| <b>Figure 16:</b> 2D section of an energy pile with double U-tube in parallel.....   | 26 |
| <b>Figure 17:</b> Typical values of thermal resistance of different configurations of energy pile, with the diameter varying between 30 cm and 140 cm, and with double, triple and quadruple U-tubes in parallel. <i>Picture from “Swiss Society of Engineers and Architects – SIA-D0190 – 2005”</i> ..... | 28 |
| <b>Figure 18:</b> A) 8-nodes three-dimensional elements, for soil and pile B) 2-nodes one-dimensional linear elements, for U-pipes. <i>Pictures from manuals of LAGAMINE – Computer Code – Bille J., Habraken A., Charlier R., Li X., 1993.</i> .....  | 32 |
| <b>Figure 19:</b> A) Perspective view of the 3D model B) 2D section of the pile. <i>Pictures taken from the numerical model made with ZSoil V18.06.</i> .....  | 33 |
| <b>Figure 20:</b> Temperature difference between the ground and the carrier fluid, over time. Steady flux conditions are highlighted.....  | 37 |
| <b>Figure 21:</b> A) Selected soil region to compute the mean temperature of the ground. B) Qualitative trend of the temperature field around the pile. ....   | 38 |
| <b>Figure 22:</b> Comparison with 2D analytical solutions provided by Swiss Code (SIA D-0190 – 2005).....  | 41 |
| <b>Figure 23:</b> Comparison between the Lagamine’s solutions and the values provided by the Swiss Code. ....  | 42 |
| <b>Figure 24:</b> Comparison between the Lagamine’s solutions and the 2D solutions provided by Loveridge and Powrie. ....  | 42 |
| <b>Figure 25:</b> 2D section of the energy pile – half geometry considered .....   | 44 |
| <b>Figure 26:</b> Stages 2-5 of the thermal response test. <i>Picture taken from “Influences on the thermal efficiency of energy piles” Cecinato F., Loveridge F.A. 2015</i> .....   | 44 |
| <b>Figure 27:</b> Comparison between the inlet and outlet temperature coming from numerical simulations and TRT data, for stage 2. <i>Data taken from the TRT done in London from Cecinato and Loveridge.</i> .....  | 45 |
| <b>Figure 28:</b> Comparison between the inlet and outlet temperature coming from numerical simulations and TRT data, for stage 4. <i>Data taken from the TRT done in London from Cecinato and Loveridge.</i> .....  | 46 |
| <b>Figure 29:</b> Comparison between the concrete temperature resulting from the numerical simulations and the TRT data. <i>Data taken from the TRT done in London from Cecinato and Loveridge.</i> .....  | 47 |
| <b>Figure 30:</b> Comparison between line source analytical approach and numerical simulations. <i>Data taken from Cecinato F., and Loveridge F.A.</i> .....   | 48 |
| <b>Figure 31:</b> Representative ground volume to calibrate the solid phase thermal properties. <i>3D mesh realized using the software ZSoil.</i> .....  | 49 |
| <b>Figure 32:</b> Comparison between the output temperature field for the equivalent single-phase and the multiphase models. ....  | 50 |
| <b>Figure 33:</b> Representative ground volume to analyse the groundwater flow. ....   | 51 |

|   |    |
|---|----|
| <b>Figure 34:</b> Increasing of water pressure on one end-face of the model. ....   | 52 |
| <b>Figure 35:</b> Water pressure distribution in hydrostatic conditions and with a flow applied. XZ view of figure 33. ....   | 52 |
| <b>Figure 36:</b> Ground temperature change over time, with a groundwater flow applied at different fluid velocity. ....  | 53 |
| <b>Figure 37:</b> A) 3D Finite element mesh of single energy pile. B) Zoom on the energy pile. <i>Mesh created with the software Zsoil.</i> ....  | 54 |
| <b>Figure 38:</b> Imposed difference of hydraulic head between the two end faces of the 3D model. ....  | 55 |
| <b>Figure 39:</b> Isothermal curves for a 2D cross section at 10m depth, with a fluid velocity of 0.7 m/day. ....   | 56 |
| <b>Figure 40:</b> Parametric analysis by varying the fluid velocity with different $\Delta H$ applied. ....   | 56 |
| <b>Figure 41:</b> A) Temperature difference between the temperature field of the analysis with flow applied and without flow. B) Pile and soil area in which the $\Delta T$ is positive. B) Soil region in which the $\Delta T$ is negative. .... | 57 |
| <b>Figure 42:</b> GHE's thermal resistance comparison between the analysis with and without the flow applied. ....  | 58 |
| <b>Figure 43:</b> A) Perspective view of the 3D FE model used for the 2xN energy piling. B) Top view of the 2xN energy piles. <i>Mesh created with the software ZSoil.</i> ....   | 59 |
| <b>Figure 44:</b> A) Geometrical parameters used for each pile. B) Schematic representation of the 2xN energy piling. ....  | 60 |
| <b>Figure 45:</b> A) Surface plot of a representative 2D section without flow applied. B) Contour plot of the 2D mid-length section of the energy piles. ....   | 61 |
| <b>Figure 46:</b> A) Surface plot of a representative 2D section with a flow of 1 m/day applied. B) Contour plot of the 2D mid-length section of the energy pile. ....  | 62 |
| <b>Figure 47:</b> A) Surface plot of the difference between figure 45(A) and figure 46(A). B) Contour plot of the difference between figure 45(B) and figure 46(B). ....  | 63 |
| <b>Figure 48:</b> A) Perspective view of the 3D FE model used for the 3xN energy piling. B) Top view of the 3xN energy piles. <i>Mesh created with the software ZSoil.</i> ....   | 64 |
| <b>Figure 49:</b> A) Surface plot of a representative 2D section in hydrostatic conditions. B) Contour plot of the 2D mid-length section of the energy piles. ....  | 65 |
| <b>Figure 50:</b> A) Surface plot of a representative 2D section with a flow of 1 m/day applied. B) Contour plot of the 2D mid-length section of the energy pile. ....  | 66 |
| <b>Figure 51:</b> A) Surface plot of the difference between figure 49(A) and figure 50(A). B) Contour plot of the difference between figure 49(B) and figure 50(B). ....  | 67 |
| <b>Figure 52:</b> Temperature difference between the heat circulating fluid and the ground, over time, for the 2xN piling. ....   | 68 |
| <b>Figure 53:</b> GHE thermal resistance of a 2xN energy piling, for different piles distance. ....   | 69 |

**Figure 54:** Temperature difference between the heat circulating fluid and the ground, over time, for the 2xN piling.....69

**Figure 55:** Pile thermal resistance for the 3x3 energy piling with and without the flow applied. ....70

**Figure 56:** A) Schematic view of the 3x3 energy pile group. B) Soil thermal resistance of the central pile. C) Soil thermal resistance of the lateral pile. D) Soil thermal resistance of the border pile.....71

# 1 INTRODUCTION

---

The last two centuries have been characterized by a rapid and huge increase of energy consumption and supply in the world anthropogenic development, and the worst consequence can be seen in a serious increase of environmental pollution. In the construction sector and more in general in the civil engineering field, international regulations are supporting the use of technologies with a low environmental impact. Applying to buildings and infrastructures technologies which can get energy from sources capable to renew themselves, in a range of time consistent with human activities and needs, can make an important contribution to achieve the objectives set by the international directives [1].

From the point of view of the building and construction sector, the net energy consumption represents the amount of thermal energy to be extracted from, or injected to, an indoor environment, using a cooling or heating system to keep the temperature at a predetermined comfort value. For instance in Swiss building sector, as in most European countries, the amount of energy consumption related to space heating and cooling or to the production of the hot water corresponds to about 85% of the total energy of the building [2] (figure 1).

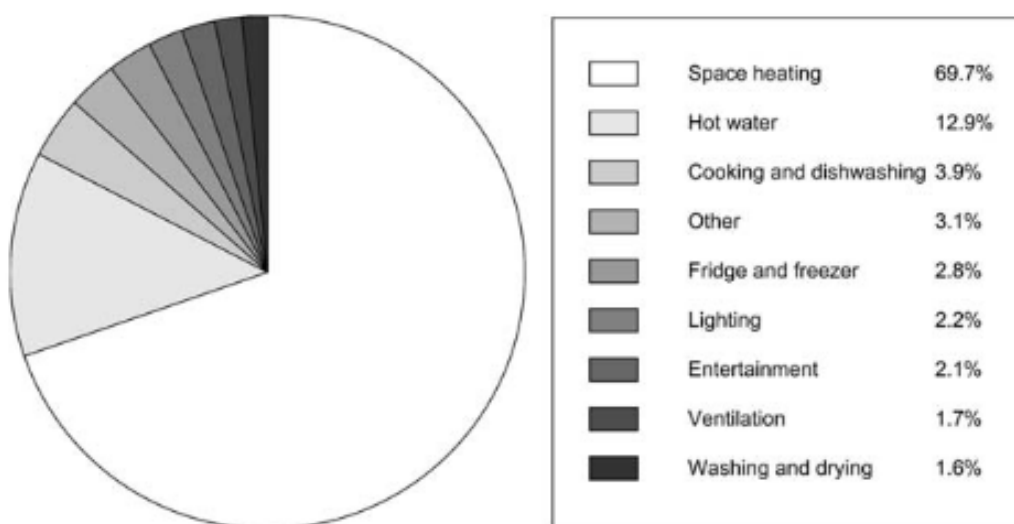


**Figure 1:** Energy consumptions related to the building area (Switzerland 2012).  
Data from Kemmler et al., 2013.

The aim of the programs promoted from ASHRAE Vision 2020 and other buildings directives is to carry on the idea of so-called “Nearly Zero-Energy Buildings (NZEB)” [3]. It means that the building sector must substantially decrease the consumption of energy and in the same time adopt the concept of “positive energy building”, for instance, building which directly gets and consumes energy from a source on-site. It is clear that accepting the development of technologies which provide heating and cooling energy from renewable sources is the right way to achieve the goals previously described.

The geothermal energy and geotechnologies play a fundamental role to such a challenge because of their limited impact on the environment and the exploitation of a renewable energy source. Considering the origin and the availability in nature, the geothermal energy belongs to the so-called primary energy sources, such as solar energy, fossil and mineral fuels, wind energy, tidal energy and biomass sources. The most important aspects which characterise these forms of energy are related to the fact that they do not need any type of conversion to be obtained and mainly are available in nature, with respect to the secondary energy sources, such as electrical energy, refined fuels and more in general energy carriers, which can only be produced from the primary sources mentioned before [1]. The primary energy sources can be further classified in renewable and non-renewable energy sources (figure 2).

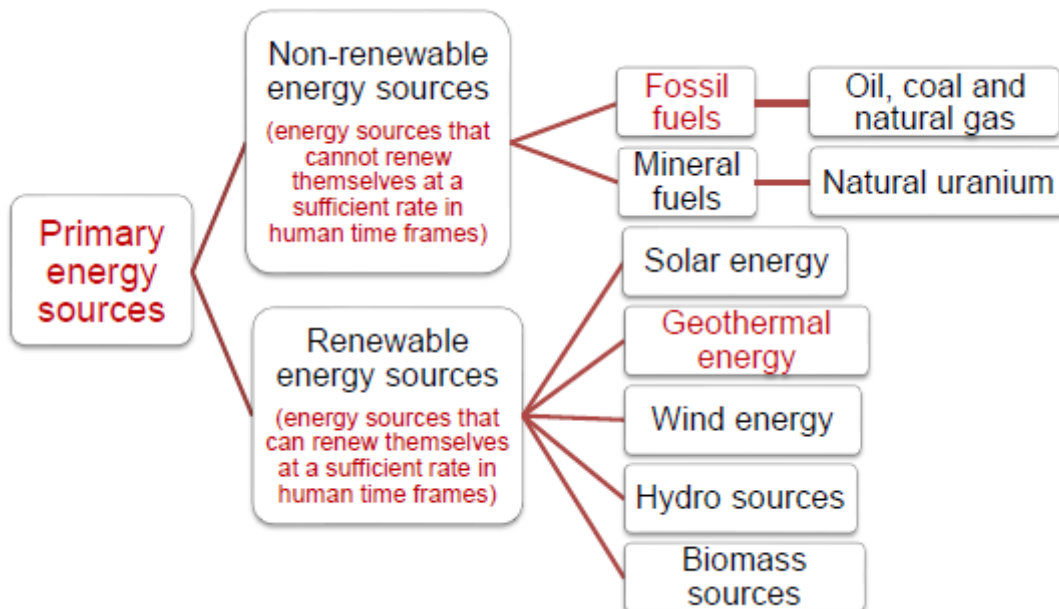


**Figure 2:** Representative scheme of renewable and non-renewable energy sources. *Graph from the slides of the course of “Energy Geostructures – Prof. L. Laloui – 2019”*

The Earth's subsurface provides the natural heat that can be used from systems based on the geothermal energy. The geothermal gradient depends on the latitude, the location and mainly the depth, but can be considered with a good approximation equal to  $3^{\circ}\text{C}$  per 100 m of depth below the upper mantle and  $1^{\circ}\text{C}$  per 100 m in continental zone of the Earth's crust [1]. The key principle on which shallow geothermal systems leverage is that the natural ground temperature field for the first 100 m, in most European countries, is on the order of  $10^{\circ} - 15^{\circ}\text{C}$ , and tends to stay relatively constant throughout the year, except for the shallow subsurface (the first 5 – 6 m), which are sensitive to the external temperature and the atmospheric conditions, rather than the temperature fluctuations due to the seasons (figure 3). For this reason, the ground temperature remains at a higher value than that of atmosphere during winter and on the contrary tends to be lower than the outside temperature during summer.

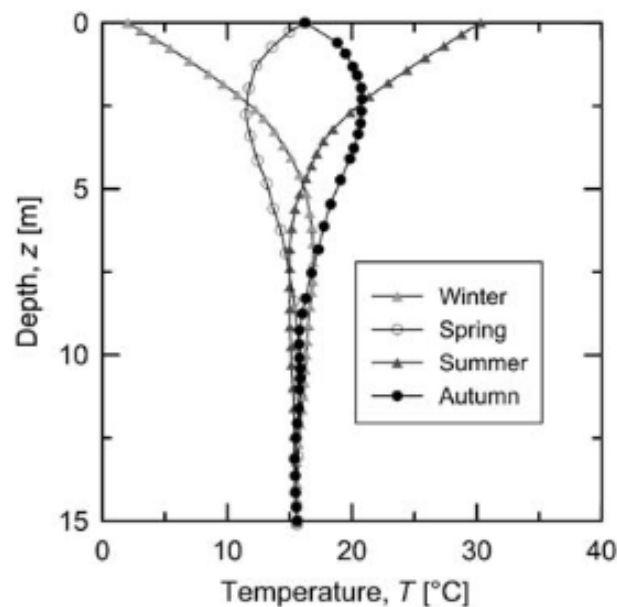


**Figure 3:** Temperature field with respect to depth in the shallow subsurface.  
*Sketch from the slides of the course of "Energy Geostructures – Prof. L. Laloui – 2019"*

In addition to the sustainable and renewable nature of the geothermal energy, other features which may spread and promote the use of the geothermal energy are linked to the fact that is available constantly, regardless the atmospheric conditions, and almost everywhere in the Earth, ensuring the energy supply to buildings and infrastructures [4].

## 1.1 Classification of geothermal systems

A technological system that exploits the geothermal energy is called geothermal system. Referring to the depth of thermal energy that is employed for the system, the geothermal systems can be classified, by definition, as shallow geothermal systems if the amount of subsurface considered is lower than 400 m, otherwise they belong to deep geothermal systems. The main difference between the two concerns the level of temperature and enthalpy you are dealing with, low for shallow systems and high for deep systems. The sectors at medium or low enthalpy concern the direct use in the civil engineering field. A schematic classification of shallow and deep geothermal systems is represented in figure 4. Regardless the technology installed, each geothermal system that works for the heating phase involves a heat source, that is usually the ground, with which the heat sink, that can be a structure or an infrastructure, exchanges heat from a heat exchanger. In the cooling phase, the heat sink is represented by the ground and the heat source is the structure.

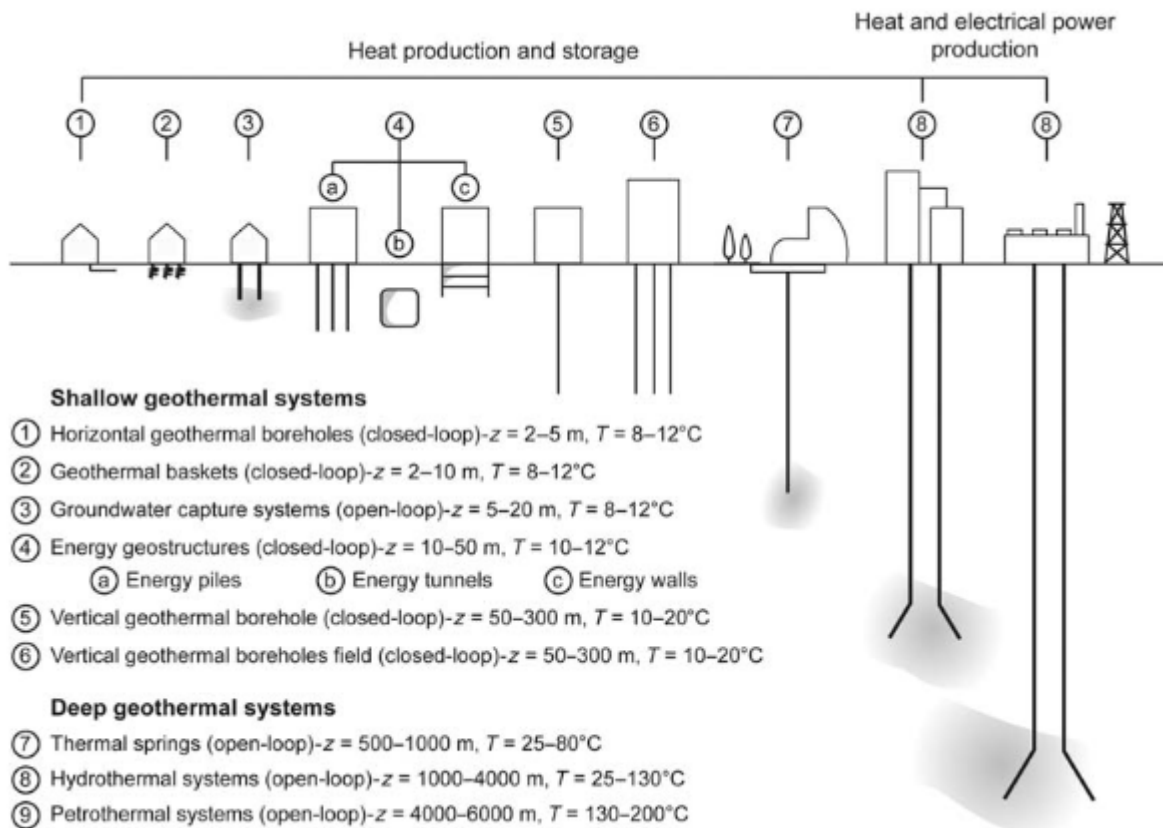


Figure 4: Examples of shallow and deep geothermal systems. Picture from L. Laloui – A.F. Rotta Loria 2019.

The heat exchanger elements are equipped with pipes in which a heat carrier fluid circulates and allows an energy exchange with the heat source.

Another difference between shallow and deep geothermal systems is related to how the thermal energy obtained is then used. In particular, in shallow systems there is a tool that transfers the geothermal energy from the ground to the structure, and in the same time a system that allows the circulation of the heat carrier fluid in the pipes, so the geothermal energy is used in an indirect way. Conversely, deep systems can be equipped with machines that directly allow the circulation of the fluid between the heat sink and the heat source [1].

## 1.2 Energy geostructures

Considering the classification of the geothermal systems in figure 4, horizontal geothermal boreholes, vertical boreholes, groundwater capture systems and energy geostructures belong to the shallow systems that work with low enthalpy. The energy geostructures can be defined as thermoactive geostructures, and from a theoretical point of view, they are a multifunctional and innovative type of shallow geothermal systems that consists of integrate a typical ground heat exchanger element (GHE) into the concrete of the structural support of any structure, as piles, walls or tunnels with a depth of  $Z = 10 - 50$  m, which is connected with the ground.

The technology of the energy geostructures consists of exploiting the ground-embedded structures as heat exchanger elements, in addition to the structural function that a pile group, a diaphragm wall, a sheet pile wall or a tunnel lining must perform. When dealing with this type of coupled technology, we talk about energy piles, energy walls, energy slabs or energy tunnels. This technique allows to get geothermal energy which can be used for heating and cooling the built environment, for the sector of agriculture to produce hot or cold water, to avoid the freezing of infrastructures, roads and platforms or more in general for energy storage. Since we are dealing with structural foundation, the materials used in this technique are concrete, steel reinforcing cage and pipes of high-density polyethylene. The pipes are embedded into the concrete and attached to the reinforcing cage, in a specific design configuration, in order to respect the design concrete cover [1].

A carrier fluid composed of water with a saline solution or in general a water-antifreeze solution is circulated inside the pipes. More than the geometrical parameters of the geostructures, which must be designed to ensure the structural stability, a fundamental design parameter is the pipe position. For this reason, an in-depth analysis must be carried out in order to get an efficient pipe configuration from an energetic point of view and in the same time maintain the structural integrity of the concrete cover. The way the pipes are fixed to the reinforced cage for the different cases of energy piles, energy walls or energy tunnel segmental lining is represented in figure 5.



**Figure 5:** Different ways in which the pipes are fixed to the steel cage, A) Energy piles B) Energy slab C) Energy tunnel D) Energy wall. *Photos from Courtesy BG Ingénieurs, BG Ingénieurs Conseils and Zublin Spezialtiefbau.*

Focusing attention on the case of energy piles, several examples of pipe configurations are represented schematically in figure 6. In particular, the U-shaped pipe configurations, with a certain number of pipes in series or in parallel, are usually applied to piles with a large diameter, despite the higher thermal potential of a W-shaped or helical pipe configuration. The latter can be adopted in more restricted situation, in which the dimensions of the pile allow the practical installation.

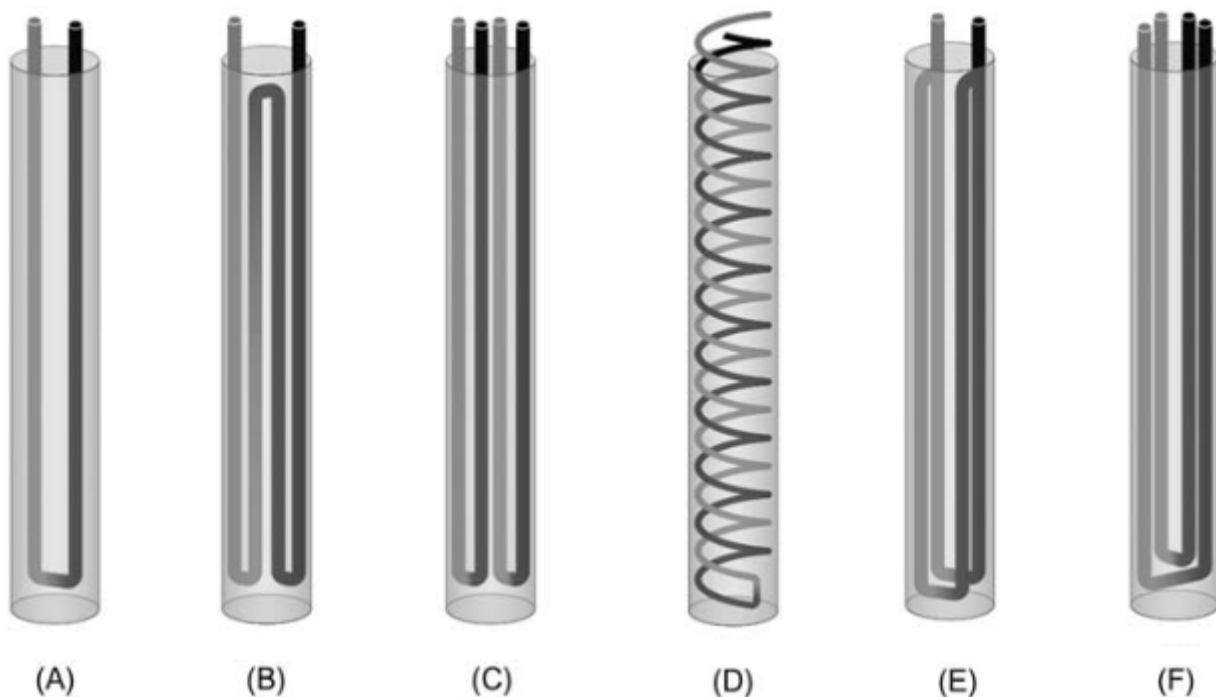


**Figure 6:** Pipe configurations: A) U-shaped pipe, B) W-shaped pipe C) parallel double U-shaped pipe D) spiral pipe E) Series double U-shaped pipe F) Multi U-shaped pipe. *Fadejev J., Simson R., Kurnitski J., Haghghat F., 2017. A review on energy piles design, sizing and modelling.*

In addition to the environment-friendly aspects of a technology which exploits geothermal energy, the main advantage linked to the use of the energy geostructures rather than standard shallow geothermal systems is the reduced installation costs of the ground heat exchanger. Foundation elements as piles, walls or tunnel lining are, in any case, required for structural reasons, therefore exploiting these elements as heat exchangers saves the installation of a conventional borehole heat exchanger. A further benefit is related to the thermal properties of the concrete, that is characterized by better thermal conductivity compared to the standard filling material, which is used for conventional systems [1].

### 1.3 Ground source heat pump system applied to the energy piles

As described in previous chapters, the ground temperature remains constant at  $10^{\circ}\text{C} - 15^{\circ}\text{C}$  throughout the year. For instance, during winter season, the inlet fluid temperature in the heat exchanger is around  $5^{\circ}\text{C} - 7^{\circ}\text{C}$ , the heat source from which the sink can extract or inject heat, would lead to have an environmental temperature in the building around  $9^{\circ}\text{C} - 11^{\circ}\text{C}$  which is not the comfort temperature for human needs. For this reason, to have a more efficient system, the energy geostructures which deal with shallow geothermal energy, are often coupled with a ground source heat pump system, which allows to have a higher ambient temperature during winter and, with a reverse heat pump, a comfortable temperature during summer.

There are several fields of application in which the heat pump plays a fundamental role: air source, water source and ground source heat pump. By definition, the ground source heat pump is a thermal machine capable to extract or inject thermal energy using mechanical energy. To better understand how it works, refer to the scheme shown in figure 7.

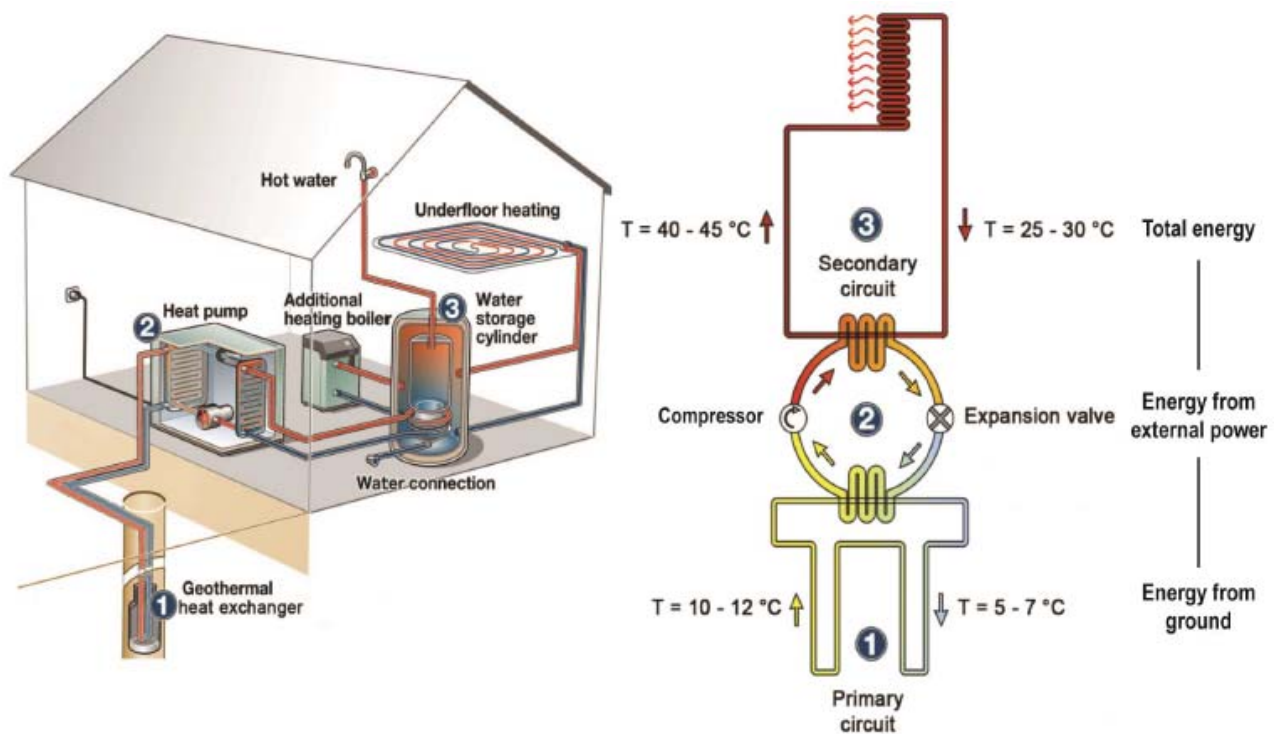


**Figure 7:** Operating scheme of a ground source heat pump, coupled with a geothermal heat exchanger. *Picture from L. Laloui – A.F. Rotta Loria 2019 – Modified after Agentur für Erneuerbare Energien*

Basically, the primary circuit concerns the heat source, represented by the ground, and the geothermal heat exchanger represented from the energy pile, the secondary circuit takes place directly in the building to be heated or cooled. Between the two circuits, the heat pump works. Referring to the winter case, the purpose of the heat pump is to absorb a low-grade heat from the ground, then to transport, concentrate and release it in the building, where it can be used for the heating or for producing hot water. In the primary circuit, a cold-water antifreeze mix at 5° - 7° C is pumped through the ground within the series of pipes integrated into the pile. As heat naturally flows from warmer to cooler places the heat carrier fluid is constantly warmed by the ground at 10°-12° C. Having increased in temperature, the anti-freeze mixture goes into a heat exchanger called evaporator, in which the thermal energy absorbed from the ground is transferred into the refrigerant which begins to boil and turn into a gas. The refrigerant never physically mixes with the heat carrier fluid in the primary circuit, but there are layers of plates which permit the heat transfer. This gas is then transferred into a compressor in which the gas pressure is increased and, as a consequence, the gas temperature rises. The hot refrigerant gas then flows into a second heat exchanger called the condenser, which features an identical set of heat transfer plates of the evaporator. The condenser delivers water hot enough to serve the space heating system, in the secondary circuit (T = 40° - 45° C). Having transferred its heat, the refrigerant gas reverts to a liquid at 25° - 30° C. This liquid is then passed through an expansion valve at the end of the cycle to reduce its pressure and temperature until 5° - 7° C ready to start the cycle all over again. Low grade heat stored in the ground has been upgraded by the refrigeration process to deliver hot water. [5]

The so-called Coefficient of Performance (COP) gives an estimate of the efficiency of a ground source heat pump system and it is defined as.

$$\text{COP} = \frac{\text{Energy output after heat pump operation [KW]}}{\text{Energy input for heat pump operation [KW]}}$$

A typical order of magnitude for energy piles is COP = 4÷5, it means that for each KW consumed by the heat pump 4 KW of energy is generated, effectively meaning the cost per KWh is quartered.

To have an idea of some applications of energy piles and how much thermal energy can be obtained, figure 8 summarizes three typical applications and the order of magnitude of extracted and injected thermal energy, as well as the associated fluid temperature.

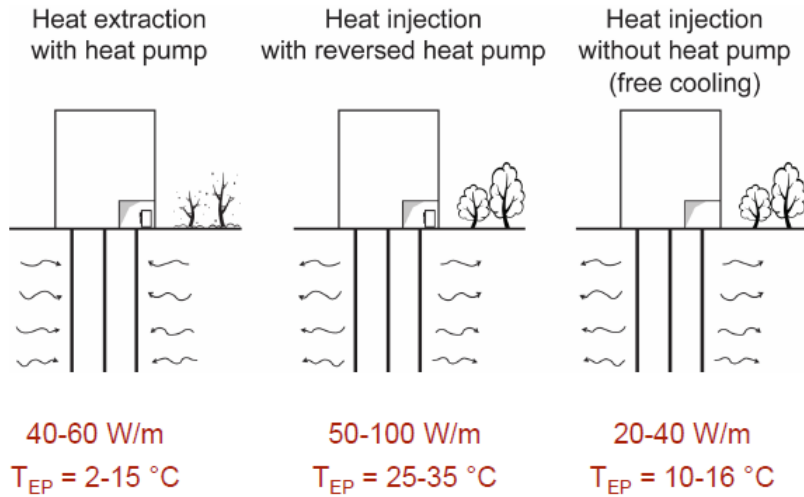


**Figure 8:** Typical orders of magnitude of thermal energy and temperature associated with energy piles. *Picture from the slides of the course of “Energy Geostructures – Prof. L. Laloui – 2019”*

To conclude this introductory part, figure 9 represents the injected and extracted energy as well as the inlet and outlet fluid temperature for each month of the year for the energy pile system installed in Zürich Airport (Dock Midfield) [1].

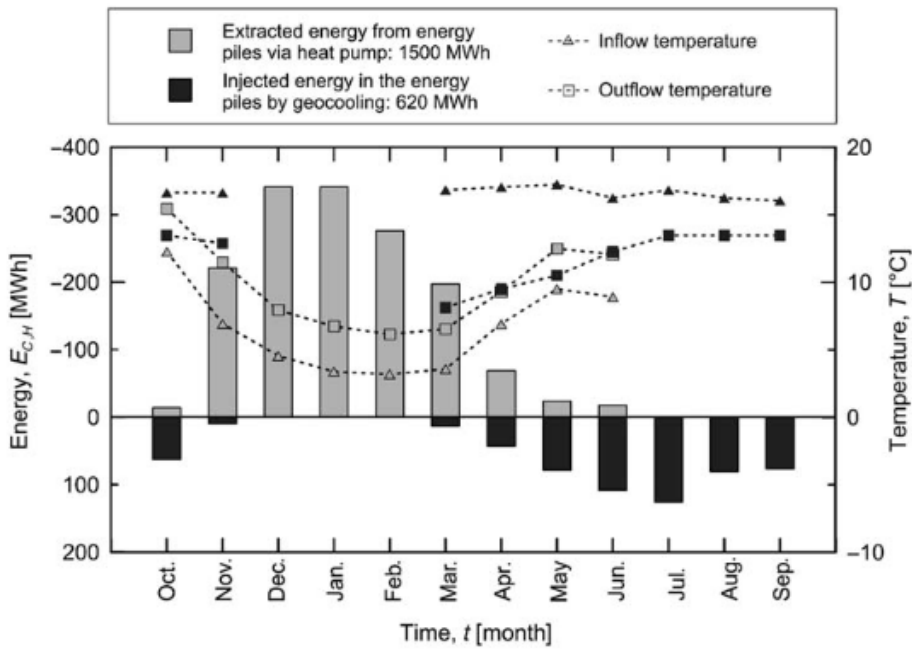


**Figure 9:** Extracted and injected energy rate for the energy piles installed in Zürich Airport. *Pahud D. Hubbuch M., 2007.*

## 2 THEORETICAL BACKGROUND

---

Heat and mass transfer, associated to the processes that occur within the energy geostructures and the ground, represent the coupled thermohydraulic response of the geothermal systems. The physical principles linked to heat and mass transfer and the energy governing equations must be analysed separately, because the effects of the thermal properties and hydraulic behaviour of the involved materials are essential for the analysis and mainly for the design of energy geostructures.

From the point of view of the constituent materials, an energy geostructure, as a whole, is characterized by: the concrete in which the steel cage is embedded, the pipes made of HDPE that are usually fixed to the steel, inside the pipes a mixture of water and antifreeze solution is pumped, and a portion of ground influenced by the Thermo-Hydro-Mechanical processes of the geothermal system. Moreover, the concrete, the heat carrier fluid and the soil present a phase heterogeneity, if we consider a certain observation scale. Since we are talking about geomaterials as concrete or soil, there are different approaches than can be adopted in the analyses. A first simplified approach considers the geomaterials as a continuum medium, leveraging on the so-called “Representative Elementary Volume”, in which the solid, liquid and gas phase are converted into a medium with equivalent properties of the multiphase geomaterial. The most rigorous approach is to consider the geomaterials as a multiphase medium, and evaluate the thermal properties of each phase, in order to get a more accurate analysis and in the same time to consider, for instance, the variation of the liquid phase pressure in presence of a groundwater flow. The two approaches mentioned are schematically represented in figure 10 [1].

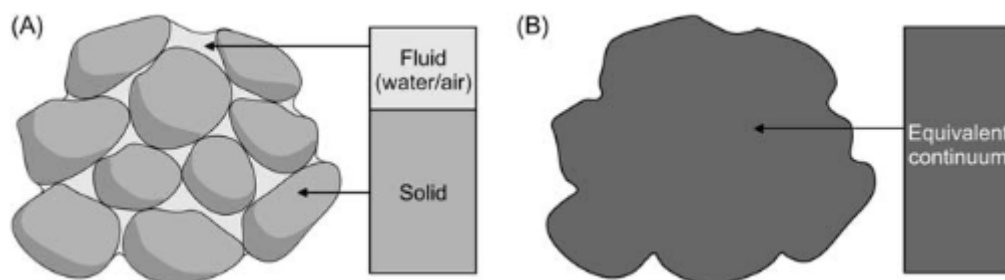


**Figure 10:** A) Multiphase model of a geomaterial B) REV, equivalent single-phase model. *Picture from L. Laloui – A.F. Rotta Loria 2019*

## 2.1 Principles of heat transfer in the energy piles

As described in the previous chapters, the principle on which the functioning of the energy piles is based, is the heat exchange (extraction or injection) between the heat carrier fluid within the pipes and the surrounding soil. To better understand how heat is actually exchanged, we must refer to the principles of heat transfer. From an engineering point of view, in the analysis and design of energy geostructures, it can be said that the exchange of heat between the circulating fluid and the ground is due to the conduction and convection, because other processes as radiation and latent heat transfer are irrelevant.

The heat transfer by conduction occurs with the mechanism of energy diffusion, whenever particles of a solid or a fluid are in contact at different temperatures. Considering the case of an energy pile, the heat transfer within the pipe wall, the grouting material and the soil is due to the conduction. The Fourier's law is the governing equation of the heat transfer by conduction, and the most important parameters of this law is the thermal conductivity which measures, by definition, the capacity of a material to conduct heat. The Fourier's law defines the heat flux density  $\dot{q}_{\text{cond}}$  due to the conduction as follows:

$$\dot{q}_{\text{cond}} = \frac{Q}{At} = \frac{\dot{Q}}{A} = -\lambda \nabla T = -\lambda \left( \frac{\partial T}{\partial x} \hat{e}_x + \frac{\partial T}{\partial y} \hat{e}_y + \frac{\partial T}{\partial z} \hat{e}_z \right) \quad (1)$$

$\lambda$  → thermal conductivity of the medium  $\left[ \frac{\text{W}}{\text{mK}} \right]$

$\frac{\dot{Q}}{A}$  → rate of heat energy transferred  $\dot{Q}$  per unit time  $t$ , for a given surface  $A$   $\left[ \frac{\text{W}}{\text{m}^2} \right]$

$\nabla T$  → temperature gradient [K]

It is worth noting that, in the case of an energy pile, the heat flux density is the heat flux rate per unit length, as follows:

$$\dot{q}_l = \frac{\dot{Q}}{L} = -\frac{\lambda A \left( \frac{\partial T}{\partial r} \right)}{L} \left[ \frac{\text{W}}{\text{m}} \right] \quad (2)$$

in which  $L$  is the length of the pile and  $r$  is the radial direction of the heat transfer [4].

The most important parameter to be defined in the Fourier's law is the thermal conductivity. In porous media it is significantly influenced by the water content (degree of saturation), the dry density and the particle size distribution. For the grouting material, in addition to the density and porosity, a key role is played by the aggregates inside the concrete. All these factors show a certain range of values that lead to having values of thermal conductivity quite different from each other. Typical values of thermal conductivity of geomaterials, water and air are summarized in Table 1.

**Table 1:** Typical range of geomaterials thermal conductivities.  
Data from Pahud 2002, Vulliet et al. 2016.

| Material | Thermal conductivity, $\lambda$<br>[W/(m °C)] |           |
|----------|---|-----------|
|          | Dry   | Saturated |
| Clay     | 0.4 – 1.0                                     | 0.9 – 2.3 |
| Silt     | 0.4 – 1.0                                     | 0.9 – 2.3 |
| Sand     | 0.3 – 0.8                                     | 1.7 – 5.0 |
| Gravel   | 0.4 – 0.5                                     | 1.8       |
| Concrete | 0.9 – 2.0                                     |           |
| Steel    | 14 – 60                                       |           |
| Water    | 0.57  |           |
| Air      | 0.025   |           |

Regarding the geomaterials, it can be said that the greater the porosity, the less the contact between ground particles, as a consequence, the thermal conductivity tends to be lower because, referring to table 1, the air is characterized by a very low thermal conductivity. Moreover, considering a saturated soil, the water inside the voids has a greater conductivity than the air, so the soil with a ground water table has a better heat exchange capacity. The last point to be discussed is the particle size distribution. For the same reasons explained before, in order to have more contact between soil particles, it is better to have a well-graded soil, and this aspect plays an important role in the mix design of the concrete. To conclude this part concerning the thermal conduction, it can be said that the choice of the thermal conductivity of each material characterising energy piles needs a thorough analysis, because most of the heat exchanged comes from the thermal conduction [1].

The second mode of heat transfer within the energy piles is the heat convection and the associated convection mass transfer. Furthermore, it is also important to differentiate the convection associated with internal and external flow, bounded by a surface, and the convection due to a seepage flow within a porous and permeable material. By definition, the heat convection occurs for a diffusion and bulk motion of a fluid. The phenomenon associated with the bulk motion and diffusion of the fluid is the so-called advection mechanism or convection mass transfer. A first distinction must be made between the free convection, which is caused from the motion of a fluid with a temperature gradient, for instance in presence of a groundwater flow, and the forced convection, in which the fluid is set in motion by an external cause, that is the case of the heat circulating fluid inside the pipes. The governing equation of the heat convection is the Newton's law for cooling. The heat flux density exchanged by convection  $\dot{q}_{\text{conv}}$  can be defined as follows:

$$\dot{q}_{\text{conv}} = h_c(T_s - T_\infty) \quad (3)$$

$h_c$  → convection heat transfer coefficient  $\left[ \frac{\text{W}}{\text{m}^2\text{K}} \right]$

$T_s$  → reference surface temperature [K]

$T_\infty$  → fluid temperature [K]

The convection heat transfer coefficient  $h$  depends on the thermal properties of the fluid and mechanical properties of the flow, as the velocity. In the context of energy piles, there are empirical approaches to determine the heat transfer coefficient of the fluid inside the pipes, depending on the mean relative fluid velocity and in particular if the flow within the pipe is laminar or turbulent [1]. The heat carrier fluid inside the pipes is characterized by a temperature gradient during the whole process, so a part of the heat exchanged is due to the convection between the heat carrier fluid and the inner surface of the pipes. In this context the Newton's law for cooling can be written as follows:

$$\dot{q}_l = \frac{\dot{Q}}{L} = - \frac{h_c A (T_s - T_\infty)}{L} \left[ \frac{\text{W}}{\text{m}} \right] \quad (4)$$

In which  $\dot{q}_l$  indicates the heat transfer rate per meter length.

To get a clearer idea of the heat exchanges that occur during the thermal process of the energy piles, figure 11 represents the typical modes of heat transfer, in a 2D section of a pile equipped with a certain number of pipes.

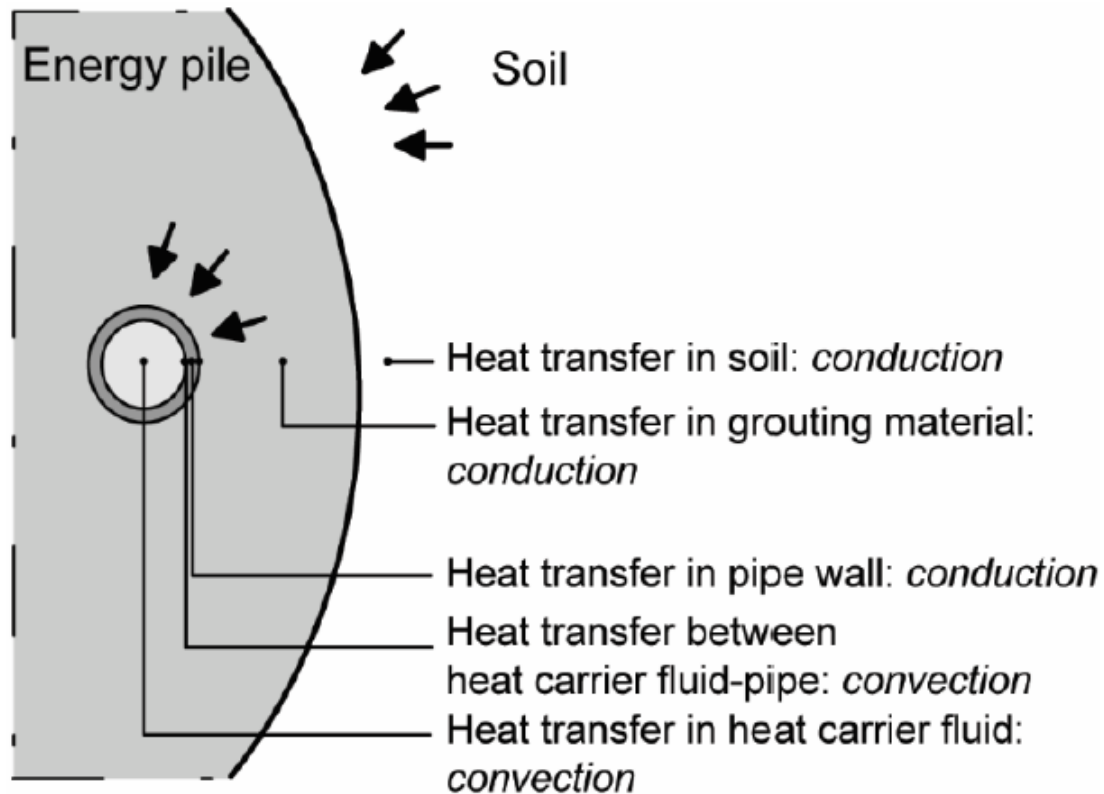


**Figure 11:** Typical modes of heat transfer within the energy piles. *Picture from the slides of the course of "Energy Geostrucures – Prof. L. Laloui – 2019" redrawn after Brandl 2006.*

While for seepage problems, Newton's law for cooling defines the heat flux density as:

$$\dot{q}_{\text{conv}} = \rho_f C_{p,f} \bar{v}_{\text{rf}} (T_s - T_\infty) \quad (5)$$

$\rho_f$  → fluid density  $\left[ \frac{\text{Kg}}{\text{m}^3} \right]$

$C_{p,f}$  → specific heat capacity of the fluid  $\left[ \frac{\text{J}}{\text{Kg K}} \right]$

$\bar{v}_{\text{rf}}$  → average relative velocity of the fluid with respect to the solid phase  $\left[ \frac{\text{m}}{\text{s}} \right]$

which is the typical case of a groundwater flow. The mean fluid velocity  $\bar{v}_{\text{rf}}$  can be calculated with the Darcy's law, considering the case of a flow in the porous media. The latter will be discussed in the chapter 2.3.

## 2.2 Energy conservation equations in energy piles

After describing the heat transfer modes within an energy pile, it is appropriate to analyse the energy conservation equations that govern the thermal processes associated with the energy geostructures and in particular, with an energy pile. The non-linear phenomena involved in thermo-hydro-mechanical processes in porous media are: thermal transfers within porous media, including conduction in geomaterial matrix and convection due to a fluid flow, and fluid flow within porous media [15].

It is possible to express the energy balance equation considering only the heat conduction through the Fourier law, as follows.

$$\nabla \cdot (\lambda \nabla T) + \dot{q}_v = \rho C_p \frac{\partial T}{\partial t} \quad (6)$$

In equation 6, the first term indicates the rate of heat passing through the bounding surfaces of a volume, the  $\dot{q}_v$  represents the rate of internal heat generation inside the elementary volume, and the term on the right-hand side indicates the rate of energy storage in the volume. It can be seen that, in equation 6 the only unknown is the temperature, as a consequence the conduction heat transfer problem can be completely solved.

Considering the case in which there is no internal volumetric heat generation  $\dot{q}_v$ , the equation 6 can be expressed as follows:

$$\alpha_d \nabla^2 T = \frac{\partial T}{\partial t} \quad (7)$$

in which, the  $\alpha_d$  represents the thermal diffusivity, that is the ratio between the thermal conductivity  $\lambda$  and the volumetric heat capacity  $\rho C_p$ . It is an important parameter representing the heat capacity per volume unit. Considering the terms on which the thermal diffusivity depends, the spread of heat inside the ground is proportional to the thermal conductivity of the medium.

As seen in the previous chapter, the thermal process of the energy piles is characterized by a heat exchange due to conduction and convection. Therefore, in the context of energy piles, in the energy governing equation an advection term that takes into account the fluid velocity within the pipes, must be added.

The energy governing equation can be expressed as follows.

$$\lambda \nabla^2 T + \dot{q}_v = \rho C_p \frac{\partial T}{\partial t} + \rho_f C_{p,f} \bar{v}_f \cdot \nabla T + h_c (T_s - T_\infty) \quad (8)$$

where,  $\bar{v}_f$  is the mean fluid velocity in the pipes. The equations 6 and 8 are partial differential equations, which need initial and boundary conditions to be solved. In the context of energy piles, the classic initial condition is to assume that the temperature within the ground, the grouting material, and the pipes is constant at the beginning of the analysis, such that:

$$T(z, 0) = T_m(z, 0) \quad m \rightarrow \text{medium} \quad (9)$$

Regarding the boundary conditions, different types of boundary conditions can be adopted in the energy piles' thermal process. The two most commonly BCs used are the so-called Dirichlet's (first kind) and Neumann's (second kind) boundary conditions. The first kind of BCs consists in imposing the temperature of the fluid, over time. For instance, it can be possible to impose the inlet fluid temperature at the beginning of the pipe  $T_{z,\text{in}} = T_{\text{in}}$ , where  $z_{\text{in}}$  is the coordinate of the pipe's inlet and  $T_{\text{in}}$  is the fixed temperature. The second kind of BCs imposes a heat flux on the inlet or outlet surface of the pipe. The heat carrier fluid is circulating within the pipe, and the heat density flow is applied at the inlet cross section of the pipe, as follows:

$$\dot{q}_{\text{in}} = -\lambda \frac{\partial T}{\partial z} + \rho_f C_{p,f} \bar{v}_f (T_f - T_{\text{ref}}) + \frac{Q_p}{S} \quad (10)$$

in which,  $T_f$  is the fluid temperature,  $T_{\text{ref}}$  is the reference temperature of the surrounding materials, and  $Q_p/S$  [ $W/m^2$ ] is the power provided to the fluid per unit of pipe section [6].

## 2.3 Mass conservation equations in porous media

As can be seen from the equation 8, the energy governing equation presents both the temperature field  $T$  and the displacement field of fluid, coming from the relative mean fluid velocity, as unknowns. As a consequence, to get the solution of a conduction-convection problem, the mass conservation equation must be added. From an engineering point of view, mass transfer caused by convection, must be considered in the analysis of energy piles. In analogy to what happens in the process of heat convection, in which there is a carrier fluid characterized by a temperature gradient, in the case of mass transfer by convection, the governing variable of the process is the difference of hydraulic head  $h$  between two regions, that can be defined from the Bernoulli's theorem, as follows:

$$H = h + \frac{\bar{v}_{rf}^2}{2g} = z + \frac{p_f}{\gamma_f} + \frac{\bar{v}_{rf}^2}{2g} \quad [m] \quad (11)$$

in which, the total head  $H$ , can be defined as the sum of the hydraulic head  $h$ , that is, in turn, the sum of the height  $z$  of the fluid with respect of a reference plane, and the fluid pressure height  $p_f/\gamma_f$ , where  $p_f$  is the fluid pressure and  $\gamma_f$  is the water specific weight, and the kinematic term  $\bar{v}_{rf}^2/2g$ , where  $\bar{v}_{rf}$  is the fluid velocity defined in equation 5 [1].

In the soil around the energy piles, the thermal processes within the piles can be affected by a groundwater seepage under laminar conditions, caused by a difference of hydraulic heads between two regions. In this case, the mean flow velocity within the ground, under steady conditions, can be computed from the Darcy's law. Assuming that the soil is characterized by an isotropic permeability  $K$ , the mean fluid velocity can be expressed as follows:

$$\bar{v}_{rf} = -K\nabla h = -K\nabla \left( z + \frac{p_w}{\gamma_w} \right) \quad K = k \frac{\rho_f g}{\mu_f} \quad (12)$$

in which, the isotropic permeability  $K$  [m/s] is function of the intrinsic permeability  $k$  [m<sup>2</sup>], the fluid density  $\rho_f$  [kg/m<sup>3</sup>], the dynamic viscosity  $\mu_f$  [kg/m s] and the gravity acceleration  $g$  [m/s<sup>2</sup>]. The minus indicates that the direction of the flow is towards a lower hydraulic head. From the equation 12, it can be noticed that, the gradient of the hydraulic head is not influenced by the hypothesis of isotropic permeability.

Therefore, the two most important variables of a groundwater flow are the soil permeability (hydraulic conductivity) and the difference of the hydraulic head between two considered regions. A significant aspect that should be highlighted is that the range of permeability values is quite wide, around ten orders of magnitude. Typical values of hydraulic conductivity of geomaterials are summarized in Table 2 [7].

**Table 2:** Typical order of magnitude of the hydraulic conductivity. *Table from “Geotecnica – Renato Lancellotta” 4<sup>th</sup> edition - 2012*

| Type of material | Hydraulic conductivity [m/s] |
|------------------|------------------------------|
| Clean gravel     | $10^{-2} \div 1$             |
| Coarse sand      | $10^{-5} \div 10^{-2}$       |
| Fine sand        | $10^{-6} \div 10^{-4}$       |
| Silt             | $10^{-8} \div 10^{-6}$       |
| Consistent Clay  | $10^{-8} \div 10^{-4}$       |
| Clay             | $<10^{-9}$                   |

The mass conservation equation governing the seepage flow within geomaterials fully saturated, derives from a mass balance for a representative volume. It is possible to assume incompressible solid grains and a volume fraction of the fluid defined as  $\rho = n\rho_f$ , where  $n$  is the porosity. It can be expressed as follows:

$$-\nabla \cdot (\rho_f \bar{v}_{rf}) + \dot{q}_v = \frac{\partial n\rho_f}{\partial t} \quad (13)$$

In the context of geomaterials we can also assume that the porous medium is incompressible and there is no volumetric mass generation  $\dot{q}_v$ . So, the equation 13 can be rewritten as:

$$\nabla \cdot \bar{v}_{rf} = 0 \quad (14)$$

In conclusion, regarding the problem of initial and boundary conditions, it is possible to make similar considerations to the heat transfer process. In this case, the boundary conditions can be defined both as a Dirichlet's condition, in which a hydraulic head  $h$  is imposed over time, and as a Neumann's condition, in which a flux  $\partial h / \partial n_i$ , in the  $n_i$  direction, is imposed [7].

## 2.4 Convective heat exchange in the pipes

It can be said that the temperature variation associated to the thermal operations of the energy piles are not constant over time, as well as the thermal loading, that are not constant in terms of energy requirement of the building, and also the boundary conditions, which depend on the day-night and seasonal cycles, in the shallowest layer of soil [1]. Therefore, the hydro-thermal processes described by the heat and mass transfer governing equations, are markedly time-dependent.

Nevertheless, after a certain time and space scales, the thermal processes within the energy piles reach the so-called steady conditions, in which the heat and mass transfer problems can be considered as time independent. In the analysis of the energy piles, first of all we must distinguish the steady state conditions and the steady flux conditions. In general, for a certain time  $t > t^*$  the variation of variables as the temperature difference, or the heat exchanged, comes from quantities that evolve with time, but with a constant rate over time, and these are the steady flux conditions. While, in the steady state conditions the variation of the variables depends on constant quantities over time.

In general, the thermal behaviour of an energy pile is characterized by three reference times and as a consequence by four different periods, and the order of magnitude of each time is function of the geometrical pile parameters, the thermal properties, and the fluid velocity inside the pipes. The first characteristic period is related to the time  $t < t_p$  to achieve a steady thermal regime in the pipes inside the energy pile, and it lasts approximately a few hundreds of seconds, in fact, it can be considered negligible from a design point of view. The second reference period of time  $t_p < t < t_{GHE}$  involves timescales ranging from a few hours to days. In this time, the ground source heat pump has reached the dynamic optimum control of its operation. The third characteristic period of time  $t_{GHE} < t < t_g$  corresponds to a long timescale in which the ground heat exchanger has reached the operative thermal behaviour and it is function of the soil thermal properties. In the last period of time  $t > t_g$  any interactions between different energy piles are considered [8]. The most important aspect of the steady flux conditions is that the thermal processes and in particular, the associated design variables can be totally analysed by a time-independent modelling approach.

The empirical equations (15) can give an order of magnitude of the aforementioned reference times of an energy pile.

$$t_p \propto \frac{L}{v_f} \quad t_{ghe} \propto (2.5 \div 5) \frac{R^2}{\alpha_{d,GHE}} \quad t_g \propto \frac{r_{soil}^2}{\alpha_{d,soil}} \quad (15)$$

in which,  $L$  is the heat exchanger depth,  $v_f$  is the heat carrier fluid velocity,  $R$  is the radius of the pile,  $\alpha_{d,GHE}$  is the thermal diffusivity of the pile,  $\alpha_{d,soil}$  is the thermal diffusivity of the soil, and  $r_{soil}$  is the radius of the soil region affected by the thermal processes of the energy pile. The latter can be calculated from the distance between two piles in an energy pile group, considering the radius of the equivalent circumference, as follows:

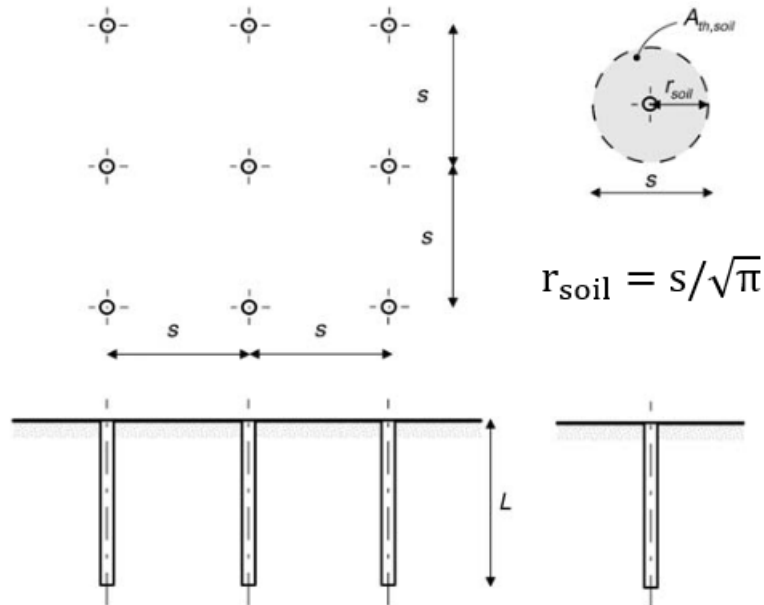


**Figure 12:** Radius of the soil affected from the thermal processes in an energy pile group.  
Picture from L. Laloui – A.F. Rotta Loria 2019.

The so-called residence time  $t_p$  is inversely proportional to the heat carrier fluid velocity. In general, the heat and mass transfer within the pipes is markedly influenced by the inlet fluid velocity and fluid temperature over time, therefore some considerations regarding the hydrodynamic entry and totally developed regions in pipes should be made. In particular, the thermo-hydrodynamic behaviour of the pile is mostly dependent on flow regime [1].

Unlike what happens during a groundwater flow, in which the variables governing the problems are essentially the soil permeability and the difference of hydraulic head between two regions, in the case of the heat circulating fluid within the pipes, the problem is completely described by the flow behaviour. In an energy piles system, it is always regulated by a pump, and therefore, the corresponding heat transfer mode is the so-called forced convection. In the context of heat transfer problem, one must distinguish the thermal entry length, which is the length of the pipe in which the fluid temperature varies with the distance and a fully developed region in which the temperature field has reached a profile that satisfies the surface conditions. Similarly, for the mass transfer problem it is possible to recognize the so-called hydrodynamic entry length, that is the entrance region of the pipe in which the fluid velocity varies with the distance, and a hydrodynamically fully developed region in which the flow velocity profile tends to be constant with the pipe length. In figure 13, the aforementioned regions are schematically represented [1].

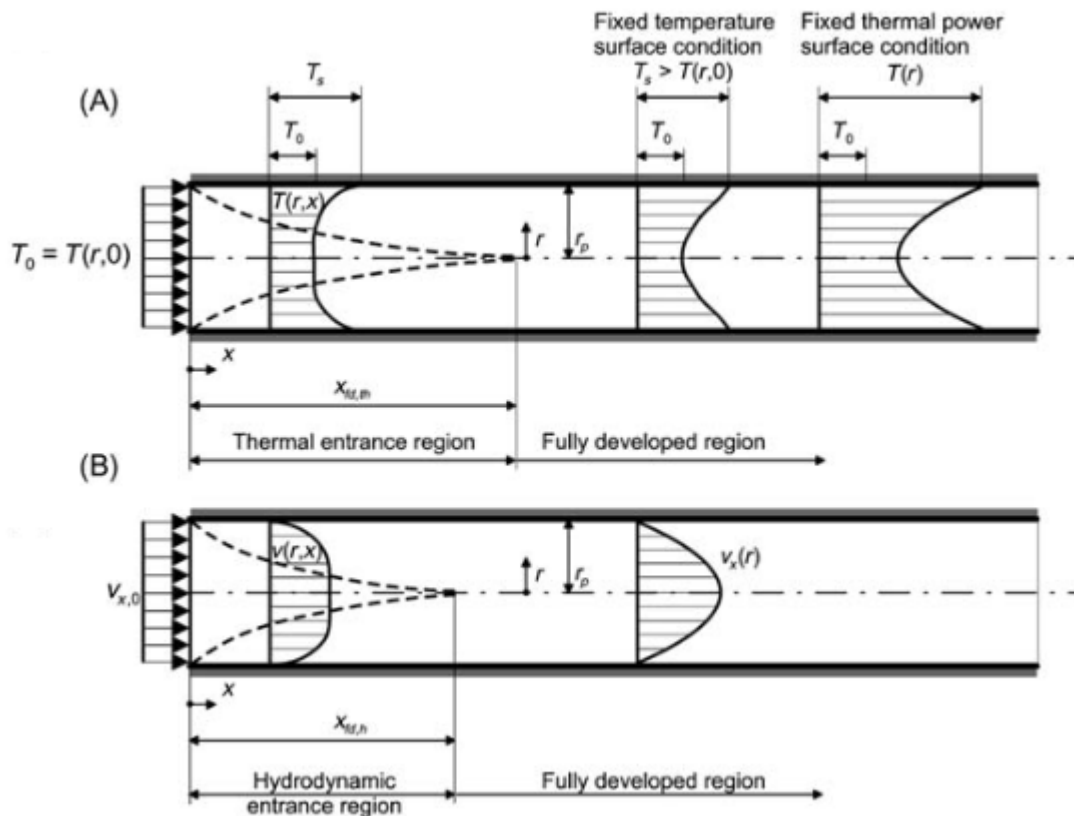


**Figure 13:** Characteristic regions of heat and mass transfer within the pipes. *Picture from Bergman T., Incropera F., Lavine A. 2011.*

An important observation on the hydrodynamic entrance region must be made. The extent of this region strongly depends on the type of flow regime.

To have an idea, under laminar flow the entrance region can reach more than 30 meters in length, while for turbulent flow it is normally of up to 2 meters. Clearly, from an application point of view, it is preferable to have a turbulent flow, to ensure the efficiency of the energy piles system. The coefficient that classifies the flow regime is the Reynolds number, that for a flow in a circular pipe can be defined as:

$$\text{Re} = \frac{v_x d_p}{\eta_f} \quad [-] \quad (16)$$

where, the  $v_x$  [m/s] is the mean fluid velocity within the pipe,  $d_p$  [m] is the inner diameter of the pipe and  $\eta_f$  [m<sup>2</sup>/s] is the kinematic viscosity, which is the ratio between the dynamic viscosity and the fluid density. With a fixed size of pipe and water properties, the parameter governing the flow regime is the fluid velocity. For Reynolds number lower than 2300 laminar flow occurs, for Re between 2300 and  $\sim 10000$  there is the transient flow domain and for Re greater than 10000, fully turbulent conditions exist [4]. The reason why it is better to have a turbulent flow within the pipe is related to the higher diffusive transfer of energy, impulse and mass. This is linked to the convection heat transfer coefficient  $h_c$  which is greater for turbulent flow than for laminar flow, and it depends on several parameters as: the pipe diameter and length, the fluid velocity, the fluid dynamic viscosity and density, the fluid specific heat and the fluid thermal conductivity. For turbulent flow,  $h_c$  can be determined through an experimental approach via Nusselt number Nu, as follows.

$$h_c = \frac{\text{Nu} \lambda_f}{d_p} \quad (17)$$

There are several approaches to determine the Nusselt number, which are basically function of the flow regime. For forced convection in turbulent pipe flow, the most common expression is the Gnielinski correlation, in which Nu is function of the Reynolds number, Prandtl number and the Darcy friction factor  $f$ .

$$\text{Nu} = \frac{(f/8)(\text{Re} - 1000)\text{Pr}}{1 + 12.7(f/8)^{1/2}(\text{Pr}^{2/3} - 1)} \quad \text{Pr} = \frac{\mu_f C_p}{\lambda_f} \quad f = (0.79 \ln(\text{Re}) - 1.64)^{-2} \quad (18)$$

### 3 THERMAL RESISTANCE CONCEPT

---

In the design of energy piles, one of the most important parameters to be analysed is the so-called thermal resistance. In analogy with the electrical field, considering the heat exchange in the energy pile as a purely resistive process, it can be possible to associate the heat conduction with the resistance, and define the thermal resistance  $R$  as:

$$R = \frac{\Delta T}{q_l} \left[ \frac{\text{mK}}{\text{W}} \right] \quad (19)$$

where  $q_l$  [W/m] is the heat transfer rate per unit length of the pile, and  $\Delta T$  [K] is a relevant temperature difference, in general, between the source and the sink. By definition, the thermal resistance of a ground heat exchanger depends on the temperature difference between the heat circulating fluid inside the pipes and the grouting material at the pile-ground interface, that can be produced as a consequence of a heat extraction or injection [9]. In other words, the thermal resistance is inversely proportional to the thermal conductivity or more in general to the heat exchange capacity of the pile. As a consequence, the lower the thermal resistance, the higher the energy efficiency of the pile. Based on what was described in the previous chapter, regarding the characteristic times and periods of an energy pile, the thermal resistance tends to be constant and time-independent in the steady flux conditions. Therefore, the thermal resistance must be computed when the steady flux conditions are reached, in order to have a constant value that, from a design point of view, can indicate the thermal efficiency of the energy piles. Figure 14 qualitatively shows the temperatures trend during the operation of the energy piles.

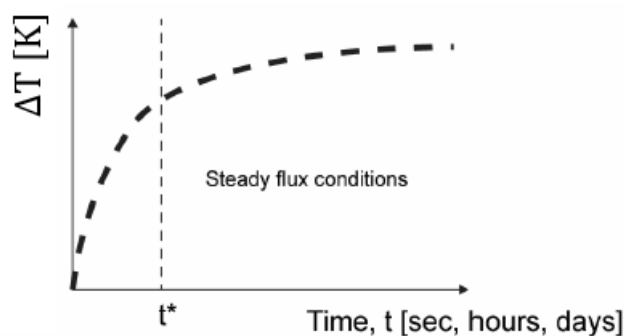


**Figure 14:** Qualitative trend of the temperature difference between the source and the sink. *Picture from L. Laloui – A.F. Rotta Loria 2019.*

### 3.1 Thermal resistance components

Since the tubes are embedded in the pile in parallel, in analogy to the electrical resistance, the total thermal resistance of the energy system  $R_{\text{tot}}$  can be considered as the sum of two terms:

$$R_{\text{tot}} = R_{\text{GHE}} + R_{\text{soil}} \quad (20)$$

where the  $R_{\text{GHE}}$  is the pile (ground heat exchanger) thermal resistance, and  $R_{\text{soil}}$  is the ground thermal resistance. The pile resistance can, in turn, be divided considering each single component related to the corresponding heat transfer mode. Heat exchange within energy piles occurs by conduction through the pipes and the concrete and convection inside the tubes, so the  $R_{\text{GHE}}$  can be expressed as follows:

$$R_{\text{GHE}} = R_c + R_{p,\text{cond}} + R_{p,\text{conv}} \quad (21)$$

in which,  $R_c$  is the thermal resistance of the grouting material (e.g. concrete), and  $R_p$  is the thermal resistance of the pipes, that can be divided into the resistance due to the conduction  $R_{p,\text{cond}}$  and the resistance due to the convection  $R_{p,\text{conv}}$  [10]. In figure 15 there are two 2D schematic sections of a single energy pile which describe each components of the pile thermal resistance.

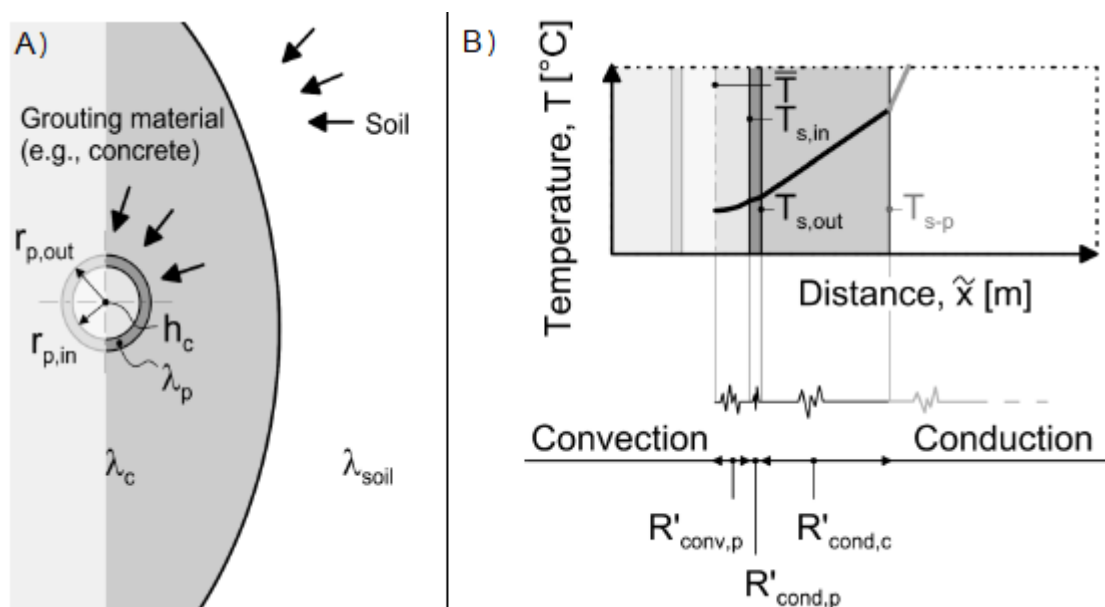


**Figure 15:** Thermal resistance components of a single energy pile. A) Top view B) Front view. *Picture from the slides of the course of “Energy Geotechniques – Prof. L. Laloui – 2019” redrawn after Loveridge, 2012.*

### 3.2 Calculation approaches

Through the analysis of thermal resistance, it is possible to consider separately the behaviour and influence of each material on the global performance of the energy pile. However, there are several approaches to determine each component of the thermal resistance, that are based on analytical models, numerical models, and empirical models. Moreover, the analytical approaches can in turn be divided into one-dimensional modelling approaches, two-dimensional modelling approaches and quasi three-dimensional modelling approaches [8].

The one-dimensional analytical models simplify the complex geometry of the energy piles (pile and pipes), replacing cylinders of infinite length, so that the temperature distribution in the surrounding space of the pipe and the thermal resistance can be computed using the existing solutions for an *infinite hollow cylinder* of constant properties. This approach can be adopted to calculate, with good approximation, the thermal resistance of the pipes due to the heat conduction and convection, as follows:

$$R_{p,conv} = \frac{1}{2n\pi r_i h_i} \left[ \frac{mK}{W} \right] \quad (22)$$

$$R_{p,cond} = \frac{\ln \left( \frac{r_o}{r_i} \right)}{2n\pi \lambda_p} \left[ \frac{mK}{W} \right] \quad (23)$$

$$R_p = R_{p,conv} + R_{p,cond} \quad (24)$$

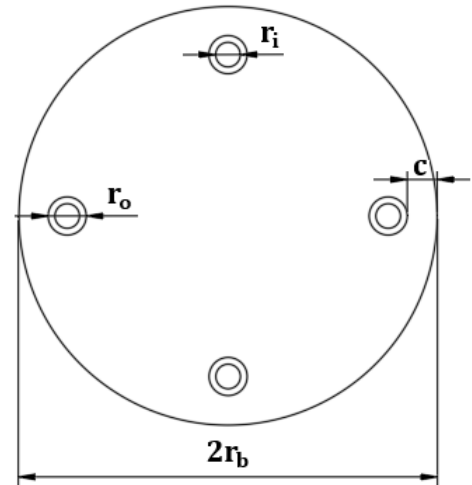


**Figure 16:** 2D section of an energy pile with double U-tube in parallel. #

where,  $h_i$  [W/m<sup>2</sup>k] is the heat transfer coefficient,  $r_i$  and  $r_o$  are respectively the inner and the outer radius of the pipe (figure 16),  $n$  is the number of pipes and  $\lambda_p$  [W/mK] is the thermal conductivity of the pipe [10]. In the context of energy piles, the flow regime within the pipes tends to be turbulent and the heat transfer coefficient can be estimated from the equation (17).

The analytical solution for an infinite hollow cylinder could be used also to calculate the concrete thermal resistance, but it can be proven that the hypothesis of considering the pile as an equivalent hollow cylinder with the outer radius equal to the pile radius  $r_b$ , and the inner effective radius assumed as  $r_{\text{eff}} = r_0 \sqrt{n}$ , leads to overestimate the thermal resistance of the concrete [10]. Therefore, to calculate the concrete thermal resistance it is more correct and realistic to adopt 2D or quasi 3D analytical approaches, or alternatively, empirical and numerical approaches. The most accurate method is the so-called line source model, in which the concrete thermal resistance, due to the heat flow between the pipes and the surrounding soil, can be computed by using a line source to characterize the position of each pipe. The total thermal resistance is then computed by making the superposition of the effects. Considering the case of two symmetric U pipes, the solution of the line source model can be expressed as follows [11]:

$$R_b = \frac{1}{4\pi\lambda_c} \left[ \ln\left(\frac{r_b}{r_0}\right) + \ln\left(\frac{r_b}{s}\right) + \sigma \ln\left(\frac{r_b^4}{r_b^4 - (s/2)^4}\right) \right] + \frac{1}{2} R_p \quad \sigma = \frac{\lambda_c - \lambda_g}{\lambda_c + \lambda_g} \quad (25)$$

where,  $r_b$  is the pile radius,  $r_0$  is the outer radius of the pipe,  $s$  is the distance between the pipes,  $R_p$  is the pipe resistance (eq. 24), and  $\lambda_c, \lambda_g$  are respectively the concrete and the ground thermal conductivity.

The same approach can also be used to calculate the thermal resistance of the soil. As described in the chapter 2.4, the thermal processes affecting a single energy pile have influence on the surrounding soil. The ground thermal resistance can be computed considering this affected area, using the line source model as follows:

$$R_{\text{soil}} = \frac{1}{2\pi\lambda_{\text{soil}}} \left\{ \left[ \frac{r_{\text{soil}}^2}{r_{\text{soil}}^2 - R^2} \right]^2 \ln\left(\frac{r_{\text{soil}}}{R}\right) - \frac{3}{4} - \frac{R^2}{2(r_{\text{soil}}^2 - R^2)} \right\} \quad (26)$$

where,  $R$  [m] is the pile radius,  $\lambda_{\text{soil}}$  [W/mK] is the soil thermal conductivity and  $r_{\text{soil}}$  [m] is the soil radius in which there is the effect of the energy pile [11]. If the ratio between the pile diameter and the distance between piles is such as to satisfy the hypothesis of energy pile group, the soil radius can be computed as shown in figure 12.

Similar to the line source model is the so-called multi-pole method based on multipole equations. Multi-poles are obtained as expansion series from the line sources, by making the derivatives. This approach is more complicated than the line source model and the greater the order of multi-poles, the higher the accuracy with the exact solution. However, it has been proven that the first order solution provides a thermal resistance with a difference of 1% from the solution got with higher order assessments [10]. Multipole method has been used from the Swiss Society of Engineers and Architects to calculate and provide the results of the pile thermal resistance of different configurations of energy piles. The values calculated and published in the Swiss Code SIA-D0190, in 2005, are represented in figure 17 [9].

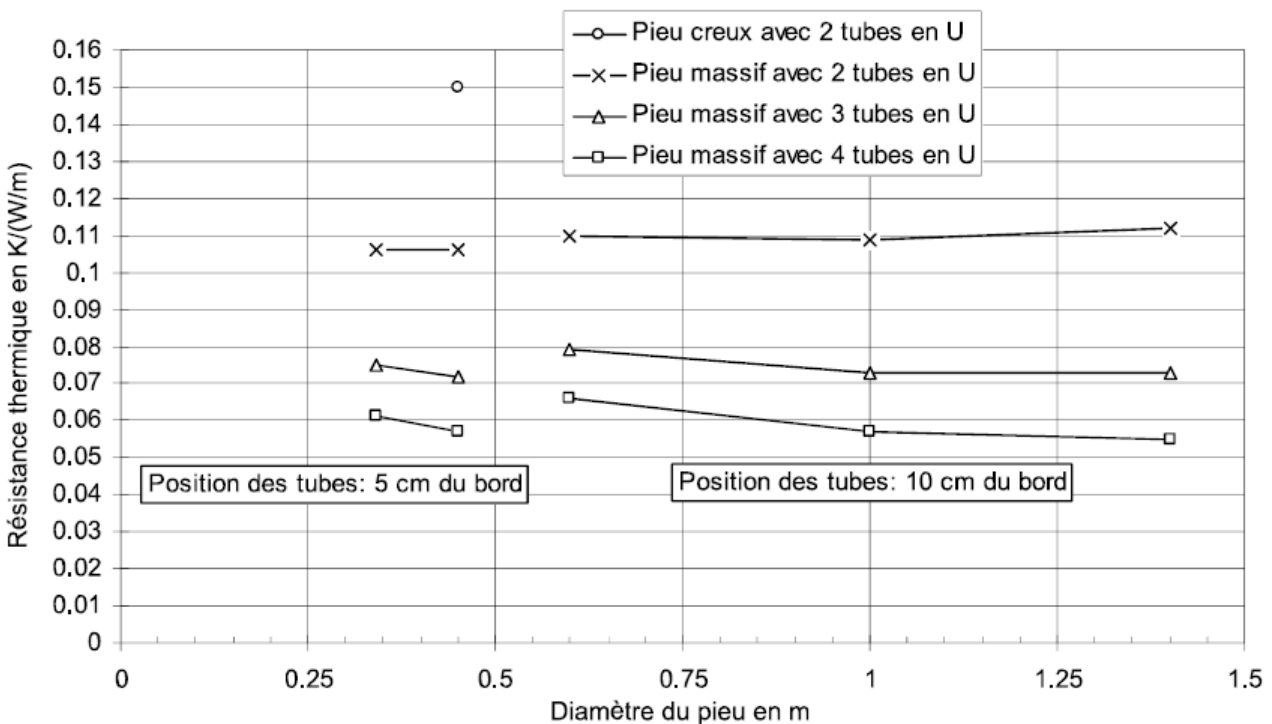


**Figure 17:** Typical values of thermal resistance of different configurations of energy pile, with the diameter varying between 30 cm and 140 cm, and with double, triple and quadruple U-tubes in parallel. *Picture from “Swiss Society of Engineers and Architects – SIA-D0190 – 2005”*

Since both the line source model and the multipole equations are based on a 2D model approach, they are not taking into account two important phenomena which actually come from the three dimensional effects, and they can have an influence on the thermal resistance. The first is related to the pipe to pipe interaction which is greater, the smaller the spacing between the pipes, the higher the fluid velocity within the pipes and the greater the pipe length. The second 3D effect is related to the thermal interactions between materials in the flow direction [10].

The thermal resistance of the pile can be also computed using empirical approach, based on experimental in situ campaigns and thermal response testing (TRT) and/or system back analysis. The idea is to determine the thermal resistance from an empirical equation, characterized by empirical coefficients. The latter are obtained by the best curve fitting of the data that come from field tests of borehole heat exchangers. Remund (1999) proposed an expression to calculate the concrete thermal resistance, in the following form:

$$R_c = \frac{1}{S_b \lambda_c} \quad (27)$$

where  $S_b$  is the so-called shape factor, that is a dimensionless parameter which is function of the ratio between the pile radius and the outer pipe radius, and other coefficients determined by curve fitting of the experimental data. The limit of this approach is linked to its applicability, because it is not always possible to know with accuracy the exact positions of the pipes inside the concrete. However, an important remark about the 1D, 2D analytical approaches and the empirical approach previously described, is that the thermal resistance of a pile depends on the geometrical parameters and thermal properties, and it is not influenced by a different temperature or different heat fluxes imposed as boundary conditions [10].

The last approach to be analysed is the numerical modelling, in which the energy pile can be represented by a finite element model and the heat and mass transfer equations can be integrated with specific boundary conditions. The thermal resistance is then calculated, by definition, from the equation 19. Loveridge and Powrie (2013) proposed a new expression for the concrete thermal resistance, based on the results of a 2D numerical modelling, by an equation of the form:

$$R_c = \frac{1}{S_c \lambda_c} \quad S_c = \frac{A}{B \ln(r_b/r_0) + C \ln(r_b/c) + (r_b/r_0)^D + (r_b/r_0)^E + F} \quad (28)$$

where the coefficients A, B, C, D, E and F come from best curve fitting of the values of the thermal resistance obtained from the 2D numerical model and are function of the conductivity ratio between ground and pile and the number of pipes, and  $r_b$ ,  $r_0$  and  $c$  are the pile radius, the outer pipe radius and the concrete cover respectively (figure 16).

### 3.3 Objective and outline of the project

In the previous chapter the concept of the thermal resistance in the context of energy piles has been described, and how it can be used in the optimization and design of the energy geostructures. The project consists in analysing the hydro-thermal processes during the operation of the energy piles, in order to provide a better assessment of the thermal resistance of the pile and the surrounding ground, accounting for 3D aspects. A new three-dimensional numerical approach is proposed to compute the energy pile's thermal resistance. The software ZSOIL v18.06 has been used to design the mesh and the software LAGAMINE, based on a finite elements code and developed in University of Liège for Chemo-Thermo-Hydro-Mechanic coupled models, has been used to run the hydrothermal analyses and integrate the heat and mass transfer equations.

Starting from the simplest case of a single energy pile, and considering the ground as an equivalent single-phase medium, the thermal resistance of the pile and the soil has been calculated. Then, a parametric analysis by varying the geometrical properties of the pile has been done, to investigate the influence on the thermal resistance of the pile diameter or the concrete cover of the pipes, and by varying the thermo-hydraulic properties of the system, as the thermal conductivity or the fluid velocity, in order to highlight the difference between the laminar and turbulent regime. Afterward, the thermal resistances obtained from these analyses have been compared with existing values from 2D numerical analysis and analytical solutions described in the chapter 3.2. To validate the 3D numerical model, a thermal response testing has been reproduced, in order to compare the output temperature field inside the pile and the ground. This TRT was performed by Cecinato F., and Loveridge F.A. on a single energy pile installed in the London clay, in 2014.

Then, a groundwater flow has been added, in order to evaluate the effects on the heat exchange capacity of the energy pile and see how the thermal resistance is changing [17]. At first, the hydro-thermal coupled constitutive law of the soil has been modified in order to have a multiphase medium. Therefore, the mechanical and thermal parameters of the constitutive law have been calibrated on a ground only model, making the output temperature

field converge with that obtained from the equivalent single-phase analysis. On a similar model, the hydraulic properties have been calibrated with a groundwater flow imposed.

To do this, a difference of hydraulic head  $\Delta H$  has been imposed between the two end faces of the model, and to investigate different fluid velocity, a parametric analysis has been made by varying both the soil permeability and the  $\Delta H$ . After that, the multiphase constitutive law and the groundwater flow have been applied to the case of a single energy pile with different diameters, and the output thermal resistance has been compared with the results of analyses made with a static groundwater table.

As a last step, a more real case of an energy pile group has been analysed. A new 3D model of 2xN and 3xN energy piles has been created, exploiting the double symmetry of a piling. Afterward, the same hydro-thermal analyses have been performed on this model. The case of a static groundwater table allowed to investigate the distance between the piles such that, there is thermal interaction between them. While, the application of the groundwater flow allowed to evaluate the screen effect of the first pile hit by the flow, on the other piles in the flow direction, and mainly the resulting thermal resistance difference from the analysis. In conclusion, the superposition principle has been adopted to create a 3x3 energy pile group. The different thermal behaviour of the central, lateral and border pile has been studied, in terms of the soil thermal resistance surrounding the pile. The dependence of the soil and pile thermal resistance on the piles distance has been highlighted.

## 4 EQUIVALENT SINGLE-PHASE ANALYSIS

The thermal resistance has been calculated for different configurations and models of energy piles. In this chapter, the hydro-thermal analyses made on a single energy pile will be presented. The pile is installed in a soil represented by an equivalent single-phase medium, whose thermal and hydraulic properties take into account the solid phase, the liquid phase and the gas phase. The pipes are embedded in the grouting material with a configuration of double U-tube in parallel (fig. 6 (C)), and with a concrete cover which ensures the correct installation and durability of the steel cage. The heat carrier fluid is circulated with different speeds, in order to evaluate both the turbulent and the laminar regime.

### 4.1 Model description and geometrical characterization

The geometry of the single energy pile is represented by a 3D finite element model, made with the software ZSOIL v18.06. The energy pile and the surrounding ground has been discretized with a 3D finite element model, which includes 8-nodes three-dimensional isoparametric elements and 2-nodes one-dimensional linear elements. The 3D brick elements have been used to discretize the soil and the pile, while the 1D linear elements to discretize the U-pipes inside the pile. Figure 18 shows the two types of elements used for the model.

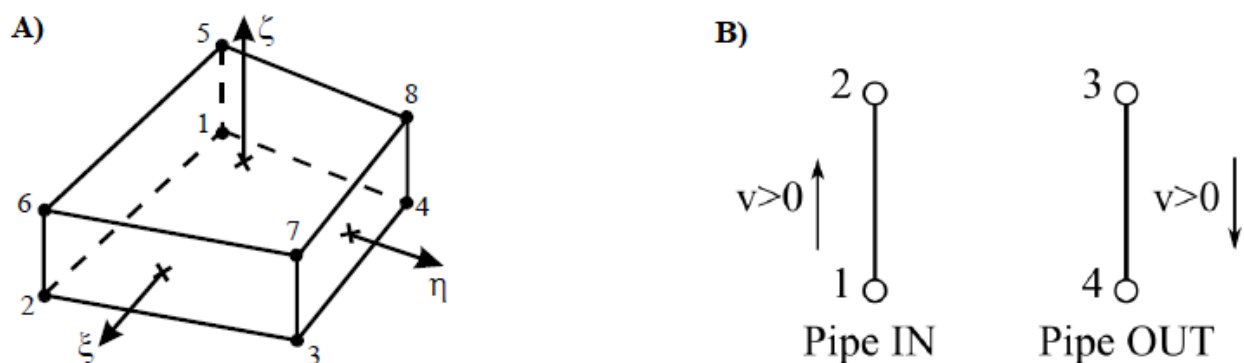


**Figure 18:** A) 8-nodes three-dimensional elements, for soil and pile B) 2-nodes one-dimensional linear elements, for U-pipes. Pictures from manuals of LAGAMINE – Computer Code – Bille J., Habraken A., Charlier R., Li X., 1993.

The geometrical parameters have been chosen based on both the orders of magnitude of a structural pile, and on previous studies and tests done by Di Donna A., Laloui L., (2014) [12].

The pile is characterized by a length  $L$  of 20 meters, a diameter  $D$  of 1 meter and the 2 U-pipes are symmetrically embedded in parallel, with a concrete cover  $c$  of 10 cm, a length of 18.8 cm, and a spacing  $s$  between them of 56 cm. The surrounding soil has been realized with a circular crown concentric to the pile, with a radius of 25 meters, in order to totally see the thermal effect of the pile in the ground. For the same reason, the depth of the ground has been taken two times the pile length. Figure 19 shows the 3D mesh, with a zoom on the pile, used for this first analysis.

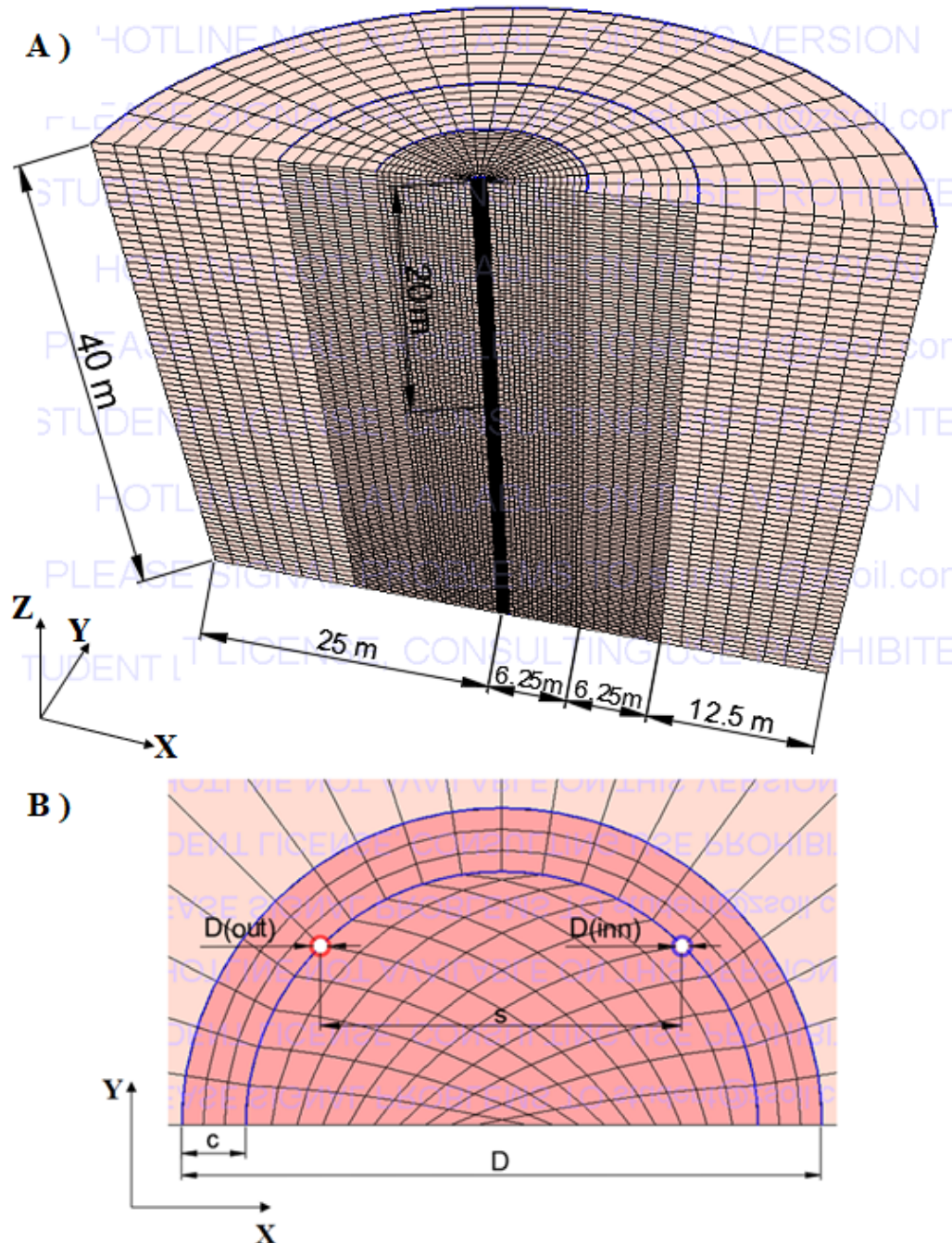


**Figure 19:** A) Perspective view of the 3D model B) 2D section of the pile. Pictures taken from the numerical model made with ZSoil V18.06.

In figure 19(B) a 2D section of the energy pile is represented.  $D(\text{out})$  and  $D(\text{inn})$  are respectively the outer and the inner diameter of the pipes. For all the analysis  $D(\text{out})$  has been fixed equal to 3.2 cm and  $D(\text{inn})$  equal to 2.6 cm.  $D$  is the pile diameter,  $c$  is the concrete cover and  $s$  is the spacing between the pipes.

To lower the computational cost, the symmetry of the single energy pile system has been exploited, therefore half geometry has been considered and the results can be extended to the whole pile. The 3D mesh is made up of 87120 brick elements and 126 1D linear elements, including 10560 elements to discretize the pile, 76560 elements for the soil and 126 linear elements for the pipes. Figure 19(A) shows that the FE discretization has been progressively thickened in the area surrounding the pile, and figure 19(B) shows that inside the pile a circular crown has been created to model the concrete cover. The U-pipes has been installed on the edge of the circular crown, with a distance from the soil-pile interface equal to the concrete cover.

## 4.2 Coupled constitutive laws and boundary conditions

The FE mesh has been subsequently implemented in LAGAMINE, with which the hydrothermal analyses have been carried out. A constitutive law has been assigned to each group of elements representative of a material. Both for the ground and for the grouting material of the pile a linear elastic constitutive law and a hydrothermal coupled constitutive law have been considered. The *WaVaT* constitutive law used for the soil and the pile is a water-air seepage-thermal coupled law for non-linear analysis, which considers coupled transient phenomena in 3D porous media [15]. For this equivalent single-phase analysis, the parameters imposed in the elastic law are the Young Modulus, the Poisson coefficient and the material density, while for the coupled law are: the initial temperature  $T_0$ , the water dynamic viscosity  $\mu_w$  and density  $\rho_w$ , the water specific heat  $C_{pw}$ . For the solid phase, equivalent parameters for the thermal conductivity and the volumetric heat capacity  $\rho C_p$  have been imposed. Thermal properties typical of a saturated coarse-grained soil and of a concrete have been chosen respectively for the ground and for the grouting material. For the pipe has been imposed the thermal properties of the high-density polyethylene, which is the most common material used for the pipes.

The aforementioned thermal and hydraulic parameters are summarized in table 3.

**Table 3:** Thermo-hydraulic properties of the ground and the grouting material imposed in the constitutive law

| <b>WaVaT COUPLED CONSTITUTIVE LAW</b> |   |   |   |                                    |
|---------------------------------------|---|---|---|------------------------------------|
| <b>T<sub>0</sub></b><br><b>[K]</b>    | <b>Water specific heat</b><br><b>[J/kgK]</b>  | <b>Water density</b><br><b>[Kg/m<sup>3</sup>]</b> | <b>Water pressure</b><br><b>[Pa]</b>                                    | <b>Air pressure</b><br><b>[Pa]</b> |
| 285                                   | 4186  | 1000  | 1.E+5   | 1.E+5                              |
| <b>MATERIAL</b>                       | <b>Equivalent thermal conductivity</b><br><b><math>\lambda_{eq}</math></b><br><b>[W/mK]</b> |   | <b>Equivalent volumetric heat capacity</b><br><b>[J/m<sup>3</sup>K]</b> |                                    |
| Saturated Fine Sand                   | 1.8   |   | 2.3E+6  |                                    |
| Concrete                              | 1.8   |   | 1.9E+6  |                                    |

The initial temperature of the pile and the soil has been set to 285 K (12°C). The mechanical parameters of the fine sand and the concrete, as the Young Modulus and the Poisson coefficient, have been imposed in the linear elastic law, but they do not influence the thermal processes and in particular the thermal resistance. The parameters of the pipe and the heat carrier fluid have been set in the law for linear heat advection-diffusion 1D elements. The *LinAdC* is implemented in Lagamine and it is used to integrate the equations of advection-diffusion of heat in a pipe. A lateral heat flow with the surrounding medium is also taken into account [6]. The parameters of the LinAdC law are summarized in table 4.

**Table 4:** Thermo-hydraulic parameters for the LinAdC law for 1D elements

| <b>LAW FOR LINEAR HEAT ADVECTION-DIFFUSION 1D ELEMENT</b> |                         |                        |                         |             |
|---|-------------------------|------------------------|-------------------------|-------------|
| <b><math>\lambda_f</math></b>                             | <b><math>v_f</math></b> | <b>T<sub>ini</sub></b> | <b><math>h_c</math></b> | <b>Q</b>    |
| W/mK  | m/s                     | K                      | W/m <sup>2</sup> K      | W           |
| <b>0,56</b>   | <b>0,8</b>              | <b>285</b>             | <b>3156</b>             | <b>1000</b> |

The heat carrier fluid velocity  $v_f$  has been set to 0.8 m/s in order to have a Reynolds number greater than 10000 (eq. 16), and as a consequence, a fully turbulent regime. The heat transfer coefficient  $h_c$  has been calculated with the Gnielinski correlation (eq. 17 and 18). For the heat

power imposed to the fluid at the inlet cross section of the pipe, has been chosen a typical order of magnitude of the heat extraction (or injection) power in the energy piles. From figure 8 it can be seen that 50 W/m is the typical value of heat extraction rate of an energy pile. The length of the pile is 20m, therefore the heat power imposed is 1000 W.

Regarding the boundary conditions, there is a distinction to be made between the design phase and the real operation of the energy piles. In reality, the energy needs of a building is not constant over time, but it could be represented with a periodic pattern, depending on the day-night and seasonal cycles. However, from a design point a view, it is known the order of magnitude of the heat exchange rate that an energy pile has to produce. Therefore, in the design phase a constant heat power is imposed to the carrier fluid, and the thermal resistance needs to be determined to estimate the mean temperature of the fluid. The latter is the so-called Neumann boundary condition. It is also possible to estimate the thermal power from the thermal resistance with a range of imposed temperature to the inlet fluid, and this is the Dirichlet boundary condition [8]. The Neumann boundary conditions has been adopted for these analyses, with a constant heat power imposed at the inlet cross section of the pipes. As initial condition, a constant temperature has been set to all materials. The numerical implementation solves the heat and mass transfer equations described in chapter 2.2, in particular the equation 10, which takes into account both the conduction and the convection between the carrier fluid, the pile and the ground. It calculates at a given time step, at each node  $k$  of the pipes, the heat transfer rate  $q_l$ , (eq. 10) with an imposed heat power  $Q$  at the inlet cross section. Then the fluid temperature change in the flow direction is computed as follows:

$$q_{l,z+dz} = q_{l,z} + \frac{\partial q_{l,z}}{\partial z} dz \quad (29)$$

$$T_{f,i}(t) = T_f(t) + \frac{q_l L}{2\rho_f C_{p,f} V_f} \quad (30)$$

$$T_{f,o}(t) = T_f(t) - \frac{q_l L}{2\rho_f C_{p,f} V_f} \quad (31)$$

where  $L$  is the pile length, and  $T_{f,i}$  ( $T_{f,o}$ ) –  $T_f$  is the temperature difference in the flow direction. The size of the model allowed to keep the temperature constant, at the lateral edge, throughout the analyses.

### 4.3 Model application

After assigning the coupled constitutive laws and the initial condition to each material and setting the boundary conditions to the to the heat carrier fluid and to the soil and pile, the numerical simulations have been made. In particular, the degrees of freedom linked to the deformation in X, Y and Z are fixed, since we are analysing the hydro-thermal processes, and the water pressure is fixed in order to consider a static groundwater table and a saturated material. For the analysis time a period of 15 days (360 hours) has been chosen, in order to consider a number of hydro-thermal cycles necessary to reach the steady flux conditions described in the chapter 2.4.

The first analyses have been made on an energy pile with a pile diameter of 1 meter and a concrete cover of 10 cm, and the case of heat injection is considered. The heat power, the heat carrier fluid velocity, and the thermal conductivity of the ground have been varied, to find the best situation from the point of view of the thermal efficiency. In other words, the thermal resistance has been calculated for each case and then compared with existing values. The case that led to obtain the lowest thermal resistance has been chosen for the subsequent analyses. The outcome of the simulations is the temperature field, at each time step, of the ground, the pile, and the carrier fluid inside the pipes. The post processing is explained below.

- 1) The situation of steady flux conditions is considered, after a certain value of time  $t^*$ .

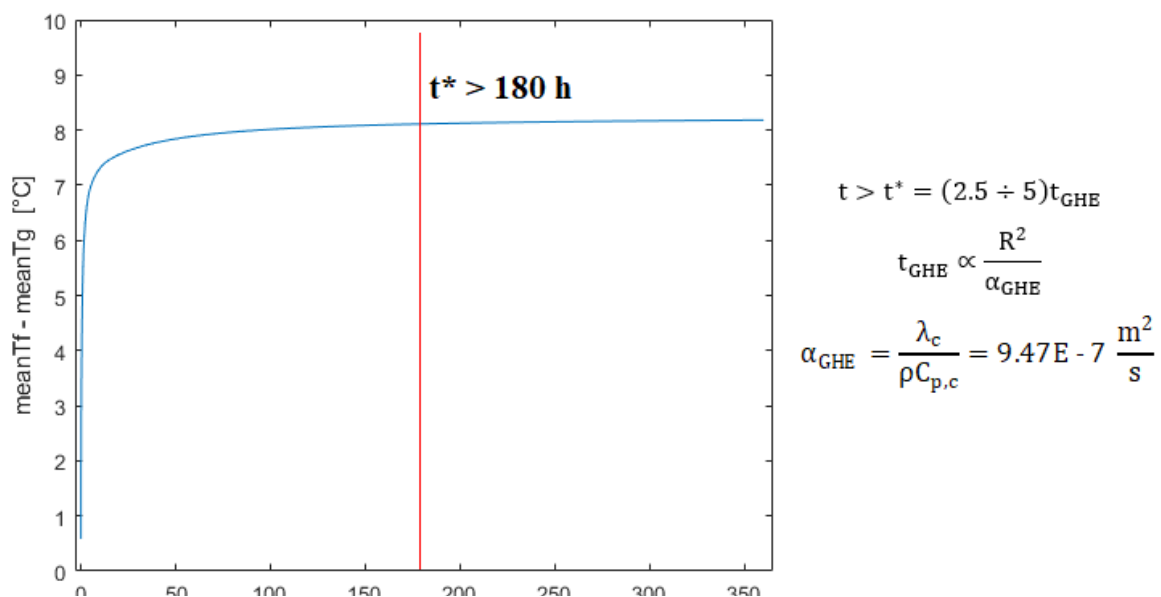


**Figure 20:** Temperature difference between the ground and the carrier fluid, over time. Steady flux conditions are highlighted.

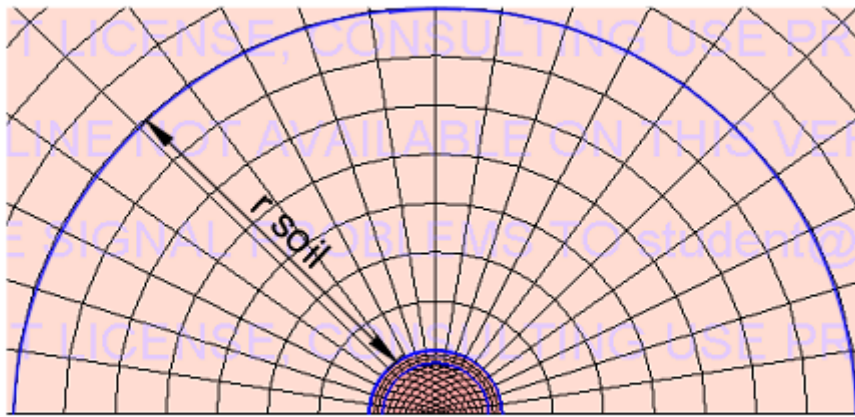
$$t > t^* = (2.5 \div 5)t_{\text{GHE}}$$

$$t_{\text{GHE}} \propto \frac{R^2}{\alpha_{\text{GHE}}}$$

$$\alpha_{\text{GHE}} = \frac{\lambda_c}{\rho C_{p,c}} = 9.47\text{E} - 7 \frac{\text{m}^2}{\text{s}}$$

2) Figure 20 shows the trend of the temperature difference between the ground and the circulating fluid. In particular, for the mean fluid temperature  $\bar{T}_f$ , it has been considered the average of the temperatures of each node of the pipes, from the inlet cross section to the outlet cross section, and then the average over time, from the steady flux conditions to the end of the process. For the mean ground temperature  $\bar{T}_g$ , it has been considered a circular crown around the pile, with a soil radius after which the temperature back to being constant at the initial ground temperature. Again, it has been done the average of the temperature of each node inside the selected region, over the whole depth, and over time, after the steady flux conditions are reached (figure 21).

**A)**



**B)**

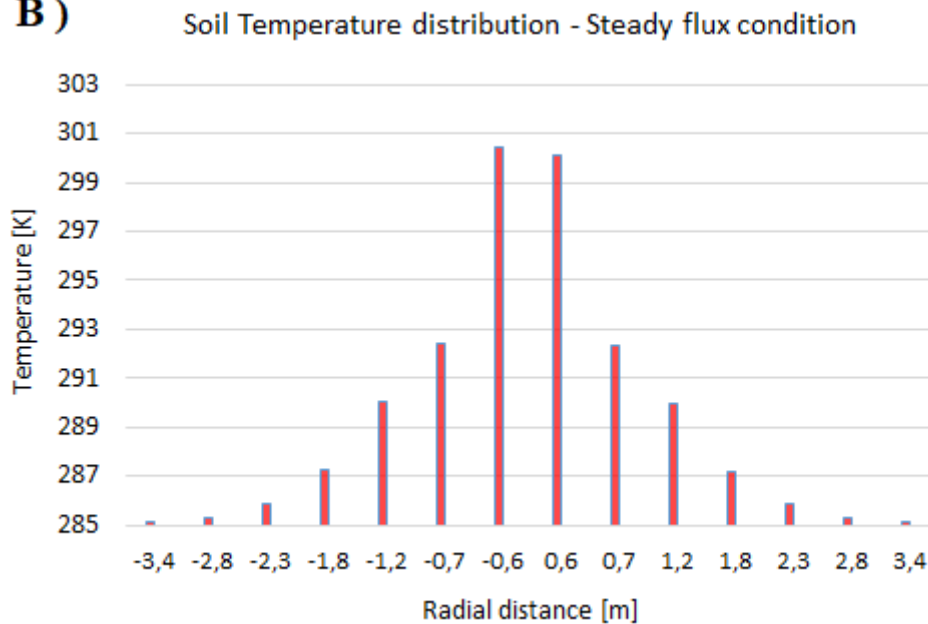


**Figure 21:** A) Selected soil region to compute the mean temperature of the ground. B) Qualitative trend of the temperature field around the pile.

- 3) Based on equations 19-20-21, the following process is applied to compute each component of the thermal resistance.

$$A) \quad \frac{\Delta T}{q} \rightarrow \begin{cases} \frac{\bar{T}_{\text{fluid}} - \bar{T}_{\text{ground}}}{q} \rightarrow R_{\text{TOT}} \\ \frac{\bar{T}_{\text{fluid}} - \bar{T}_{\text{interface}}}{q} \rightarrow R_{\text{GHE}} \\ R_{\text{soil}} = R_{\text{TOT}} - R_{\text{GHE}} \end{cases}$$

where,  $\bar{T}_{\text{interface}}$  is the mean temperature of the nodes on the edge of the pile, over time, and  $q$  is the heat transfer rate  $Q/L = 50 \text{ W/m}$ .

$$B) \quad \begin{cases} R_{\text{P,conv}} = \frac{1}{2n\pi r_i h_i} \\ R_{\text{P,cond}} = \frac{\ln(r_{\text{out}}/r_{\text{in}})}{2n\pi\lambda_p} \\ R_c = R_{\text{GHE}} - R_{\text{P,conv}} - R_{\text{P,cond}} \end{cases}$$

- 4) To verify the process, the analytical expression proposed by Hellstrom (eq. 26) and based on a line source model has been used. With a back analysis, the calculated soil thermal resistance  $R_{\text{soil}}$  has been imposed in the Hellstrom's equation, and the soil radius that satisfy the equation has been obtained.

$$R_{\text{soil}} = \frac{1}{2\pi\lambda_{\text{soil}}} \left\{ \left[ \frac{r_{\text{soil}}^2}{r_{\text{soil}}^2 - R^2} \right]^2 \ln\left(\frac{r_{\text{soil}}}{R}\right) - \frac{3}{4} - \frac{R^2}{2(r_{\text{soil}}^2 - R^2)} \right\} \quad R \rightarrow \text{pile radius}$$

- 5) As a last step, the soil radius got from the previous equation has to be consistent with the one chosen in point 2). If not, a larger (or smaller) soil radius has been considered until the convergence between the two values has been reached.

#### 4.4 Comparison with 2D analytical and numerical solutions

The analyses have been made for four different cases, with a fixed pile diameter of 1 meter and a concrete cover of 10 cm. Table 5 shows the four different cases, in which the heat power, the flow velocity and the soil conductivity have been varied.

**Table 5:** Equivalent single-phase analyses – simulations parameters

| CASE | Pile Diam. [cm] | Concrete c. [cm] | Heat Power Q [W] | Soil cond. $\lambda_s$ [W/mK] | Flow rate [m/s] |
|------|-----------------|------------------|------------------|-------------------------------|-----------------|
| 1    | 100             | 10               | 500              | 1.8                           | 0.1             |
| 2    |                 |                  | 1000             | 1.8                           | 0.1             |
| 3    |                 |                  | 1000             | 1.8                           | 0.8             |
| 4    |                 |                  | 1000             | 1.5                           | 0.8             |

From table 4 it can be seen that, in the first two cases a laminar regime has been set due to the fluid velocity equal to 0.1 m/s, and the heat power has been varied. In the case 3 and 4, the fluid velocity set to 0.8 m/s has produce a fully turbulent regime, and the soil conductivity has been varied in order to see its effect on the heat exchange. The thermal resistance has been computed with the post-processing analysis explained in the previous chapter. In particular, the total thermal resistance ( $R_{soil} + R_{ghe}$ ) has been computed from the output temperature of the analysis and the resistance of the pipe (conduction + convection) has been calculated with an analytical approach. The results of each component of the thermal resistance are summarized in table 6.

**Table 6:** Thermal resistance components resulting from the equivalent single-phase analysis

| CASE | R tot [mK/W] | R ghe [mK/W] | R soil [mK/W] | R p,cond [mK/W] | R p,conv [mK/W] | Rc [mK/W] |
|------|--------------|--------------|---------------|-----------------|-----------------|-----------|
| 1    | 0,29         | 0,21         | 0,08          | 0.0207          | 9.6E-4          | 0.188     |
| 2    | 0,33         | 0,23         | 0,10          |                 |                 | 0.208     |
| 3    | 0,27         | 0,16         | 0,11          |                 |                 | 0.142     |
| 4    | 0,35         | 0,23         | 0,13          |                 |                 | 0.208     |

As expected, the case 3 has produced the lowest thermal resistance. In fact, the best situation for an energy pile is characterized by a fully turbulent flow and a soil and pile thermal conductivity as high as possible. Comparing the results with the values provided by the Swiss Code (chapter 3.2) [9] (figure 22), it can be seen that the case 3 shows a GHE thermal resistance quite consistent.

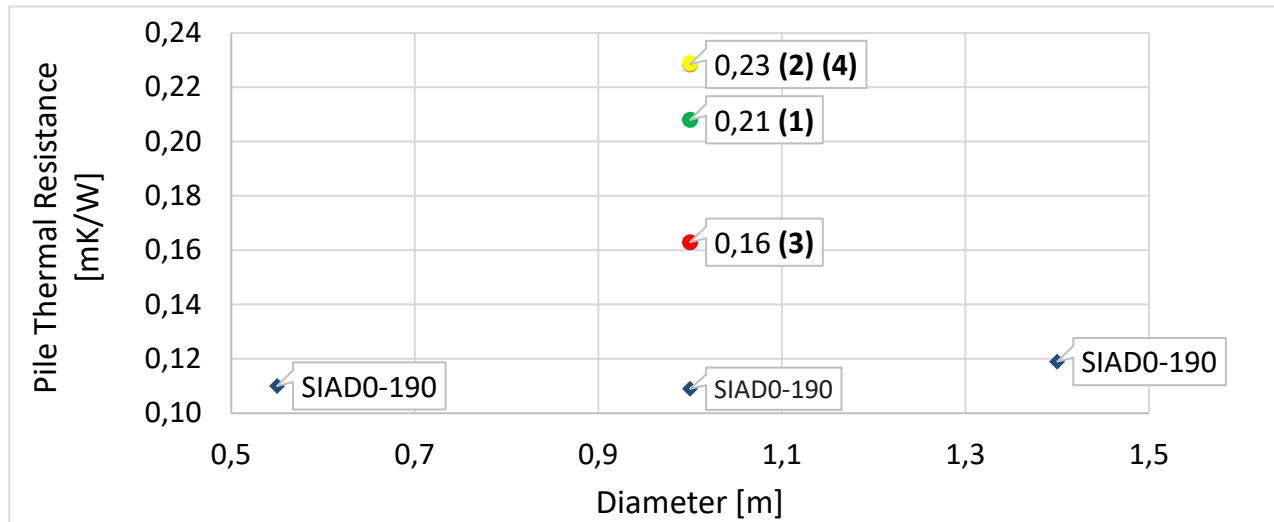


**Figure 22:** Comparison with 2D analytical solutions provided by Swiss Code (SIA D-0190 – 2005)

Then, considering the parameters of the case 3, other analyses have been made by varying the diameter and the concrete cover (table 7).

**Table 7:** Numerical results of the thermal resistance for different pile diameters and concrete covers

| Pile Diameter | c    | t steady | R tot  | R ghe  | R soil | Rc     |
|---------------|------|----------|--------|--------|--------|--------|
| [m]           | [cm] | [h]      | [mK/W] | [mK/W] | [mK/W] | [mK/W] |
| 0,3           | 5    | >100     | 0,332  | 0,157  | 0,174  | 0,137  |
| 0,4           | 5    | >130     | 0,321  | 0,154  | 0,166  | 0,133  |
| 0,6           | 10   | >130     | 0,350  | 0,171  | 0,149  | 0,163  |
| 1             | 10   | >180     | 0,288  | 0,163  | 0,126  | 0,142  |
| 1,2           | 10   | >200     | 0,270  | 0,162  | 0,109  | 0,141  |
| 1,4           | 10   | >200     | 0,250  | 0,153  | 0,096  | 0,133  |

The results in terms of pile thermal resistance  $R_{ghe}$  are shown in figure 23.

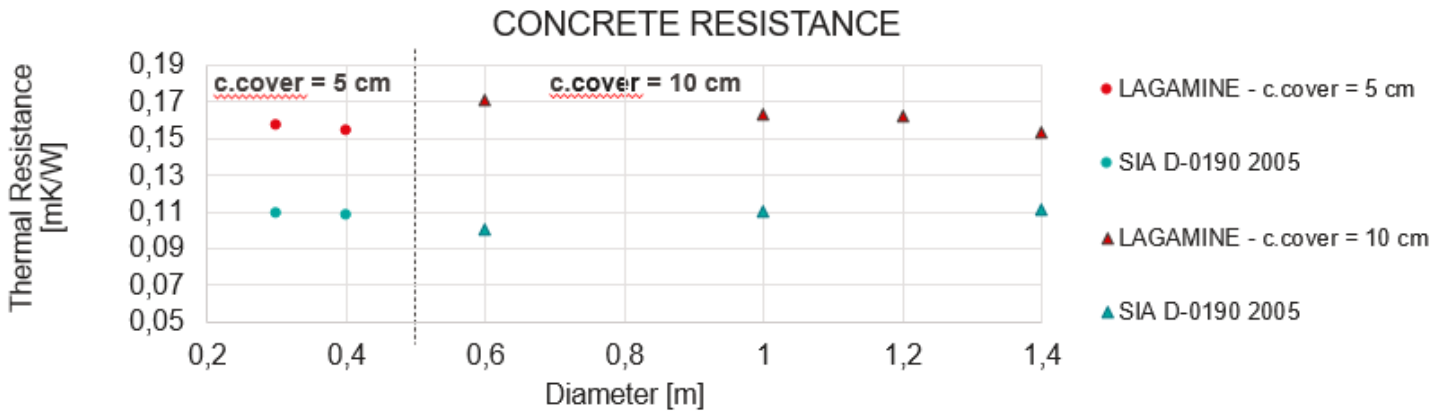


**Figure 23:** Comparison between the Lagamine’s solutions and the values provided by the Swiss Code.

Another comparison has been made with the solutions provided by Loveridge and Powrie. They investigate the effects of the pipes’ configurations and pile diameter on the concrete thermal resistance. To do that they implemented two-dimensional heat transfer models using the finite element software COMSOL v4.1. The output of their simulations are the different components of the thermal resistance, but they adopted the Dirichlet B.C., so they imposed constant temperatures at the pile edge and the pipe surface, and they ran steady state analyses. They provided an empirical formulation determined by curve fitting of the results coming from the numerical solutions (chapter 3.2 – eq. 28). In particular, their solution is function of the ratio between the soil and the pile thermal conductivity, and the number of pipes [10]. The comparison of the 3D and 2D numerical solutions is shown in figure 24.

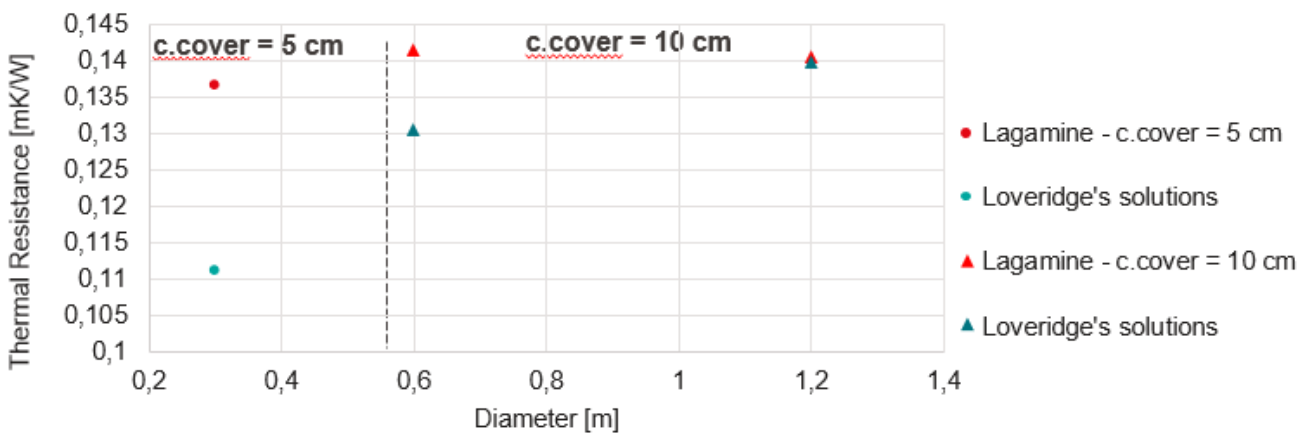


**Figure 24:** Comparison between the Lagamine’s solutions and the 2D solutions provided by Loveridge and Powrie.

## 4.5 Model validation – Reproduction of TRT field data

The three-dimensional finite element model implemented in Lagamine has been validated both by reproducing a multi-stage thermal response testing and by comparing a numerical solution obtained by a 3D finite element model. The TRT is used to design a ground source heat pump and consists in indirect in-situ measurements of the thermal properties of the ground. Basically, it involves the use of a device with which a constant power is injected into (or extracted from) a ground borehole, and in the same time the borehole temperature is measured [13].

The TRT field data has been taken from a test carried out in London, by Cecinato F. and Loveridge F.A. (2014). They have implemented a 3D numerical model of a single energy pile, and they have used the TRT field data for the validation. The 3D finite element model has been implemented using the software ABAQUS, with which 3D transient conduction through the solids and convection heat transfer between the fluid and the soil have been integrated. As boundary conditions, the measured inlet fluid temperature history of the TRT has been imposed at the first node of the U-pipe throughout the simulation time (Dirichlet B.C.). In this way, they have taken into account the fluctuations of the input power around the nominal value. As a result, the temperature field of the fluid, the pile and the ground has been obtained. The geometrical parameters of the pile and the hydro-thermal properties of the system have been taken from the borehole, and the ground on which the TRT has been made. The energy pile is characterized by a length  $L$  of 26.8 m and a diameter  $D$  of 30 cm. A single U-loop of pipes is embedded in the pile with a pipe diameter of 3.2 cm. The ground is characterized by a saturated, firm to stiff London Clay. The inlet and outlet fluid temperatures have been measured during the test. Moreover, couples of vibrating wire strain gauge have been installed at 4 different depths, embedded in the concrete with a symmetric configuration. Therefore, temperature measurements from the concrete area have been taken [14].

The aforementioned thermal properties and geometrical parameters have been adopted for the 3D model implemented in Lagamine. Exploiting the symmetry of the system, half geometry of the energy pile is considered, and as the single U-loop of the pipe is installed on the symmetry plane, just half of it is considered.

In table 8 are summarised the hydro-thermal properties of the energy pile and the and in figure 25 a 2D section of the pile is represented.

**Table 8:** Thermal properties of the pile and the ground

| Material | $\lambda$<br>W/mK | $C_p$<br>J/KgK | $\rho$<br>Kg/m <sup>3</sup> |
|----------|-------------------|----------------|-----------------------------|
| Concrete | 2.8               | 1050           | 2210                        |
| Clay     | 2.3               | 1820           | 1900                        |

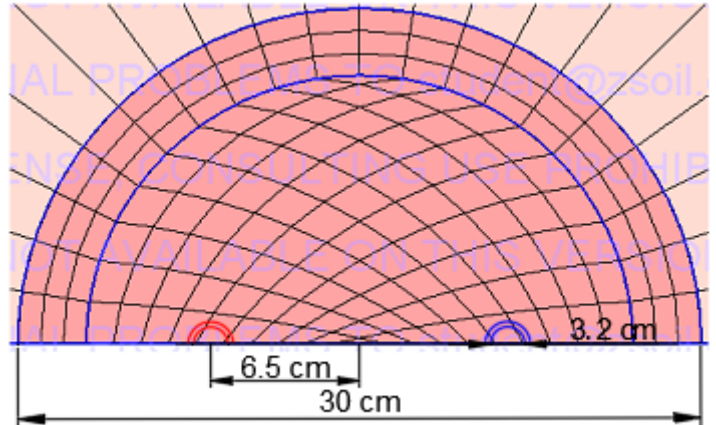


**Figure 25:** 2D section of the energy pile – half geometry considered

However, in these simulations a constant heat flux has been set as Neumann boundary condition, and the applied power is nominally constant during each stage of the test. Actually, there are significant fluctuations with time around the nominal value, of the order of 3.7 W/m (100 W). The test lasted for about 316 hours. The stages of the thermal response test are schematically represented in figure 26.

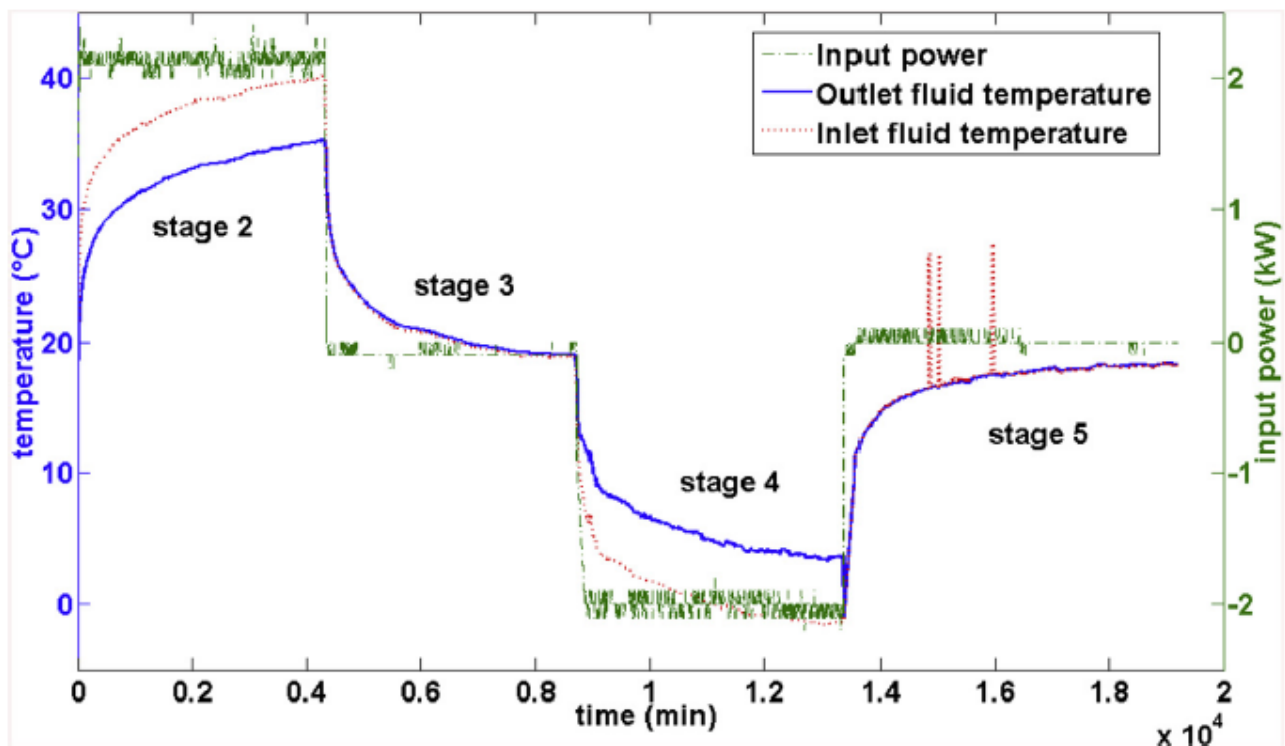


**Figure 26:** Stages 2-5 of the thermal response test. Picture taken from “Influences on the thermal efficiency of energy piles” Cecinato F., Loveridge F.A. 2015

In figure 26 the stage 1 of initial isothermal circulation is not represented but, as initial condition for the simulations, the equilibrium temperature for all the materials has been set to 17.4° (290.4 K). Then, it can be seen that the TRT involves a heat injection test during stage 2 (summer season), a recovery period in stage 3, followed by a heat extraction test during stage 4 (winter season) and again a recovery period in the final stage 5.

The stage 2 (heat injection) and the stage 4 (heat extraction) have been simulated in Lagamine and the comparison between the inlet and outlet fluid temperatures over time, coming from the TRT data and the numerical simulations for the stage 2, is represented in figure 27. Table 9 shows the analysis' parameters adopted for this stage.

**Table 9:** Parameters adopted to simulate the stage 2 of the TRT

| <b>STAGE 2 – HEAT INJECTION – SUMMER SEASON</b> |                              |                             |                  |                               |                                   |                     |
|---|------------------------------|-----------------------------|------------------|-------------------------------|-----------------------------------|---------------------|
| <b>Q<br/>W</b>                                  | <b>Pile<br/>Length<br/>m</b> | <b>Pipe<br/>Depth<br/>m</b> | <b>q<br/>W/m</b> | <b>Mass flowrate<br/>Kg/s</b> | <b>Fluid<br/>velocity<br/>m/s</b> | <b>Time<br/>min</b> |
| +2100   | 26.8                         | 23.8                        | 88.2             | 0.108                         | 0.134                             | 4300                |

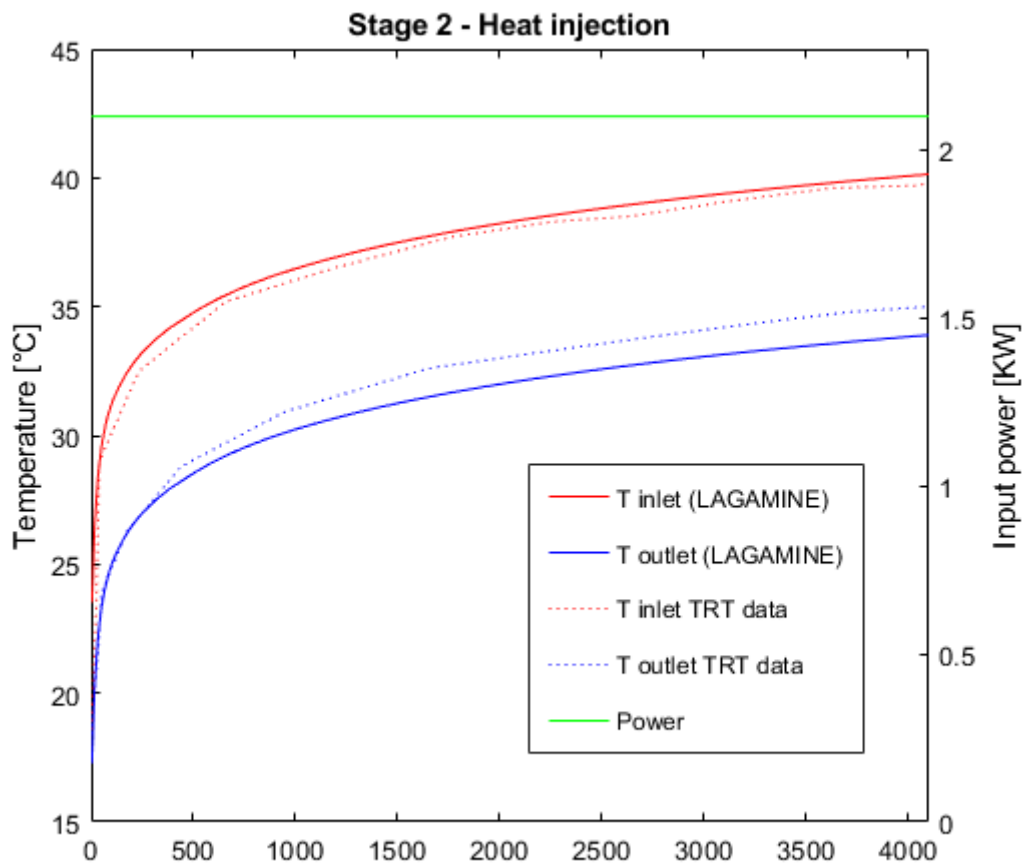


**Figure 27:** Comparison between the inlet and outlet temperature coming from numerical simulations and TRT data, for stage 2. Data taken from the TRT done in London from Cecinato and Loveridge.

During the heat extraction test (stage 4) the equilibrium temperature for all materials has been set to 18,9° (292 K). A constant and negative heat flux condition has been set as boundary condition. Figure 28 shows the same comparison made for the stage 2. In this case the constant heat flux has been set to -1900 W (-79.8 W/m), in order to take into account the fluctuations around the nominal value. The simulation time has been set to 4660 min.

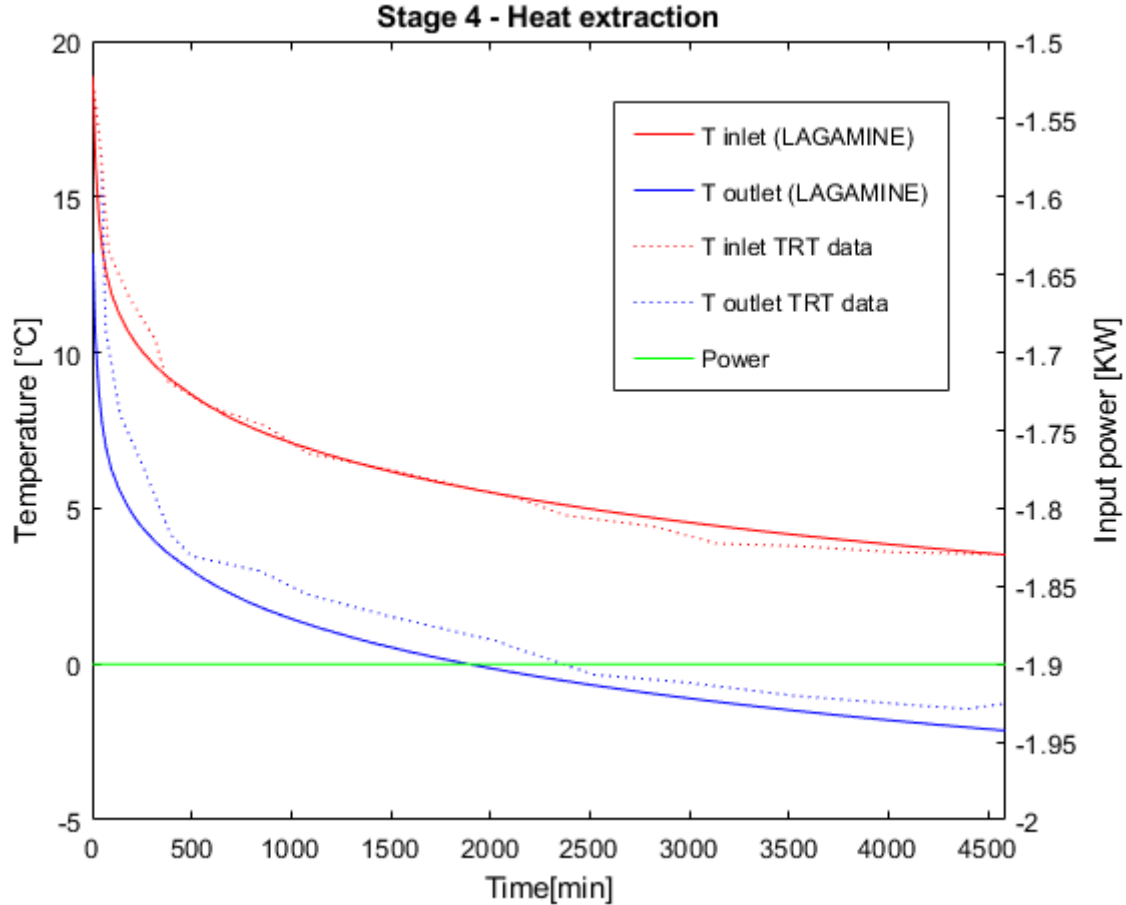


**Figure 28:** Comparison between the inlet and outlet temperature coming from numerical simulations and TRT data, for stage 4. Data taken from the TRT done in London from Cecinato and Loveridge.

The energetic efficiency of the energy piles is related to the total exchanged energy for a given time, which is the integral of the curves in figure 27 and 28. Considering the exchanged power  $q(t)$  for a certain period of time  $t$ , it is possible to assess the energy efficiency as follows.

$$\dot{q}(t) = \dot{m}C_{pf}[T_{in}(t) - T_{out}(t)] \quad (32)$$

$$E_{tot} = \int_0^{t_f} \dot{q}(t) dt \quad t_f = 5000 \text{ min} \cong 3.5 \text{ days} \quad (33)$$

In both cases of heat injection and extraction  $E_{tot}$  it is equal to 14.1 MJ and -14.1 MJ, respectively. It means that the pile shows a linear behaviour for the two analyses.

As an addition validation step, to check the concrete behaviour, a comparison between the concrete temperature at two depths, resulting from numerical simulations and VWSG measurements, has been carried out. The stage of heat extraction has been considered for the simulations, with the same analysis parameters indicated before. Figure 29 shows the results.

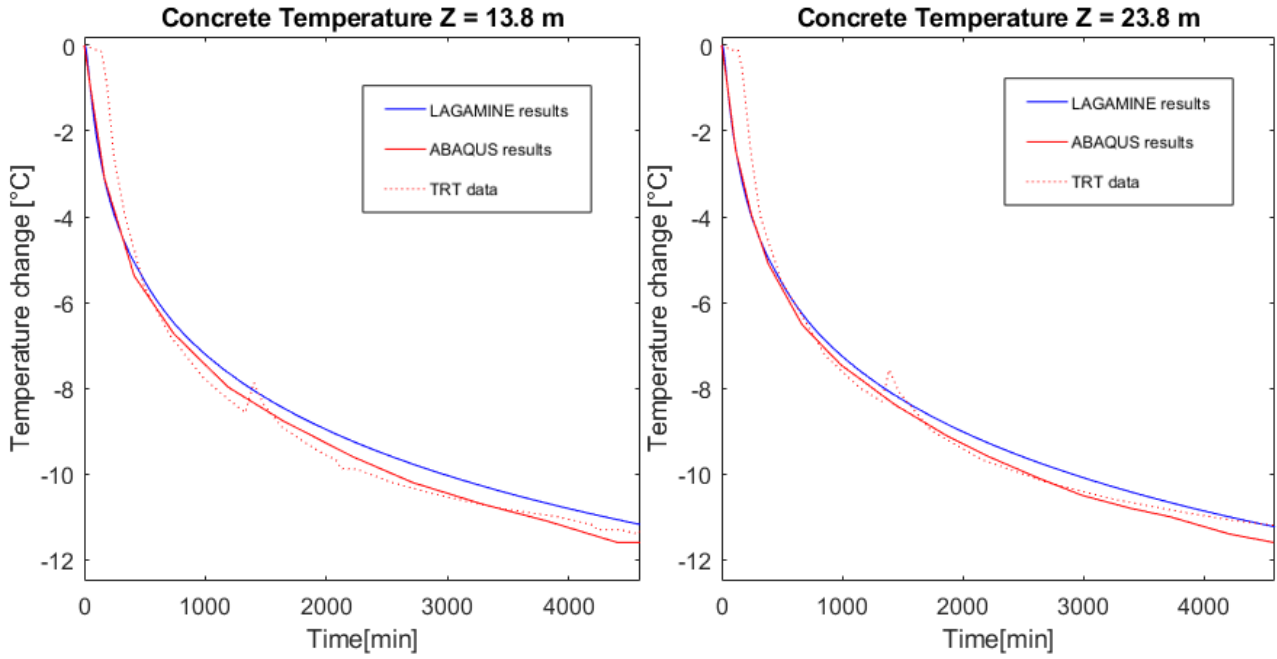


**Figure 29:** Comparison between the concrete temperature resulting from the numerical simulations and the TRT data. Data taken from the TRT done in London from Cecinato and Loveridge.

In conclusion, to validate the thermal behaviour of the ground, the infinite line source analytical approach has been used to calculate the temperature change in the ground,  $\Delta T_g$ , over time, at different radial distances  $r$ . An infinite line heat source of constant power  $q$  equal to 85.9 W/m, per unit depth is assumed, for each pipe. The thermal conductivity of the medium has been taken equal to 2.5 W/mK, as an average between the concrete and the ground conductivity. Equation 34 shows the line source approach.

$$\Delta T_g = \frac{q}{4\pi\lambda_g} \int_{r^2/4\alpha_g t}^{\infty} \frac{e^{-u}}{u} du \quad (34)$$

where,  $\lambda_g$  is the thermal conductivity of the medium,  $r$  is the radial distance from the pipe, and  $\alpha_g$  is the thermal diffusivity of the ground, assumed equal to 6.26E-7 m<sup>2</sup>/s. The simulation time has been imposed to 7 days.

Figure 30 shows the comparison between the analytical solutions obtained from the equation 34 and the numerical results from the 3D simulations, at three different radial distances.

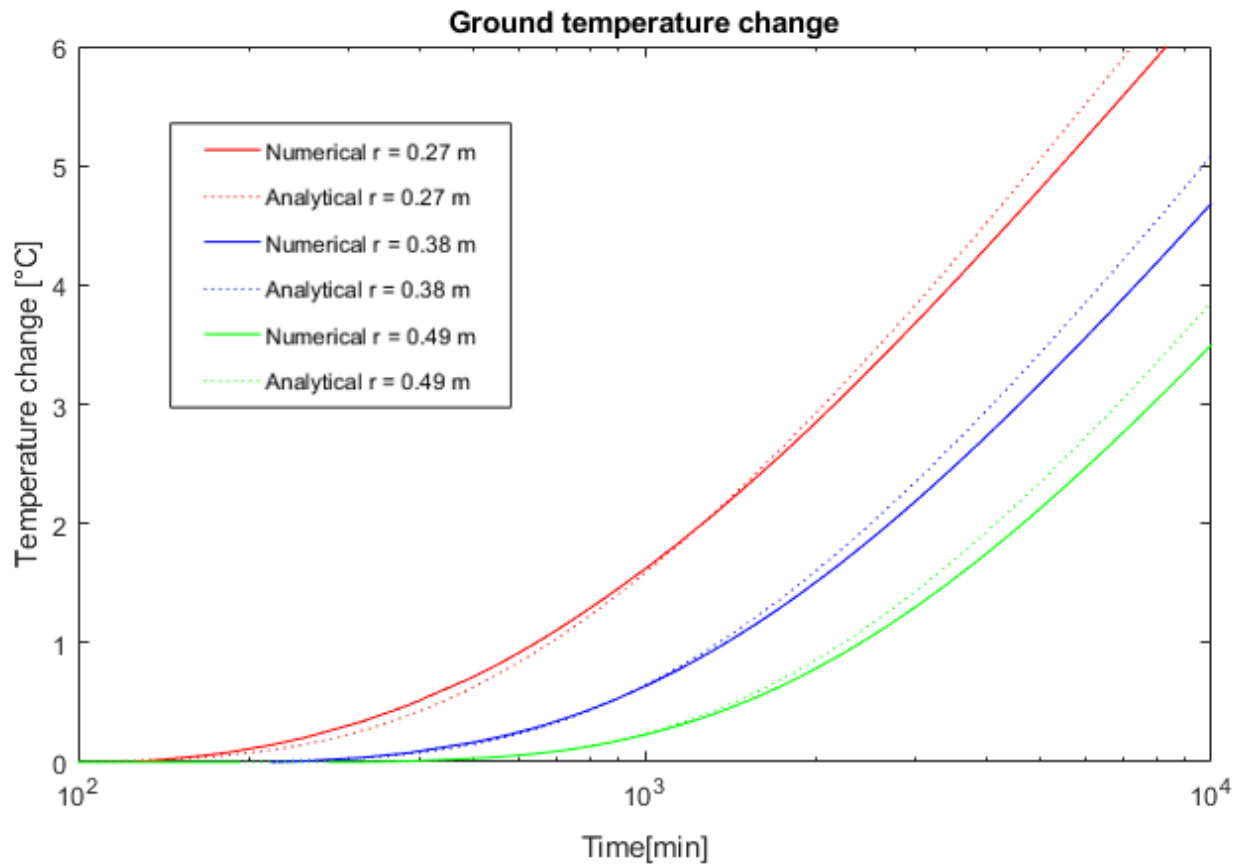


**Figure 30:** Comparison between line source analytical approach and numerical simulations. *Data taken from Cecinato F., and Loveridge F.A..*

Figure 30 shows how the analytical approach leads to have a lower ground temperature change than the numerical approach's results, during the beginning of the simulation, and then, after a certain time, there is an opposite trend, with a greater ground temperature change for the analytical approach. This is due to both the three-dimensional effect that the line source model cannot take into account, and the inability of the analytical solutions to capture the transient effects when the steady flux conditions are reached [14].

## 5 MULTIPHASE ANALYSIS

The analyses described in the chapter 4 have been done considering the ground as an equivalent single-phase medium, in saturated conditions. In order to switch to a multiphase medium, the HT coupled constitutive law of the soil has been modified. The thermo-hydraulic properties of the solid, liquid and gas phase have been calibrated on ground only models.

### 5.1 TH coupled constitutive law for multiphase analyses

A three-dimensional representative ground volume has been defined to calibrate the thermal properties of the ground solid phase, considering the WaVaT coupled constitutive law described in the chapter 4.2. The 3D mesh has been created in order to simulate the region of the soil affected from the thermal processes of an energy pile. Figure 31 shows the three-dimensional mesh used for the analyses.

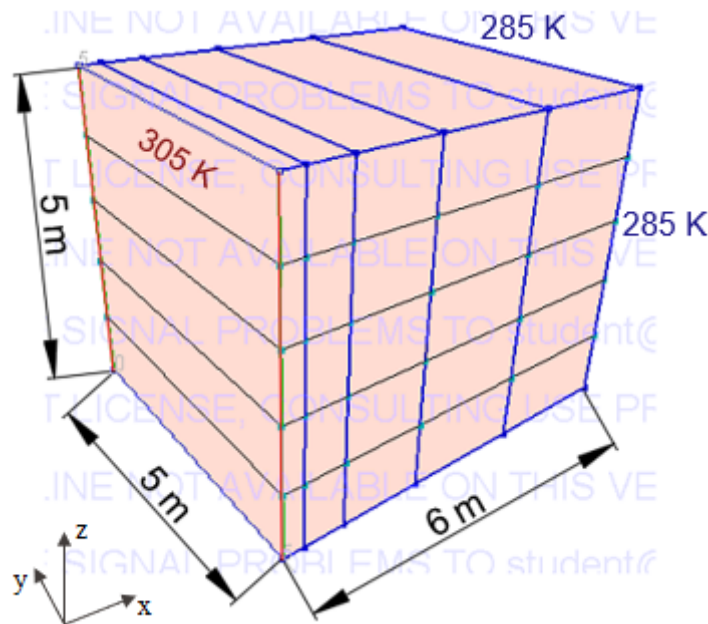


**Figure 31:** Representative ground volume to calibrate the solid phase thermal properties. 3D mesh realized using the software ZSoil.

From figure 31, it can be seen that a fixed temperature difference of 20°C between the two columns of nodes in red and the ground has been imposed, in order to have the same response of the ground in presence of an energy pile. The time for the analysis has been set to 120 days and the temperature output has been recorded at different time steps, until the analysis has reached the steady conditions.

The first analyses have been made considering a saturated sand with the properties of an equivalent single-phase medium, indicated in table 3. Then, starting from the results of the equivalent single-phase analysis, the parameters of the multiphase constitutive law have been varied, until the convergence between the temperature field in output for both the analyses is reached. The water thermal conductivity  $\lambda_w$  has been set to 0.6 W/mK, the soil porosity  $n$  has been set to 0.3, the soil tortuosity to 0.8 and the soil density to 2000 kg/m<sup>3</sup>. Averaging the resulting temperature of the nodes at the same distance from the source, the temperature field in the ground has been plotted for both the analysis at different time steps. Figure 32 shows the results for both the analyses.

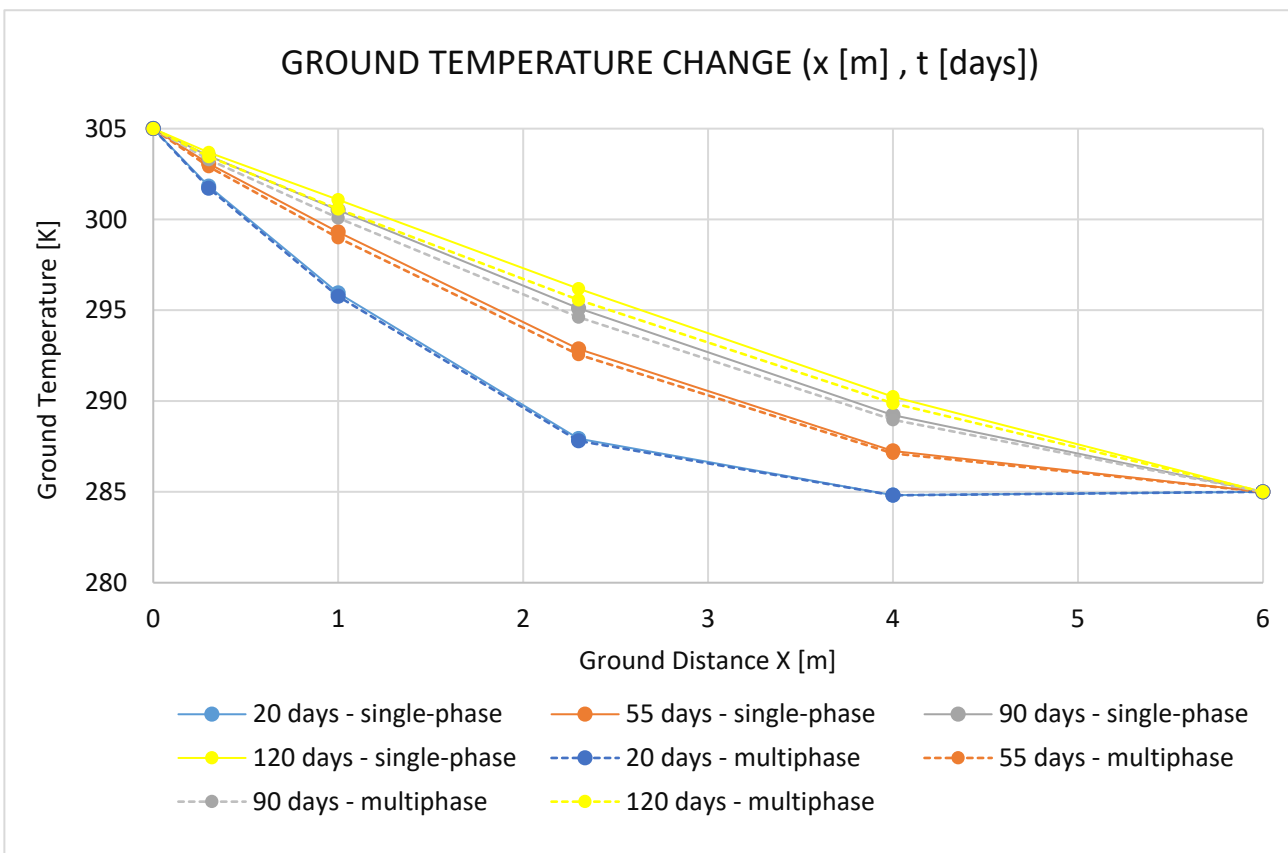


**Figure 32:** Comparison between the output temperature field for the equivalent single-phase and the multiphase models.

By converging the two analyses it has been possible to evaluate the thermal properties of the solid phase of the medium. In particular, the thermal conductivity  $\lambda_s$  of the saturated sand has been set to 2.5 W/mK and the specific heat capacity to 1200 J/KgK. Furthermore, to validate the process, it has been verified that the solid phase thermal conductivity  $\lambda_s$ , substituted in the equation 35 of the ground thermal conductivity  $\lambda_g$ , gives the same value of the equivalent single-phase conductivity.

Considering the case of a saturated sand, with a degree of water saturation  $S_w$  equal to 1 and degree of air saturation  $S_a$  to 0 and soil porosity and the materials thermal conductivities previously mentioned, the ground thermal conductivity is defined as follows.

$$\lambda_g = nS_w\lambda_w + nS_a\lambda_a + (1 - n)\lambda_s = n\lambda_w + (1 - n)\lambda_s \quad (35)$$

As expected, from equation 35 the same value of the equivalent soil thermal conductivity  $\lambda_{eq}$  has been obtained.

Once characterized the thermal properties of the solid, liquid and gas phase of the ground constitutive law, a second ground volume has been defined to investigate the presence of a groundwater flow and his influence on the temperature field of the ground. To calibrate the hydraulic properties as the soil permeability, different analyses by varying the fluid velocity inside the ground have been made. Figure 33 shows the three-dimensional FE mesh to analyse the groundwater flow.

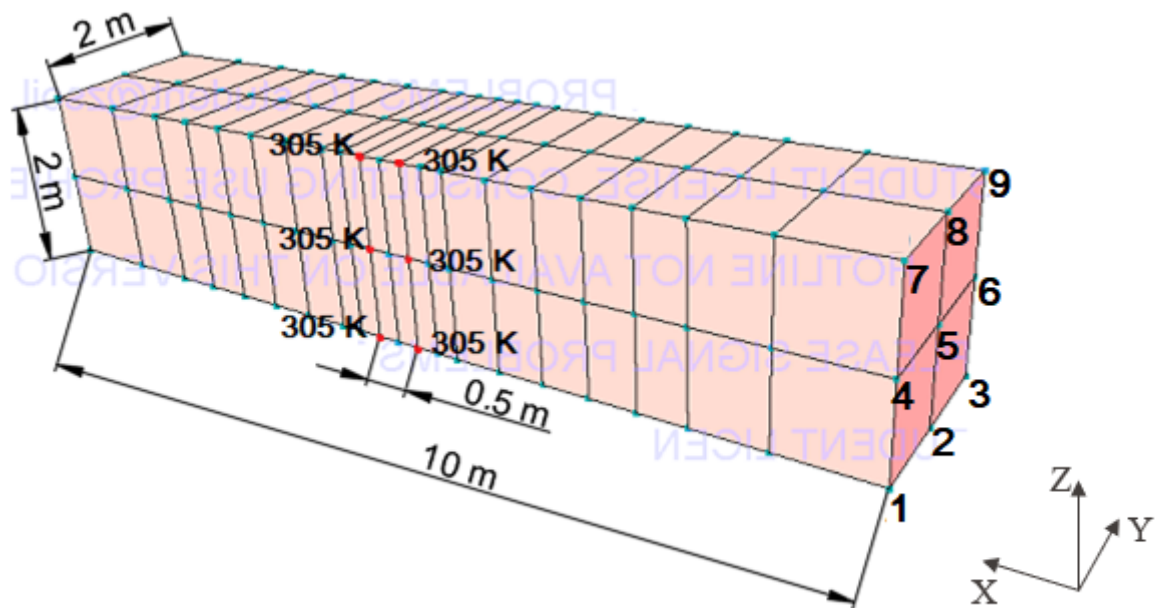


**Figure 33:** Representative ground volume to analyse the groundwater flow.

For the solid phase, the parameters obtained from the previous model have been adopted. The soil porosity  $n$  has been set to 0.3, the soil thermal conductivity  $\lambda_s$  to 2.5, and the initial value of intrinsic permeability  $k$  to  $5.0E-14$  m<sup>2</sup> which leads to have a soil permeability of  $5.0E-7$  m/s (eq. 12). To simulate the operations of the energy piles, a temperature difference of 20°C between the two central columns of nodes and all the other nodes has been set.

In order to create a groundwater flow in the medium, a difference of hydraulic head has been imposed between the two end faces of the model. To do this and to have the soil always saturated, starting from the hydrostatic conditions, the water pressure of the nodes 1 to 9 has been increased of 20 KPa (figure 33). Figure 34 schematically shows the process [16].

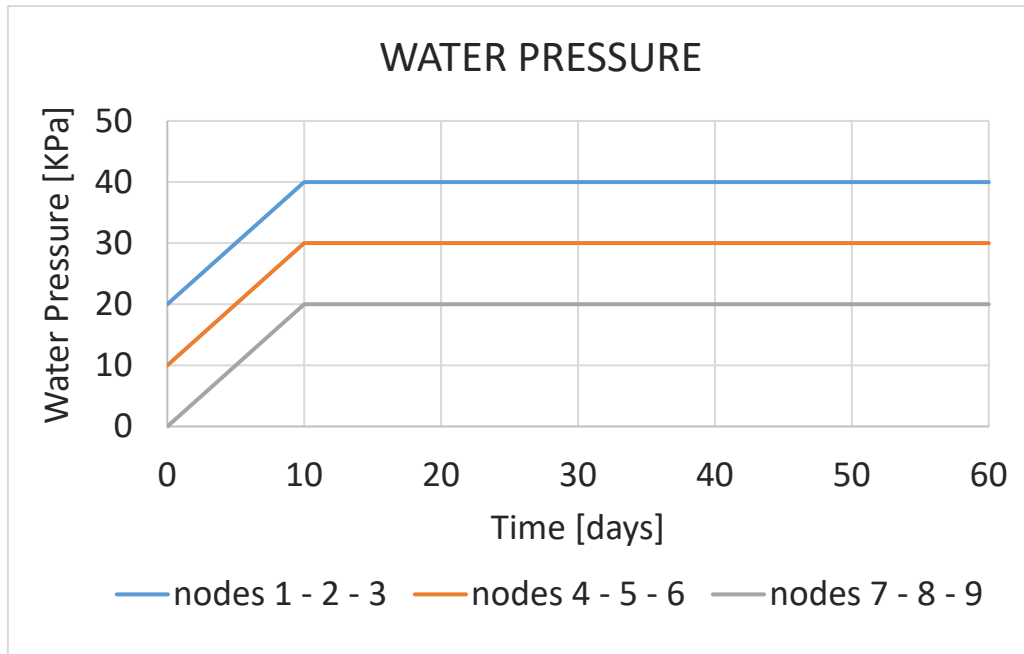


Figure 34: Increasing of water pressure on one end-face of the model.

The simulation time has been set to 60 days (1440 hours) and the results in terms of water pressure distribution have been obtained both with hydrostatic conditions and with a flow applied and they are shown in figure 35.

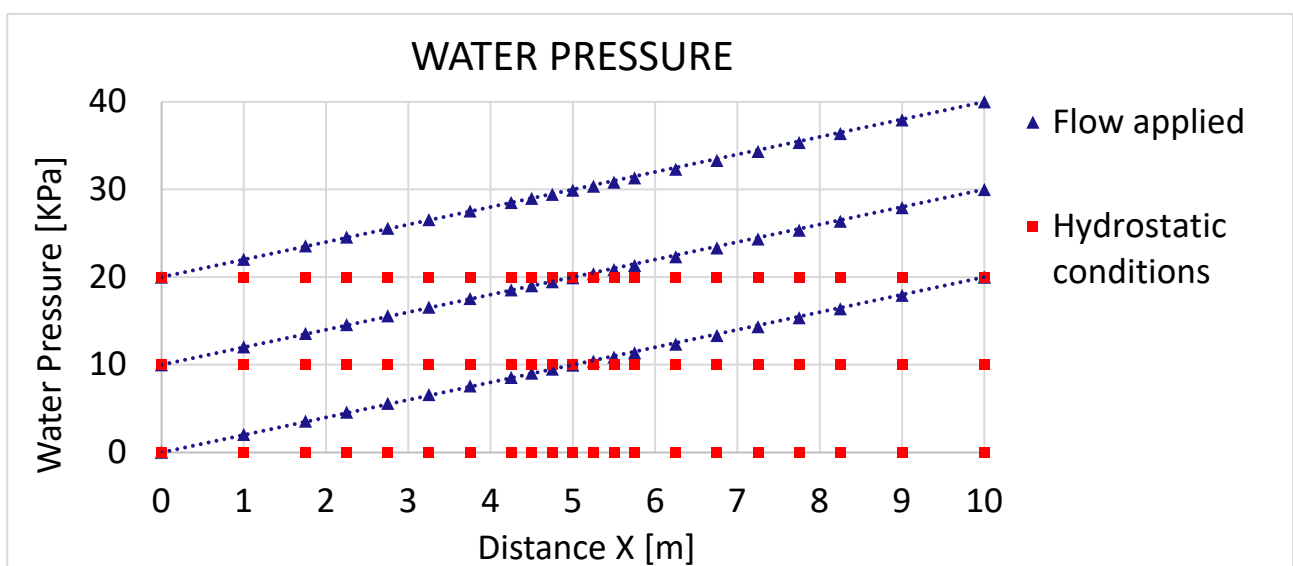


Figure 35: Water pressure distribution in hydrostatic conditions and with a flow applied. XZ view of figure 33.

From figure 35, it can be seen that the equilibrium velocity of the groundwater flow is reached with a linear distribution of the water pressure. This is due to the fact that the mechanical behaviour of the ground is not considered, and in other words the compressibility  $m_v$  of the medium tends to 0. From the theory of the consolidation, we have:

$$\delta\varepsilon_{zz} = m_v \delta\sigma'_{zz} \quad m_v \rightarrow 0 \quad (36)$$

$$C_v = \frac{\lambda}{m_v g \rho_w} \rightarrow \infty \quad t_{100} = \frac{T_v H^2}{C_v} \rightarrow 0 \quad (37)$$

where  $T_v$  is the adimensional time factor and  $H$  is the medium height. Equation 36 shows that the deformation of the ground  $\delta\varepsilon_{zz}$  tends to 0, while equation 37 shows that consolidation's coefficient  $C_v$  leads to have a time to get the total consolidation,  $t_{100}$ , equal to 0.

Once the applied flow has reached the equilibrium velocity, the temperature field inside the ground volume has been plotted at different time step. Figure 36 shows the results for two different soil permeabilities.

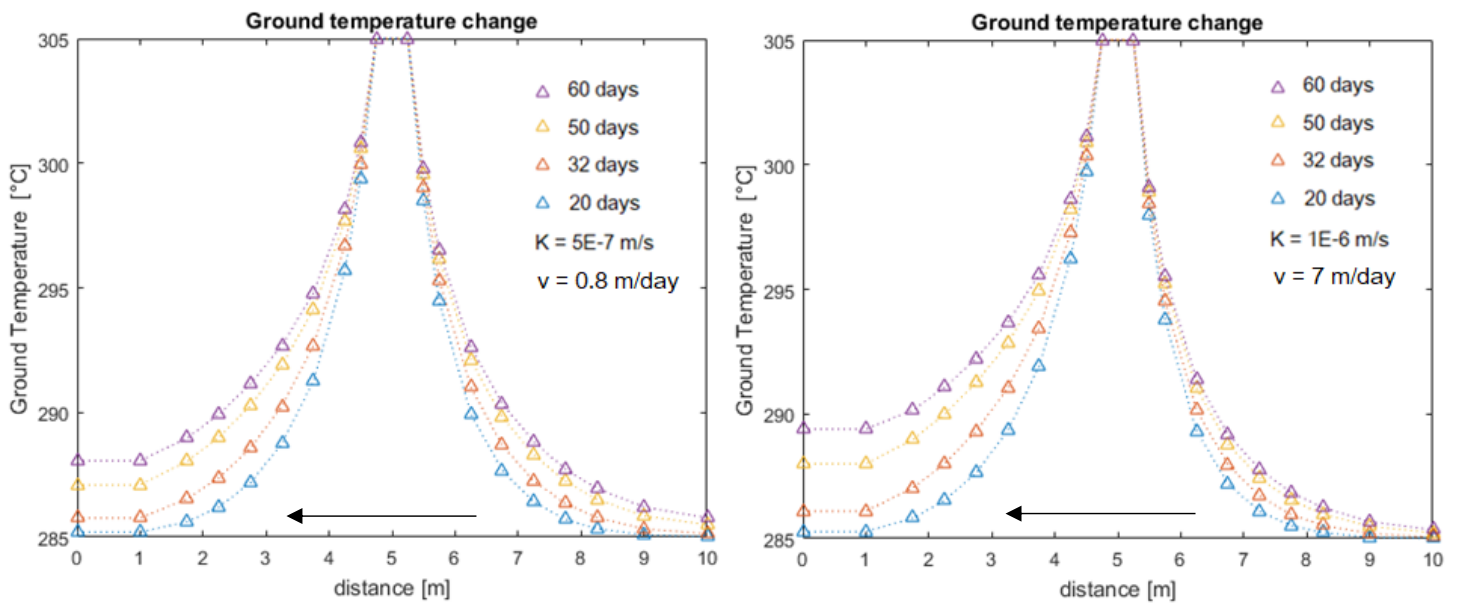


**Figure 36:** Ground temperature change over time, with a groundwater flow applied at different fluid velocity.

The two main effects that can be seen in figure 36 are: the increase of ground temperature in the area adjacent to the source, and mainly the translation of the temperature range in the flow direction. The latter effect is higher the greater the soil permeability. In conclusion, to have a significant groundwater flow and an order of magnitude of the soil permeability typical of a coarse ground, the value of  $K = 1E-6$  m/s has been assumed for the next analyses.

## 5.2 Application of the multiphase model to the single energy pile

After calibrating the parameters of the hydrothermal coupled constitutive law for soil, the multiphase model has been applied to the single energy pile. Analysing the model with both hydrostatic conditions and applied groundwater flow, it has been possible to evaluate the effects of the flow on the temperature field coming from the thermal processes of the pile. Then, computing the pile thermal resistance for different pile diameters, the difference between the groundwater flow applied and the hydrostatic conditions has been quantified.

To apply the groundwater flow in the X direction perpendicular to the pile, the FE mesh has been defined with brick elements in order to create a box of soil. The mesh has been thickened in the direction of the pile. Figure 37 (A)(B) shows the 3D mesh and a zoom on the pile.

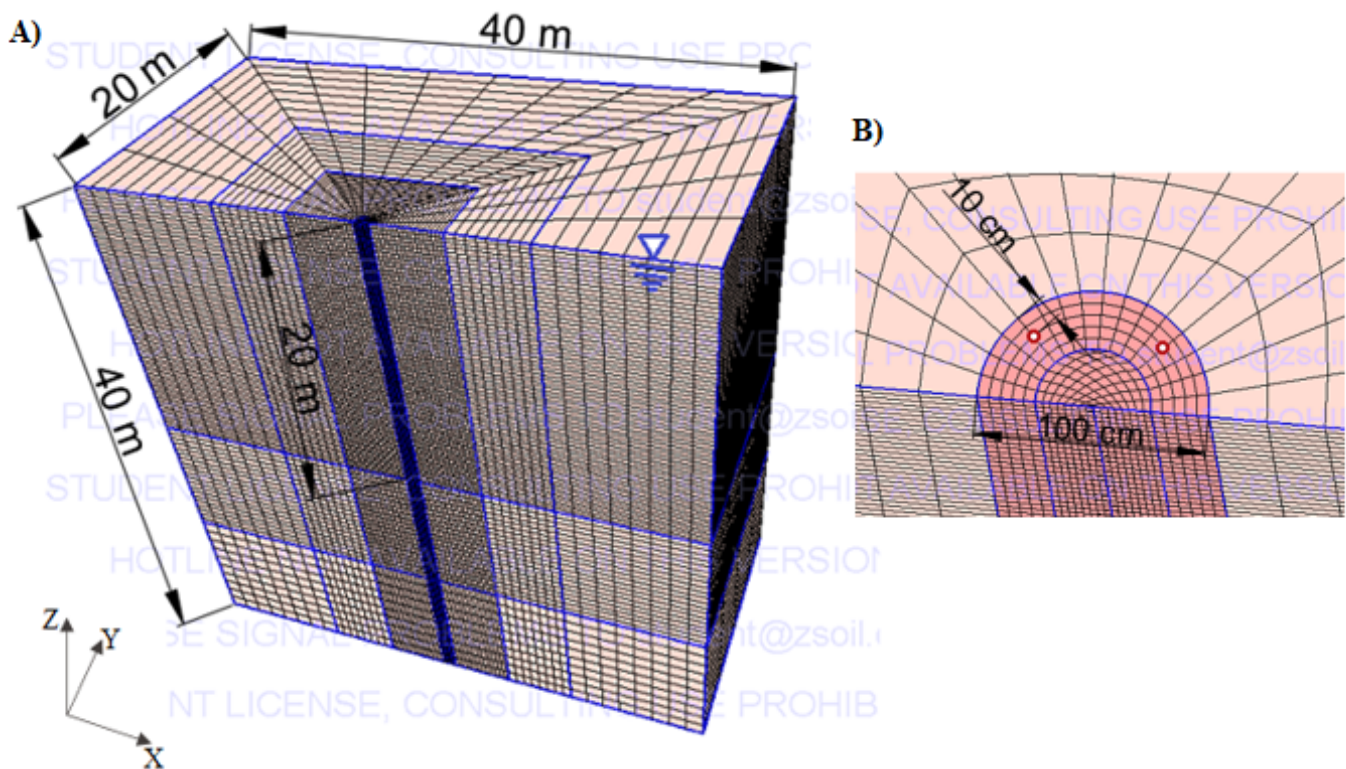


**Figure 37:** A) 3D Finite element mesh of single energy pile. B) Zoom on the energy pile. Mesh created with the software Zsoil.

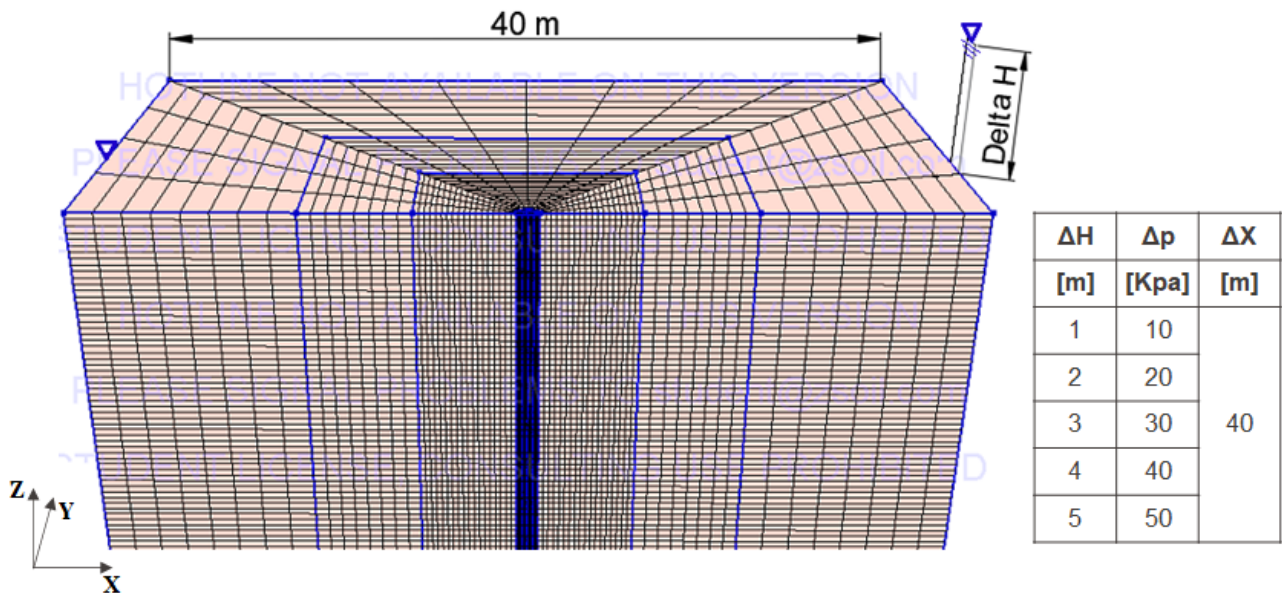
As a starting point, the hydrostatic conditions with a groundwater table at the ground level are considered. A pile length of 20 m, a pile diameter of 1 m and a concrete cover of 10 cm have been adopted. The pile is equipped with a double U-pipes in parallel and the geometrical and hydro-thermal properties of the heat carrier fluid are summarised in table 4.

Table 10 shows the WaVaT coupled law's parameters obtained from the ground only models in chapter 5.1, adopted for these analyses, and the grouting material's parameters.

**Table 10:** WaVaT coupled constitutive law's parameters for ground and pile, multiphase analyses.

| WaVaT Coupled Constitutive Law |                |        |                   |           |           |
|--------------------------------|----------------|--------|-------------------|-----------|-----------|
| Soil                           | k              | K      | Porosity          | $\lambda$ | T initial |
|                                | m <sup>2</sup> | m/s    | [-]               | W/mK      | K         |
|                                | 1.0E-13        | 1.0E-6 | 0.3               | 2.5       | 285       |
| Pile                           | $\lambda$      |        | $\rho C_p$        |           | T initial |
|                                | W/mK           |        | J/Km <sup>3</sup> |           | K         |
|                                | 1.8            |        | 1.9E+6            |           | 285       |

The groundwater flow has been applied considering five cases, with an imposed difference of hydraulic head,  $\Delta H$ , between the two end faces of the 3D model (fig. 38). So, an increase of water pressure has been imposed on the right end face of the model, from the initial time step. The flow velocity range is from about 0.1 m/day with an increase of water pressure set to 10 KPa, to 1 m/day with 50 KPa applied on the right-end face.



**Figure 38:** Imposed difference of hydraulic head between the two end faces of the 3D model

The analysis time has been set to 15 days (360 hours) and the equilibrium velocity of the flow is reached in the early hours of the simulation. As boundary conditions, a constant heat power  $Q$  has been imposed at the inlet cross section of the pipes. As initial condition, a constant temperature has been set to all the materials.

The results in terms of temperature field of the heat circulating fluid, the pile and the soil around the pile, have been obtained, over time. Then considering the last time step, the isothermal curves for a representative 2D cross section at the mid-length of the pile have been plotted. Figure 39 shows the results for a groundwater flow of 0.7 m/day.

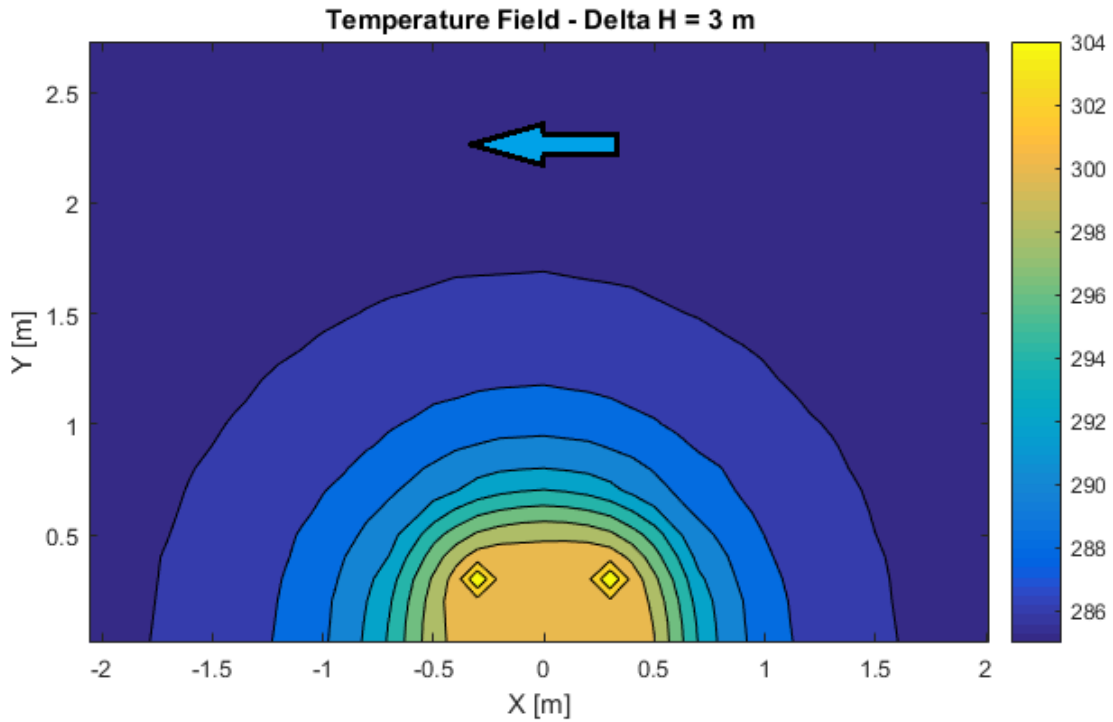


**Figure 39:** Isothermal curves for a 2D cross section at 10m depth, with a fluid velocity of 0.7 m/day

A first clear effect of the flow is the translation of the temperature field of the pile and the surrounding ground, in the flow direction.

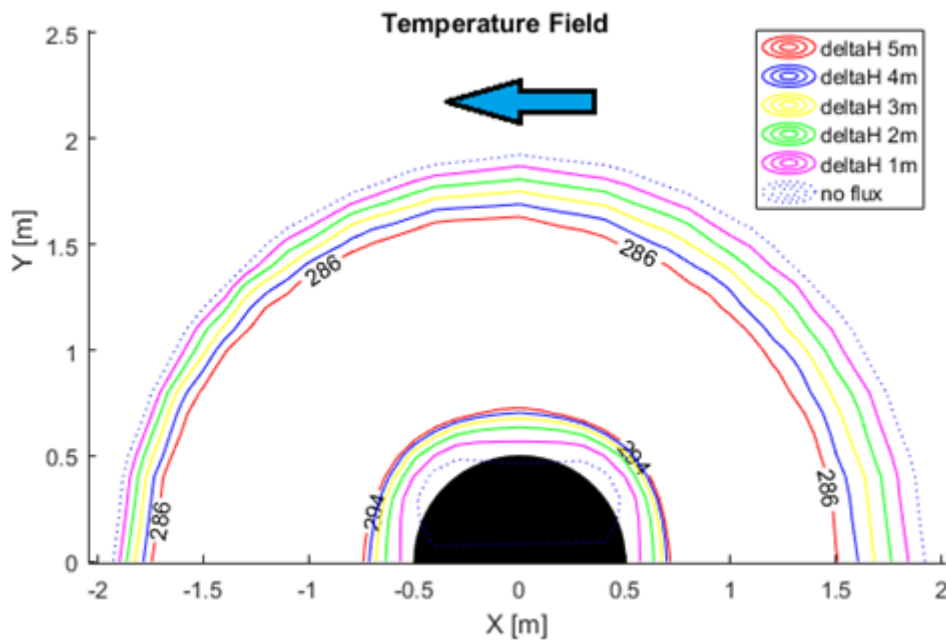


**Figure 40:** Parametric analysis by varying the fluid velocity with different  $\Delta H$  applied.

Then, a parametric analysis by varying the  $\Delta H$  with a fixed permeability has been done, and the results are shown in figure 40. The latter shows that the translation of the temperature field in the flow direction is higher the greater the  $\Delta H$  applied. Moreover, it can be seen that there are other two significant effect. The first is the screen effect of the pile in the flow direction, and this can be observed considering the distance between the isothermal curves. In other words, the fluid velocity decreases in the soil area shielded by the pile. The second, and most important effect of the groundwater flow on the thermal process of the pile, is the increase of the heat exchange capacity of the energy pile. In fact, figure 40 illustrates that the temperature field until a certain distance from the pile tends to increase, while after this distance it tends to decrease. This inversion effect can be better understood by making the difference between the temperature field coming from the analysis with flux of 0.7 m/day and the one without the flux. Figure 41(A)(B)(C) shows the results.

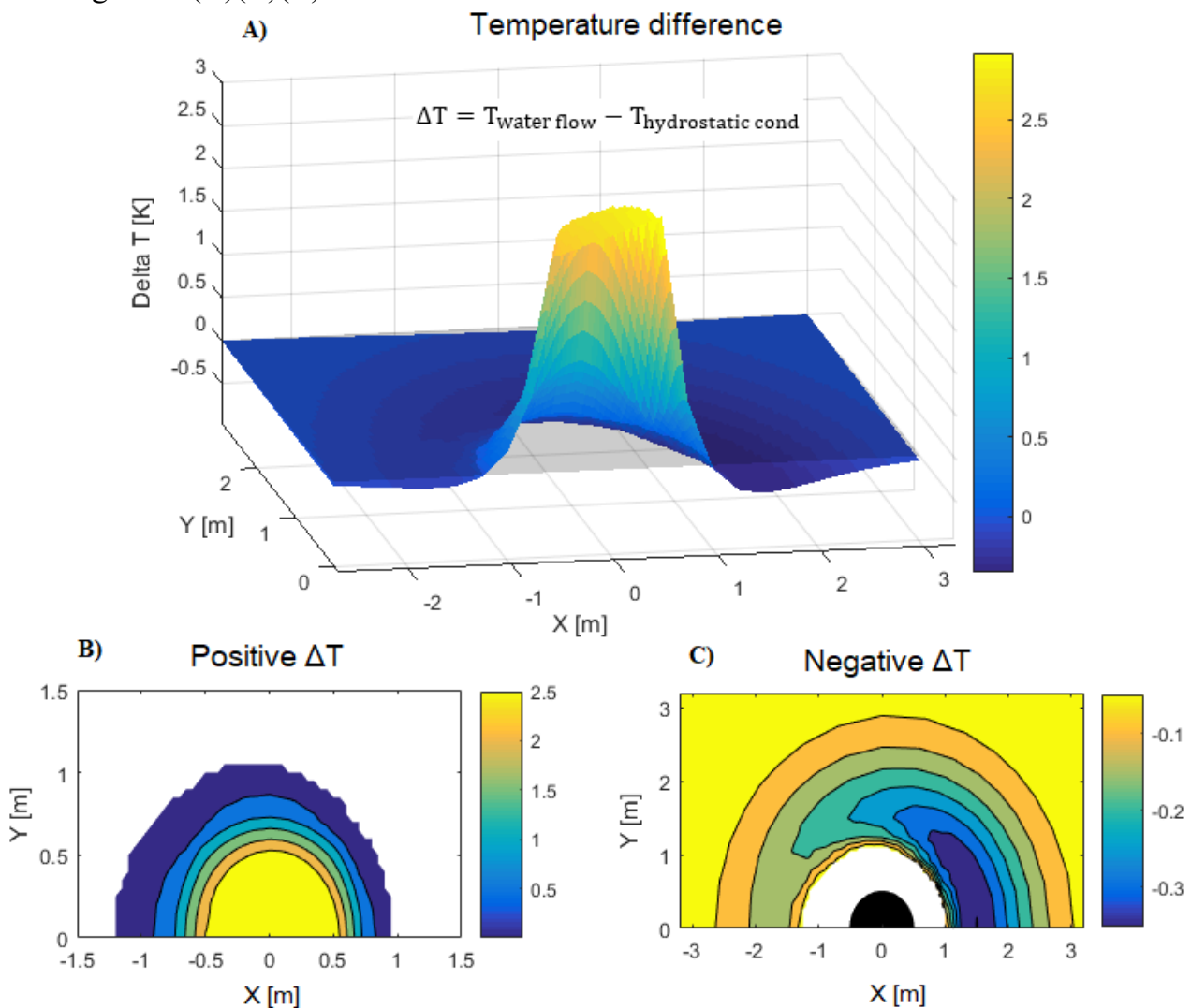


**Figure 41:** A) Temperature difference between the temperature field of the analysis with flow applied and without flow. B) Pile and soil area in which the  $\Delta T$  is positive. C) Soil region in which the  $\Delta T$  is negative.

Figure 41 (A) shows that the temperature of the heat circulating fluid has increased with the flow applied. Since we are considering the heat injection phase, it means that the heat exchange capacity of the energy pile has improved. Figure 41 (B) (C) shows that, after about 50 cm away from the pile, the temperature difference is negative, because the temperature field has decreased with the flow. This inversion effect is also a consequence of the constant heat power that is injected into the pipes, which is the same for both the analyses. In addition, figure 41 (C) shows the screen effect of the pile to the groundwater flow.

To conclude the study on the behaviour of the single energy pile, a parametric analysis to investigate the effect of the groundwater flow on different pile diameters has been done. Then a comparison between the GHE thermal resistances, obtained from the analyses with the flow applied, and the analyses in hydrostatic conditions, has been carried out. The results are summarised in figure 42.

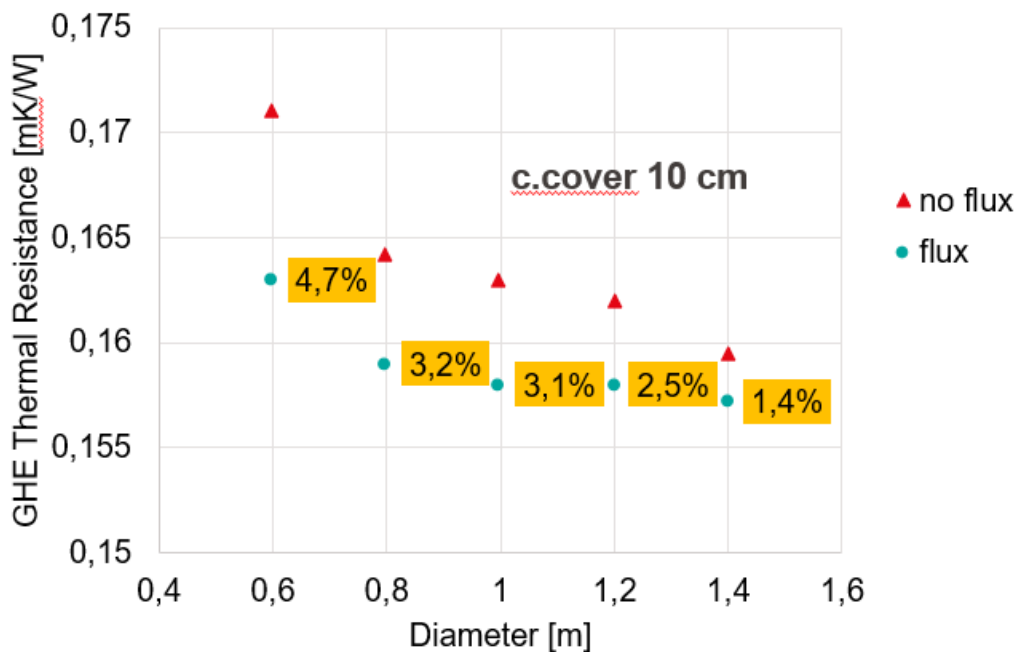
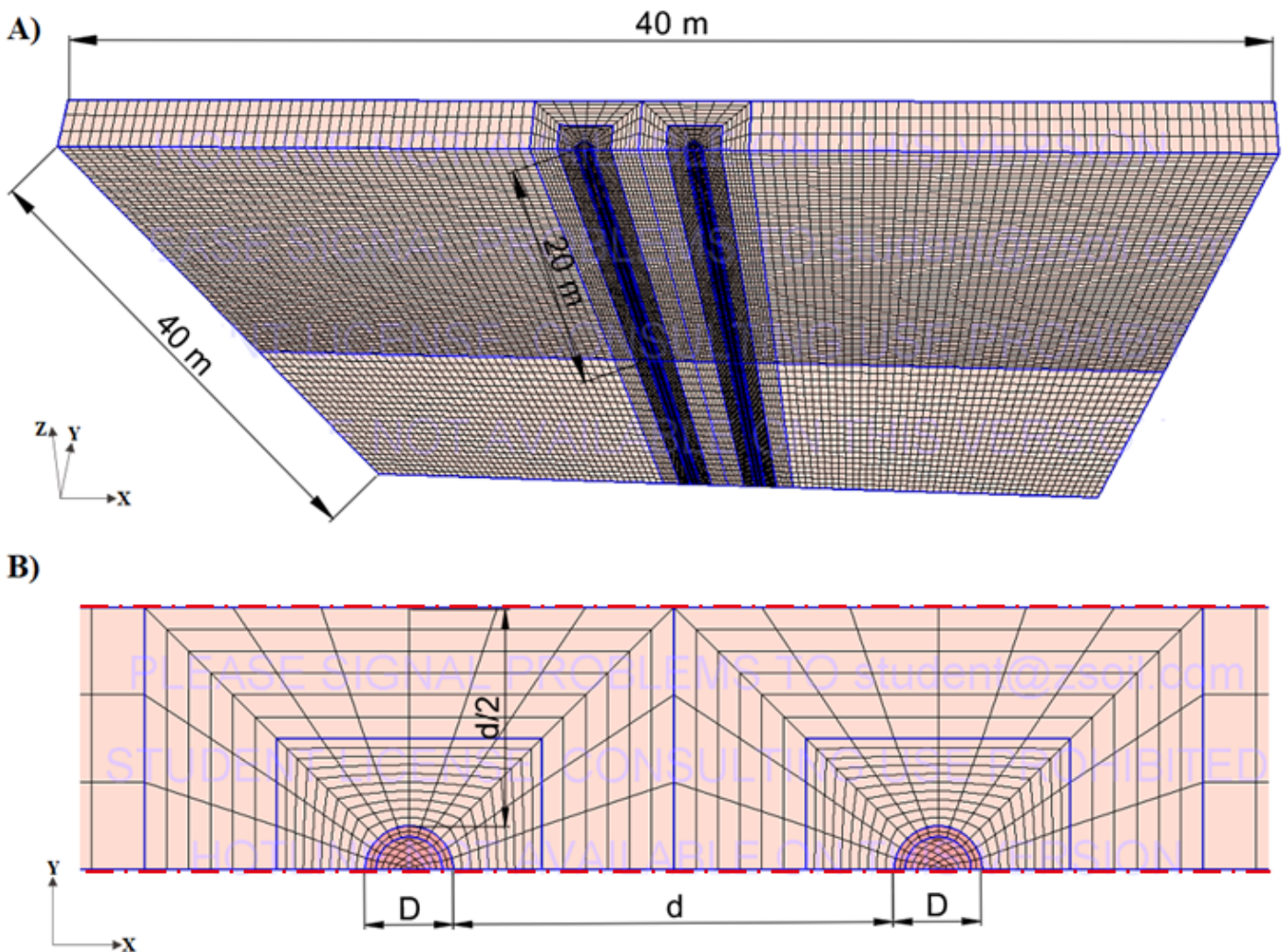


Figure 42: GHE's thermal resistance comparison between the analysis with and without the flow applied.

As expected, the pile thermal resistance tends to decrease with the diameter, and this is due to the lower interaction between the pipes. It tends to decrease for the presence of the flux, for the increase of heat exchange capacity. Moreover, the smaller the diameter, the higher the effect of the flow on the temperature around the pile and, as a consequence, on the thermal resistance, and this is due to the lower screen effect of a smaller diameter.

### 5.3 Application of the multiphase model to a 2xN energy piling

In the previous chapter, the case of a single energy pile, in the presence or absence of a groundwater flow, has been analysed. As a next step, a more real case represented by an energy pile group is proposed. In particular, exploiting the double symmetry of a piling, 3D FE models of 2xN and 3xN energy piles have been created. Then, the hydrothermal coupled phenomena of the energy piles groups have been studied, by applying the same multiphase analyses performed on the single energy pile. Table 10 shows the parameters used for the WaVat coupled law for soil and concrete.



**Figure 43:** A) Perspective view of the 3D FE model used for the 2xN energy piling. B) Top view of the 2xN energy piles. Mesh created with the software ZSoil.

Starting from the case of a 2xN piling, figure 43 shows the 3D FE model used for the analyses. Different simulations, by varying the distance between the piles  $d$  have been performed to investigate the limit values, for which there is thermal interaction between the piles (fig. 44).

In the same time, a groundwater flow has been applied and the screen effect to the flow has been evaluated. In particular, the pile diameter that leads to have a lower screen effect has been adopted. The analyses have been ran considering a 60 cm pile diameter, and 20 m pile length. The 2 U-pipes are 18.8 m long and installed symmetrically with a concrete cover of 7.5 cm (figure 44). The parameters adopted for the WaVaT coupled constitutive law for soil and concrete are summarized in table 10. As boundary condition, a constant heat power of 1000 W is imposed at the inlet cross section of the pipe and as initial condition, the temperature for all materials is fixed to 285K and. The simulation time is set to 15 days.

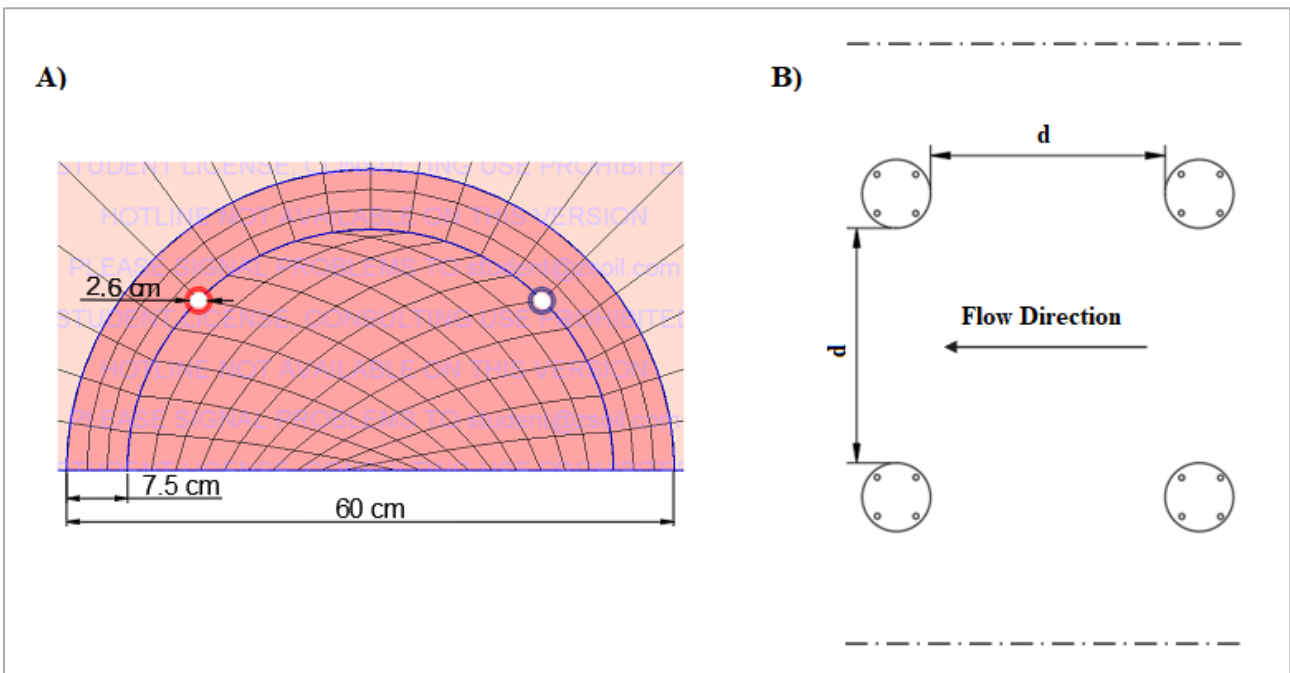


**Figure 44:** A) Geometrical parameters used for each pile. B) Schematic representation of the 2xN energy piling.

The first simulation has been done considering the hydrostatic conditions, and a groundwater table at the ground level. Then, a groundwater flow with different fluid velocity has been applied. The temperature field has been plotted for a 2D representative section of the 2xN piling at the mid-length of the piles, for both the analysed cases. For all the simulations, the pile distance has been varied to 3m, 4m and 5m. Table 11 shows the hydraulic parameters used for the simulations.

**Table 11:** Simulations' hydraulic parameters.

| Difference of Hydraulic Head $\Delta H$ | Fluid velocity $v_{ff}$ |
|---|-------------------------|
| [m]                                     | [m/day]                 |
| 0 – ground level                        | 0                       |
| 3                                       | 0.7                     |
| 5                                       | 1                       |

The results have been investigated by using a three-dimensional surface plot, in which the X-Y plane corresponds to a representative 2D section of the energy pile, and the Z variable represents the temperature field at the final time step. Moreover, a contour plot has been created, to better evaluate the isothermal curves and the effect of the flow on the temperature field. Figure 45 shows the results of the analysis without flow for a 2xN piling with a pile distance of 3 m, in hydrostatic conditions.

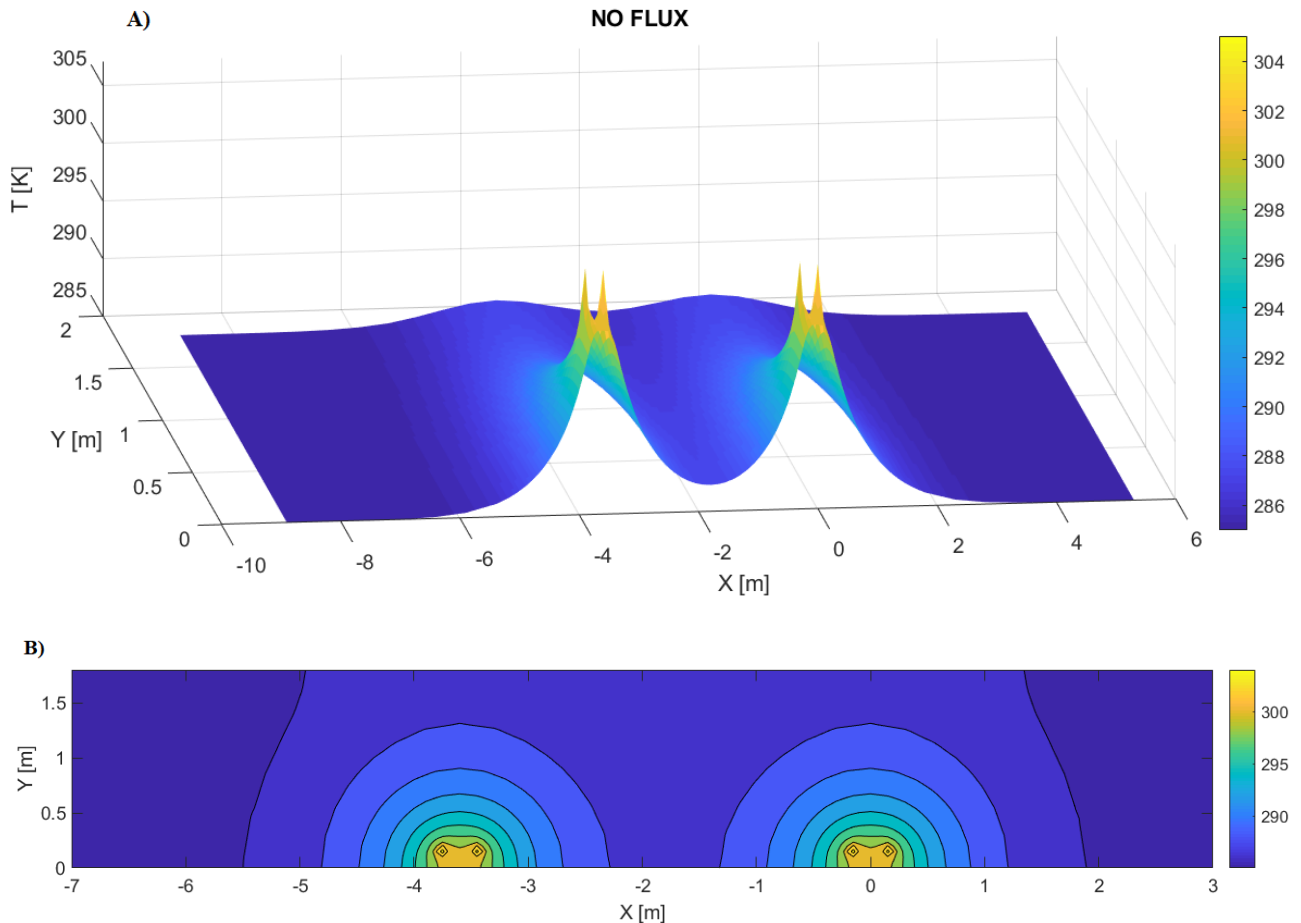


**Figure 45:** A) Surface plot of a representative 2D section without flow applied. B) Contour plot of the 2D mid-length section of the energy piles.

Figure 45 shows that, unlike the single energy pile, the soil area between the two piles is characterized by a higher temperature, and this can be seen from the isothermal curves. As expected, this effect is greater the smaller the piles distance. So, the same 2xN energy piling has been analysed with a pile distance equal to 4 m and 5 m. The effect shown in figure 45 (B) is lower for the case of 4 m piles distance and tends to disappear for the case of 5 m piles distance. Then, a groundwater flow has been added to the 2xN piling, with a difference of hydraulic head applied (table 11) between the two end faces of the model (figure 43 (A)).

The same surface plot and contour plot done for the previous analysis, have been computed for the case with a groundwater flow. Figure 46 shows the results for the case of 3 m piles distance, at the final time step.

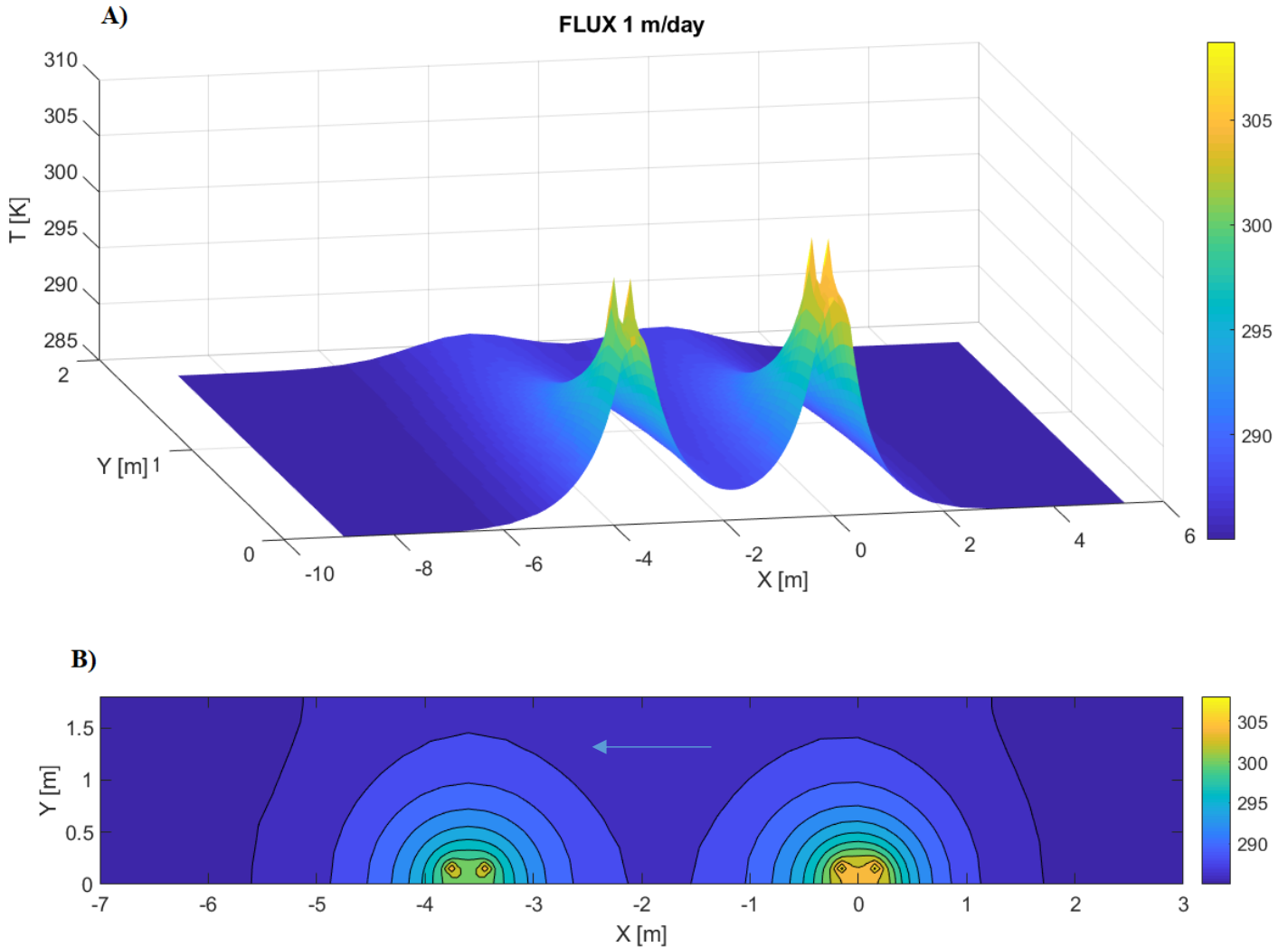


**Figure 46:** A) Surface plot of a representative 2D section with a flow of 1 m/day applied. B) Contour plot of the 2D mid-length section of the energy pile.

Figure 46 shows that, the first energy pile hit by the groundwater flow has a fluid temperature inside the pipes, greater than the case without a flow (figure 45). As we are dealing with the heat injection phase, the groundwater flow increases the heat exchange capacity, and this is related to the convective component of the flow. Figure 46 shows a second important result, related to the flow applied: the first pile behaves as a screen for the second pile, in the flow direction. It means that, for a pile distance of 3 m, the effect of a flow parallel to the piles row is most affected by the first pile. The screen effect tends to decrease for the case of 4 m and 5 m piles distance (Appendix A).

Then, a clearer view of the effects of the flow on the 2xN piling has been created. In figure 47 is represented the difference between the temperature field, coming from the two analyses with and without a groundwater flow, at the last time step, for a piles distance of 3 m.

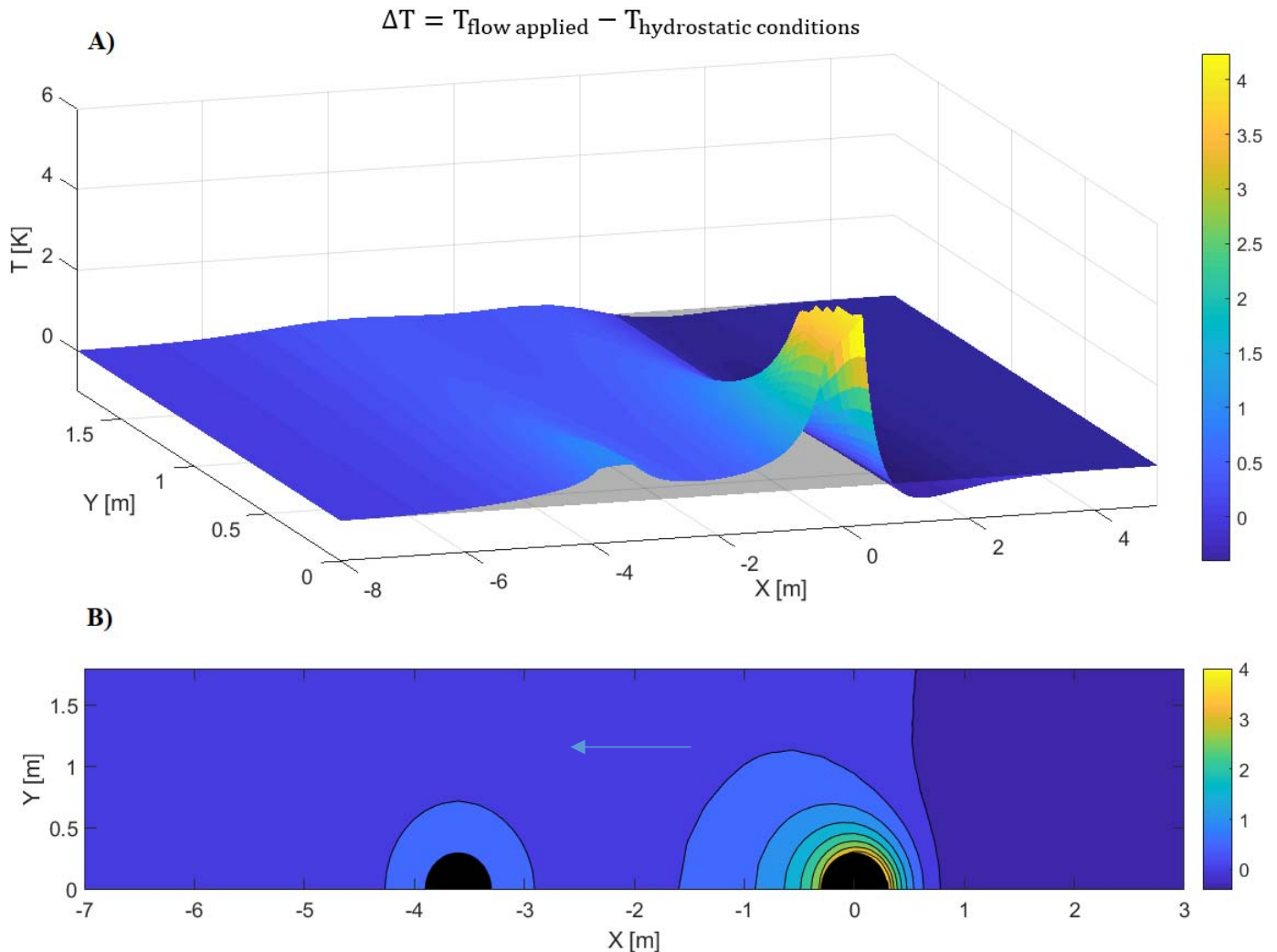


**Figure 47:** A) Surface plot of the difference between figure 45(A) and figure 46(A). B) Contour plot of the difference between figure 45(B) and figure 46(B).

Figure 47 shows that the final temperature of the heat circulating fluid, resulting from the analysis with the flow, has reached around  $4.5^{\circ}\text{C}$  more than the analysis in hydrostatic conditions. While, the shielded energy pile shows roughly the same behaviour with and without the flow applied. The plots in figure 47 have also been made for the cases of 4 m and 5 m piles distance, and the results in terms of heat carrier fluid temperature are similar to the case of 3 m piles distance (Appendix A).

## 5.4 Application of the multiphase model to a 3xN energy piling

In this chapter, the results coming from the application of the hydro-thermal analyses to a 3xN energy piling are proposed. In order to save computational time, exploiting the double symmetry of the problem, also in this case only half geometry of the piling is considered. The three-dimensional FE mesh is represented in figure 48. The piles have been discretized in the same way of the previous analyses.

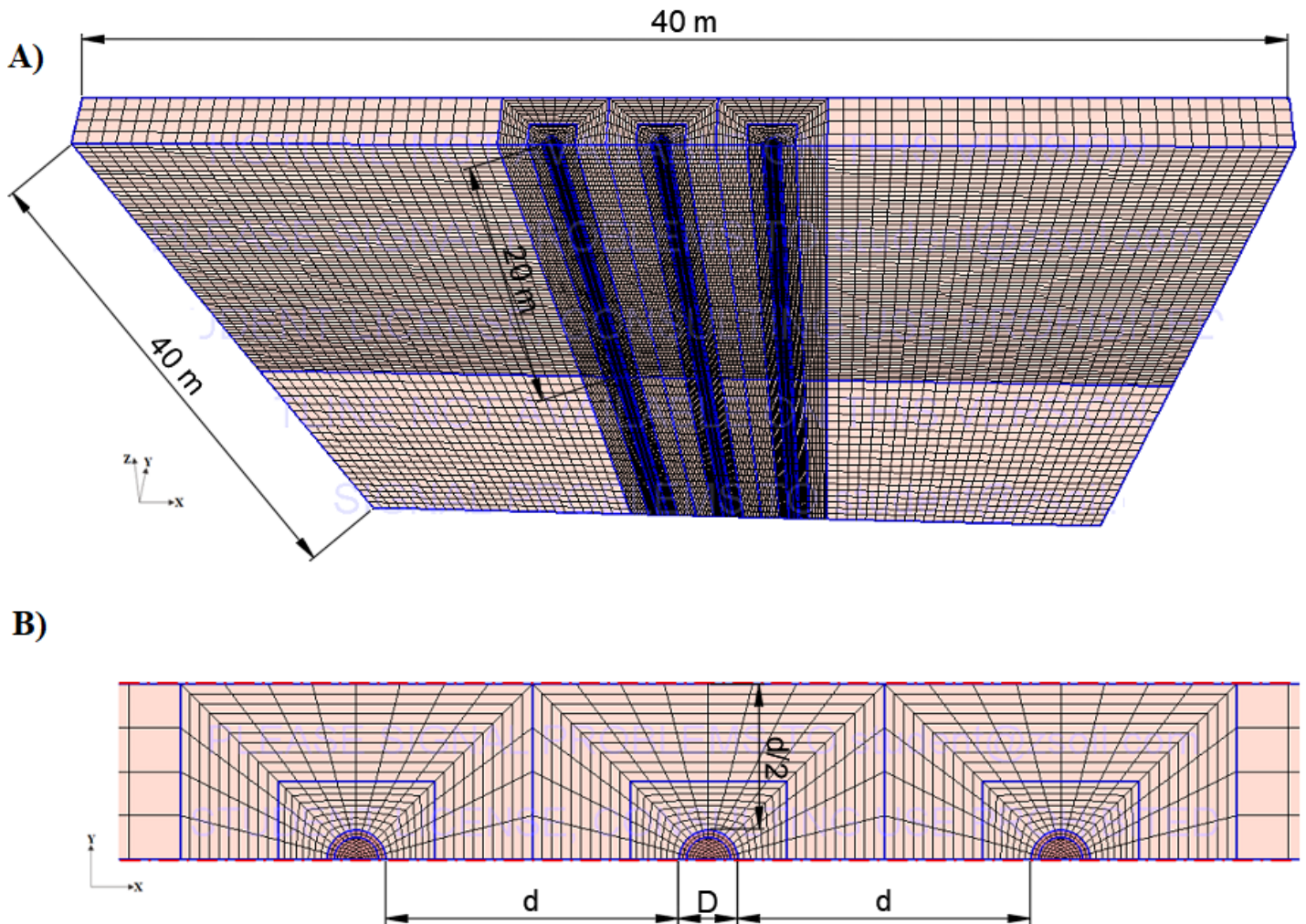


**Figure 48:** A) Perspective view of the 3D FE model used for the 3xN energy piling. B) Top view of the 3xN energy piles. Mesh created with the software ZSoil.

The parameters used for the WaVaT coupled constitutive laws for soil and concrete are summarized in table 10. Each pile is 20 m long and has a diameter of 60 cm and a concrete cover of 7.5 cm. The piles are equipped with 2U pipes in parallel and the 2D section is represented in figure 44 (A). A distance  $d$  of 3 m between the piles has been considered, to study both the thermal interaction between the piles and the screen effect to the flow.

As boundary conditions, a constant heat power of 1000 W is injected into the inlet pipe cross section, and as initial condition, the initial temperature for all materials is fixed to 285 K. The time analysis has been set to 15 days. The thermal behaviour of the energy piles has been analysed both in the presence and in the absence of a groundwater flow. A three-dimensional surface plot and a contour plot have been created to study both the cases. The first simulation has been done in hydrostatic conditions and the results are represented in figure 49.

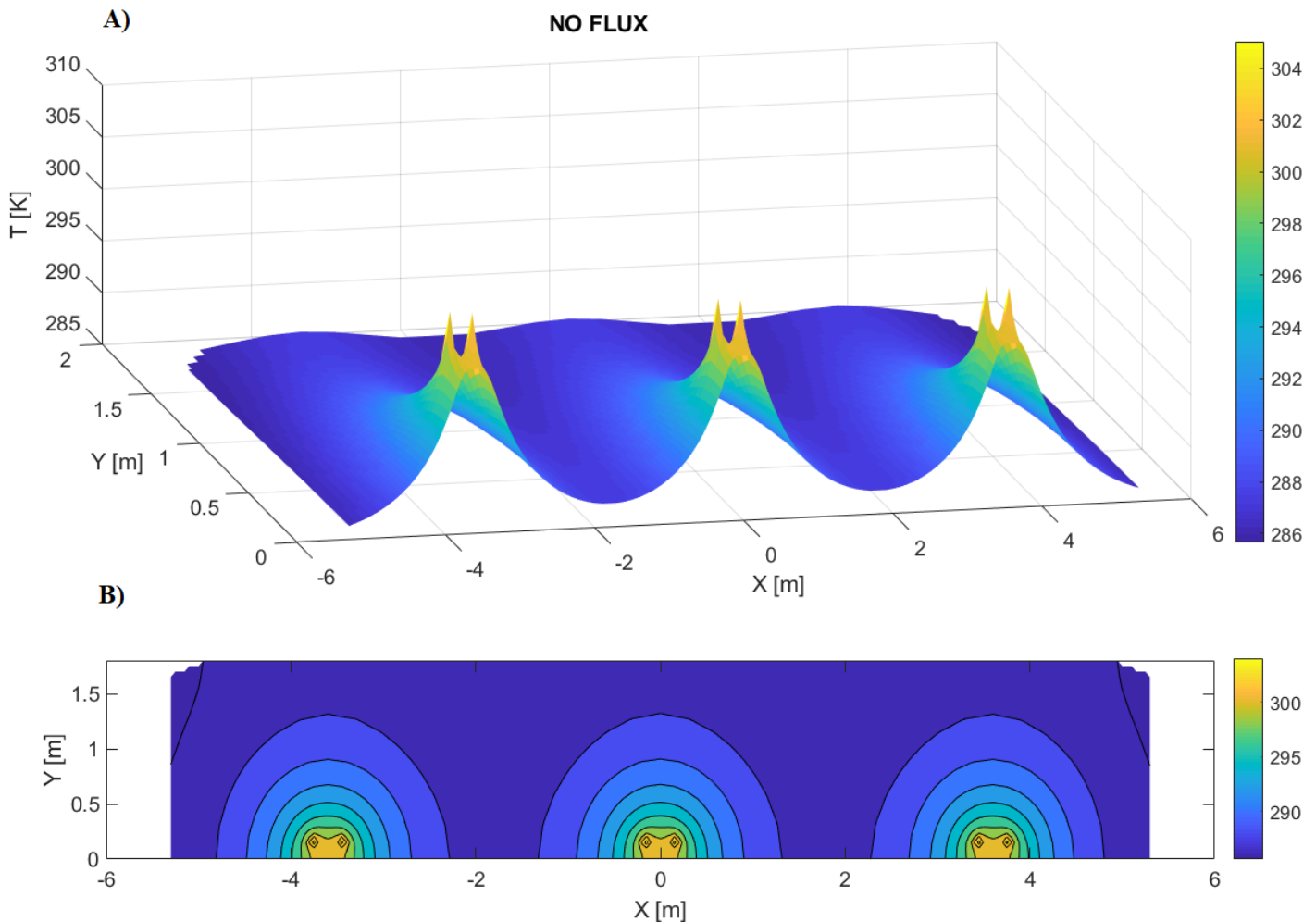


**Figure 49:** A) Surface plot of a representative 2D section in hydrostatic conditions. B) Contour plot of the 2D mid-length section of the energy piles.

Figure 49 shows the temperature field of the piles and the surrounding soil, at the final time step. The 3xN energy piling reaches a temperature of around 305K inside the pipes, and the thermal behaviour is similar to the 2xN piling. The only difference is related to the central pile, whose surrounding soil is most affected by the operations of the external piles, and this effect can be seen from figure 49 (B). Then, on the same configuration of piles has been applied a groundwater flow, imposing a pressure gradient on the right end-face of the model.

A difference of hydraulic head has been created between the two end faces (figure 48A), and a groundwater flow has been established with an equilibrium velocity of 1 m/day. So, considering the representative 2D section at the mid-length of the piles and at the final time step, the surface plot and the contour plot of the temperature field have been created, and the results are shown in figure 50.

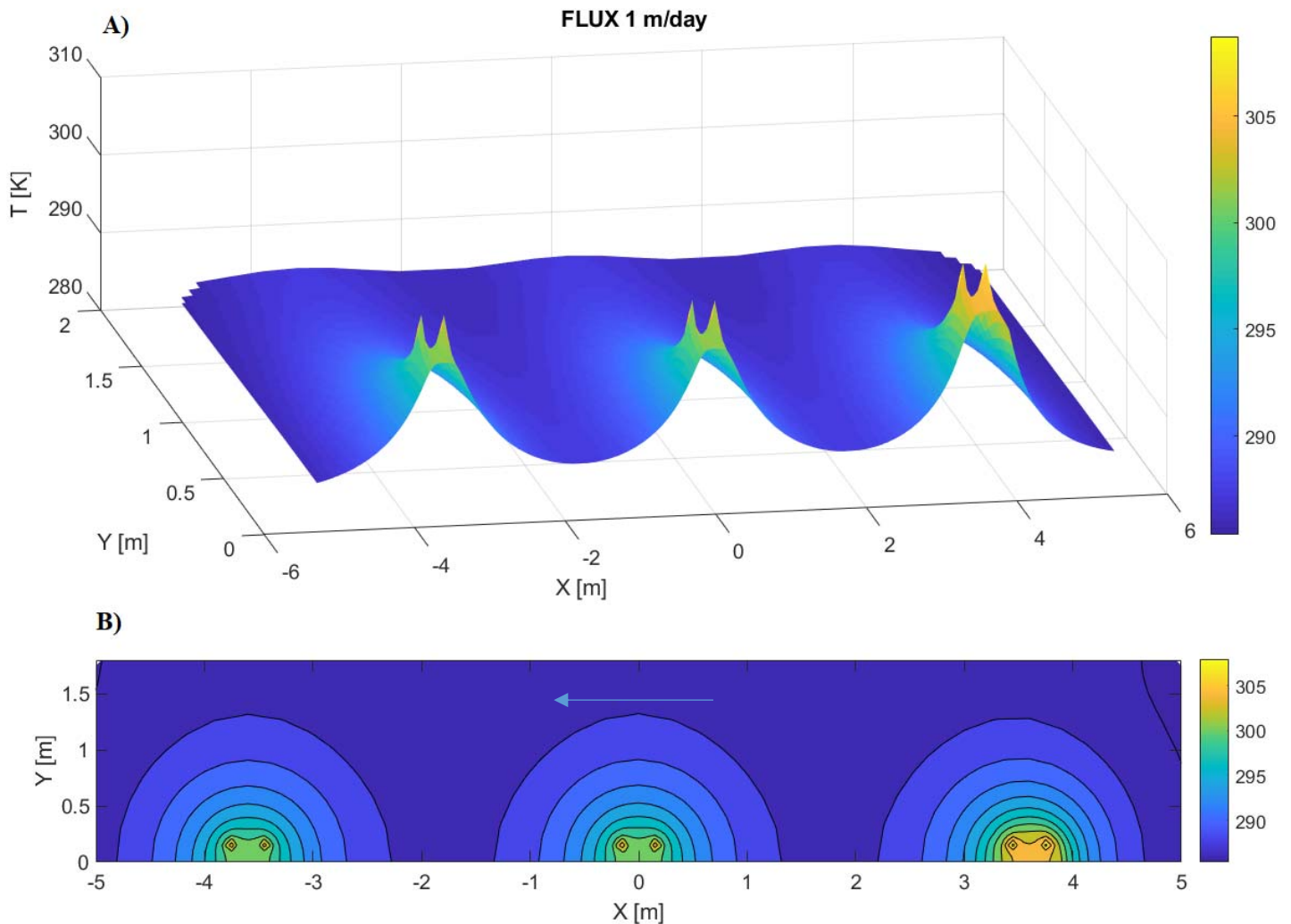


**Figure 50:** A) Surface plot of a representative 2D section with a flow of 1 m/day applied. B) Contour plot of the 2D mid-length section of the energy pile.

Figure 50 shows that, the heat circulating fluid of the first pile hit by the flow reaches a higher temperature than the other piles. It means that a groundwater flow applied parallel to the piles row affects the thermal process of the first pile, while the shielded piles behave as in absence of flow. Then, the difference between the temperature field of the simulations with and without the flow has been computed, and figure 51 shows the results. In conclusion, it can be said that, the two shielded piles show roughly the same behaviour of the 2xN piling in hydrostatic conditions.

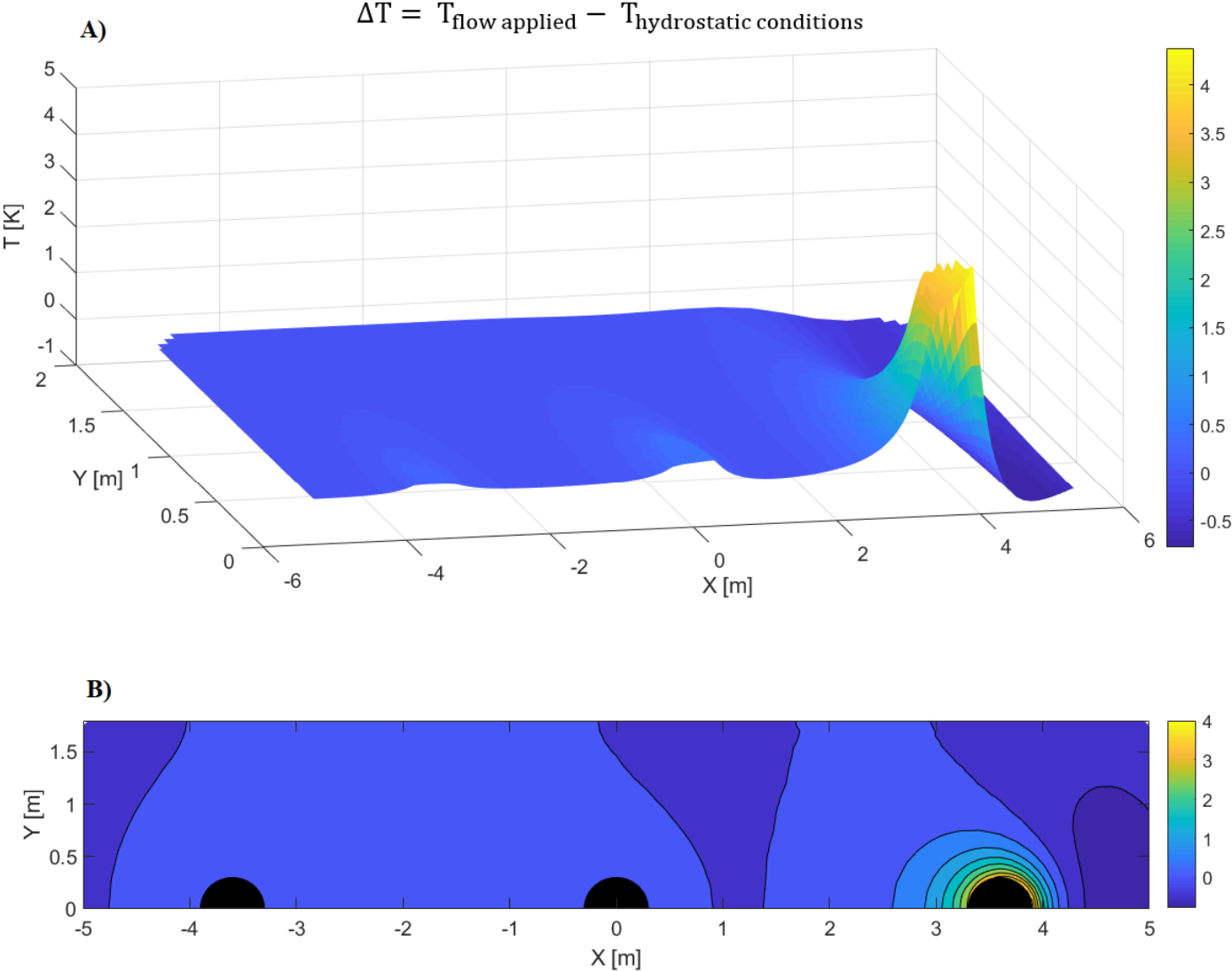


**Figure 51:** A) Surface plot of the difference between figure 49(A) and figure 50(A). B) Contour plot of the difference between figure 49(B) and figure 50(B).

## 6 THERMAL RESISTANCE RESULTS

In the previous chapter, the effects of a groundwater flow on the energy piles have been described. In particular, the temperature field of the heat circulating fluid and the surrounding ground is markedly affected by the convective component of the flow. This temperature variation has a consequence on the thermal efficiency of the pile. To quantify the latter, in this chapter, the thermal resistance of the energy piles and the ground has been calculated, with the same approach used for the single energy pile.

At first, the case of the 2xN energy piling (figures 45-46-47), with a groundwater flow of 1 m/day, has been considered. The piles distance  $d$  has been varied from 3 m to 5 m and the pile thermal resistance has been computed. Figure 52 shows the difference between the mean fluid temperature within the pipes and the mean ground temperature, with respect to the time.

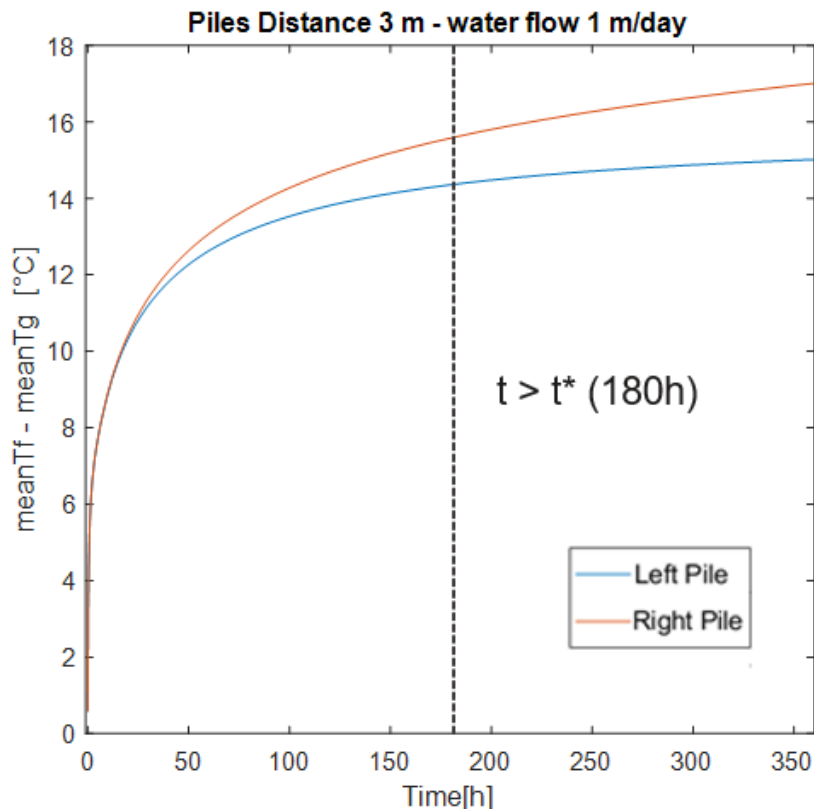


**Figure 52:** Temperature difference between the heat circulating fluid and the ground, over time, for the 2xN piling.

Figure 52 shows that, for the right pile, the temperature difference between the fluid and the ground is higher than the left pile, which is not affected by the flow. As the case of heat injection has been simulated, the right pile has a better heat exchange capacity.

Then, the energy efficiency has also been studied in terms of pile thermal resistance. In particular, figure 53 shows the values of pile thermal resistance of the 2xN energy piling, for different piles distance, with a groundwater flow of 1 m/day.

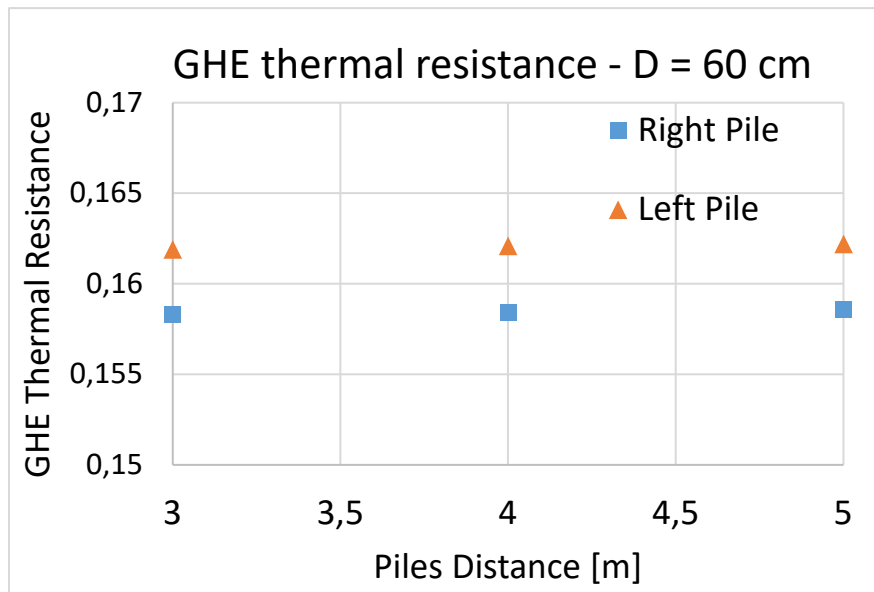


Figure 53: GHE thermal resistance of a 2xN energy piling, for different piles distance.

As expected, the thermal resistance of the pile affected by the flow is lower than that of the shielded pile. Then, the same procedure has been applied to the 3xN energy piling, and the results in terms of temperature difference and resistance are shown in figure 54 and 55.

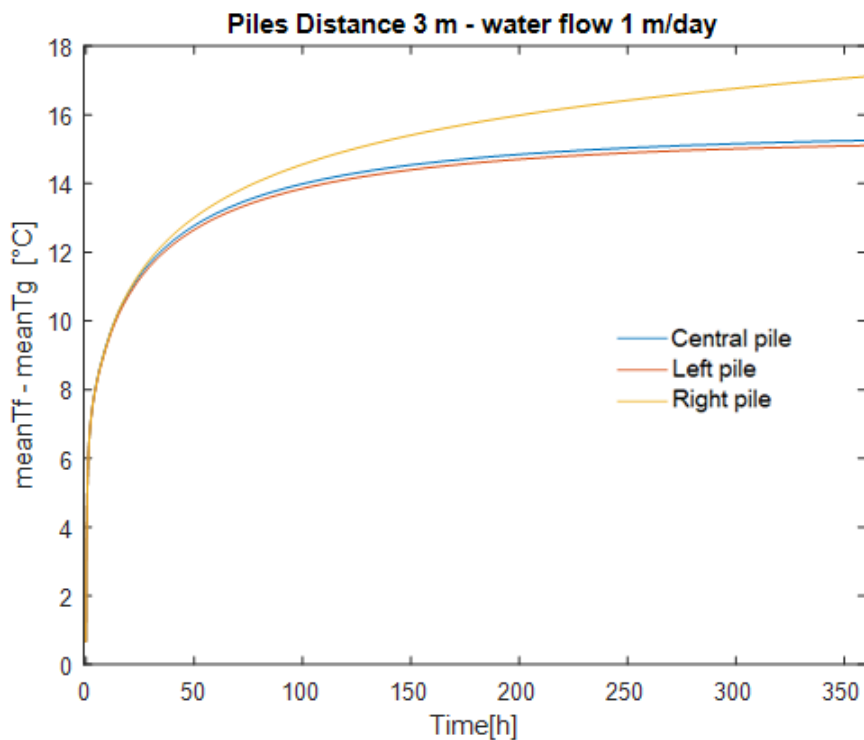
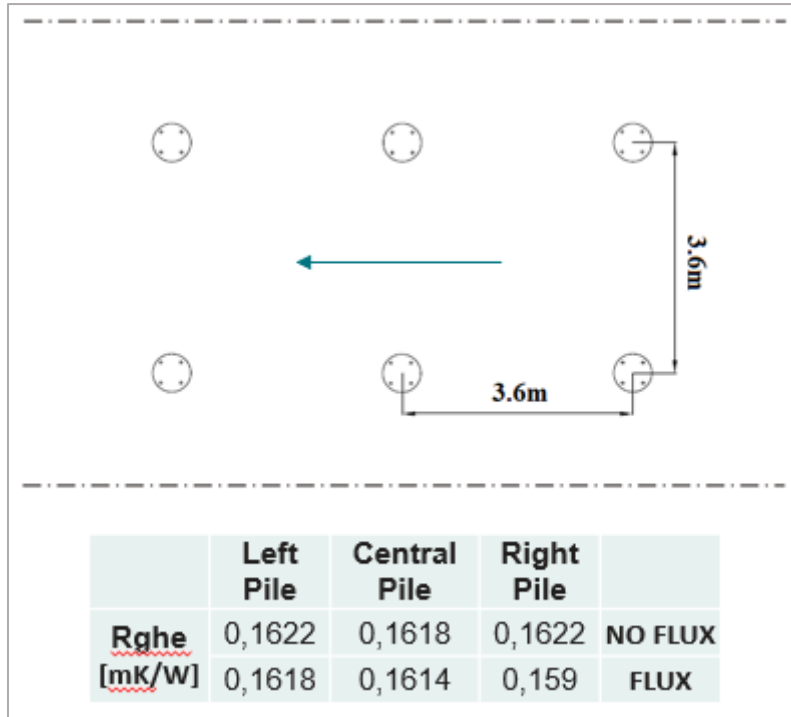


Figure 54: Temperature difference between the heat circulating fluid and the ground, over time, for the 2xN piling.



**Figure 55:** Pile thermal resistance for the 3x3 energy piling with and without the flow applied.

Furthermore, figures 53-55 show that the pile thermal resistance is almost independent of the distance between the piles, because it depends mostly on the thermal properties of the pile and eventually on the presence of a groundwater flow.

In an energy pile group, the thermal resistance component affected by the piles distance is the resistance of the soil surrounding the piles. The superposition principle has been adopted to create a 3x3 energy pile group, and to study the soil thermal resistance. Considering a single energy pile and replicating it in different positions, it has been possible to define a 3x3 energy pile group, making an interpolation of the temperature field around the pile. Then, applying the procedure to compute the thermal resistance components, the soil thermal resistance has been evaluated by varying the piles distance in X and Y direction, as follows:

$$\frac{\bar{T}_{fluid} - \bar{T}_{ground}}{q} \rightarrow R_{TOT} \quad (38)$$

$$\frac{\bar{T}_{fluid} - \bar{T}_{interface}}{q} \rightarrow R_{GHE} \quad (39)$$

$$R_{soil} = R_{TOT} - R_{GHE} \quad (40)$$

The 3x3 energy pile group has been analysed in hydrostatic conditions, and the soil thermal resistance has been studied with a contour plot on a 2D section. Figure 56 shows the results.

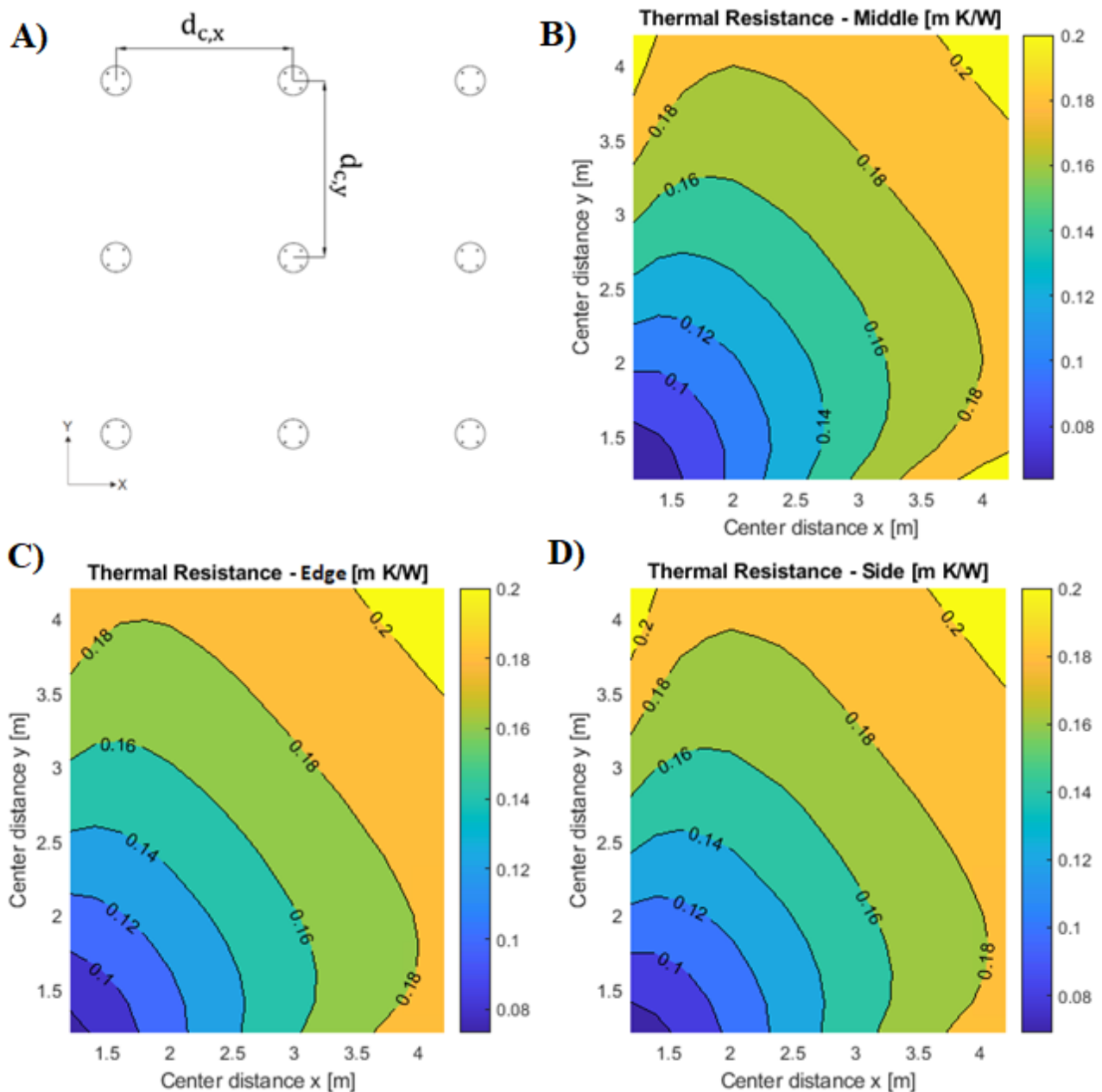


**Figure 56:** A) Schematic view of the 3x3 energy pile group. B) Soil thermal resistance of the central pile. C) Soil thermal resistance of the lateral pile. D) Soil thermal resistance of the border pile.

Figure 56 shows that the soil thermal resistance strongly depends on the piles distance. As expected, the greater the distance between the piles, the greater the soil thermal resistance. From another point of view, the closer the piles, the greater the thermal interaction between them and the higher the ground temperature. To conclude, the central pile shows slightly less soil resistance than the edge and lateral pile, with the same center distance. This effect is related to the number of piles with which the single energy pile interacts.

## 7 CONCLUSION

---

The three-dimensional numerical models presented in this work, have been used to study the thermal behaviour and the energy efficiency of energy piles. The analyses of the single energy pile have shown the key controlling parameters for the thermal resistance. In particular, the influence of the thermal properties of the pile and the ground, as the thermal conductivity, the configuration of the pipes embedded in the concrete, as well as the concrete cover of the pipes has been explored. The higher the concrete cover, the greater the resulting pile thermal resistance. Then, a parametric analysis by varying the pile diameter has shown that the larger the diameter, the lower the thermal interaction between pipes, and as a consequence, the lower the pile thermal resistance. Moreover, to make the most of the energy piles efficiency, the effect of the flow regime has been studied. A fully turbulent flow leads to a better heat exchange between the heat circulating fluid and the ground, thanks to the higher convective component of the heat transfer. Then, the simulations have demonstrated that, energy piles with a diameter of 1m, characterized by a turbulent flow within the pipes, reach the steady flux conditions after several days. The results coming from the 3D finite element model let to values of thermal resistance greater than the 2D numerical and analytical models. This is due to the three-dimensional effect of the flow in the pipe direction, and mostly to the potential interaction between the pipes. In fact, the amount of concrete cover and the spacing between the pipes have a significant influence on the outlet temperature of the fluid.

A multiphase ground model has been defined, in order to characterize the solid, liquid and gas phase of the hydro-thermal coupled soil constitutive law. In this way, it has been possible to apply a groundwater flow to the case of the single energy pile and see the effects on the thermal behaviour. The water tends to carry the heat in the flow direction; hence one effect is the translation of the temperature field around the pile. Then, the most important effect of the groundwater flow is the improvement of the heat exchange capacity of the energy pile. In fact, the heat circulating fluid within the pipes reaches a temperature higher than the case without a flow applied, while the surrounding ground shows a lower temperature. Moreover, considering the fluid velocity field around the pile, it has been proven that the pile acts as a screen to the flow.

Afterward the thermal resistance has been computed, and a parametric analysis by varying the pile diameter has been done. The comparison between the values coming from the analyses with and without the flow applied has shown that, the pile thermal resistance tends to decrease with a flow applied, because the heat exchange capacity increase. Furthermore, the smaller the diameter, the higher the effect of the flow on the temperature surrounding the pile, and the higher the reduction of the thermal resistance.

Then, the configuration of the energy pile group has been studied. Starting from the case of a 2xN and 3xN energy piling, the thermal interaction between the piles has been analysed. The simulations have been done with different piles distances and different groundwater flow velocities. As expected, for a piles distance of 3 m, the soil area between the piles reaches a higher temperature than the case of a single energy pile. While, considering 4 m and 5 m of piles distance, the energy piles behave almost independently. After that, the analyses have been done with a groundwater flow of 1 m/day applied, and the results have shown two important effects. The first is that the flow is improving the heat exchange capacity of the energy piles, the second is related to the screen effect of the first pile hit by the flow. In fact, the shielded piles in the flow direction, show the same behaviour of the piling without the flow applied. To conclude the analyses of the energy piling, the thermal resistance of the piles has been computed, and the results have shown an important aspect: the pile thermal resistance is not really affected by the piles distance, but it changes with different groundwater flow's conditions.

In an energy pile group, the soil thermal resistance is affected by the piles distance. Exploiting the superposition principle, a 3x3 energy pile group has been defined, and the soil thermal resistance has been studied. Considering the hydrostatic conditions, the soil thermal resistance has been computed around the central, the lateral and the edge pile, and a contour plot with different piles distance, in X and Y direction, has been created. The results show that the soil thermal resistance tends to increase with the piles distance, because of the lower thermal interaction between piles, and the lower temperature of the soil. In addition, the soil resistance around the central pile is slightly lower than that of the lateral and border pile, because the central pile interacts with more piles and the surrounding soil temperature is higher.

## Conclusion

In conclusion, the 3D numerical model presented in this work is intended to serve a new numerical approach, to evaluate the thermal resistance of energy piles and a range of values of it. Coupled phenomena as hydrothermal effects in hydrostatic conditions and in presence of a groundwater flow have been analysed, for a single energy pile and energy pile groups.

## 8 REFERENCES

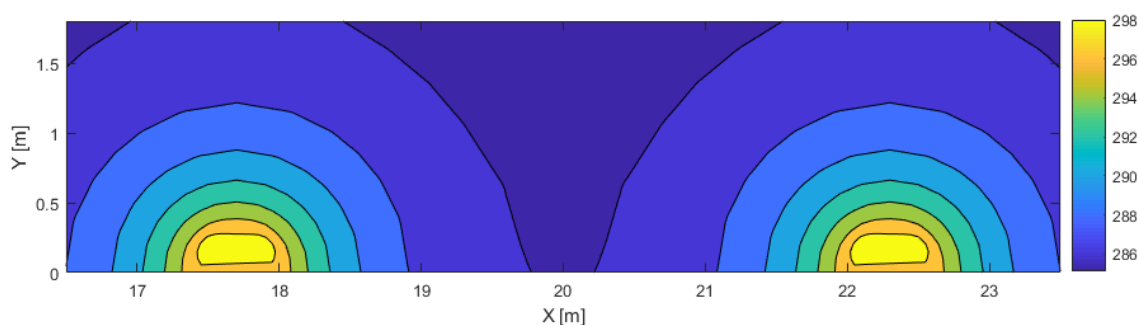
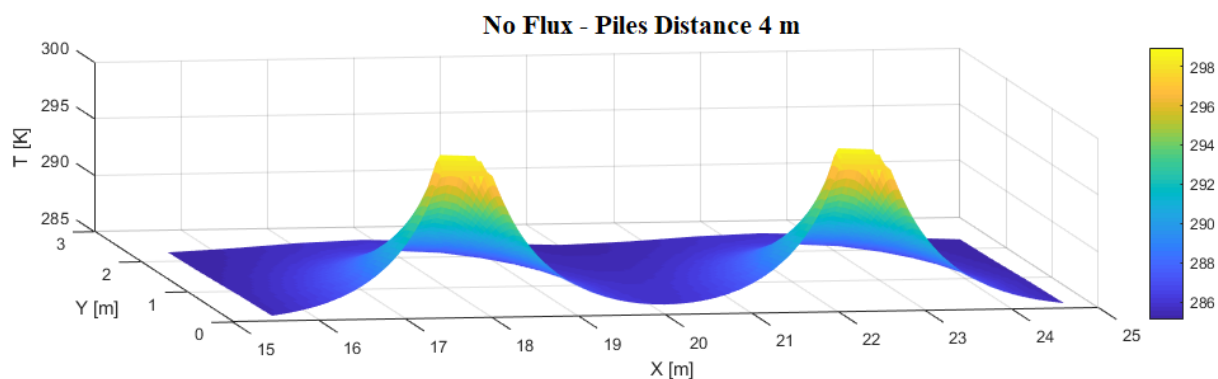
---

- [1] L.Laloui, A.F. Rotta Loria 2019 “*Analysis and Design of Energy Geostructures : Theoretical Essentials and Practical Application*” (1<sup>st</sup> ed.), Elsevier Academic Press (2019).
- [2] Kemmler, Piégsa A., Ley A., Keller, Jakob M., Catenazzi, G. 2013 “*Analysis of the Swiss Energy Consumption according to the End Use*” Swiss Federal Office of Energy, Bern.
- [3] ASHRAE Vision 2020 “*American Society of Heating, Refrigerating and Air-Conditioning Engineers*” Producing Net Zero Energy Buildings (NZEBs).
- [4] Brandl, H., 2006 “*Energy foundations and other thermo-active ground structures*” Geotechnique 56 (2), 81-122.
- [5] Batini N., Rotta Loria A.F., Conti P., Testi D., Grassi W., Laloui L., 2015. “*Energy and geotechnical behaviour of energy piles for different design solutions.*” Appl. Therm. Eng.
- [6] Cerfontaine B., Radioti G., Collin F., Charlier R., 2016. “*Formulation of a 1D finite element of heat exchanger for accurate modelling of the grouting behaviour: Application to cyclic thermal loading*”. Elsevier Ltd.
- [7] Renato Lancellotta “*Geotecnica*” Quarta edizione - Zanichelli – giugno 2012.
- [8] Min Li, Alvin Lai C.K., 2015. “*Review of analytical models for heat transfer by vertical ground heat exchangers (GHEs): A perspective of time and space scales*” Elsevier Ltd.
- [9] SIA Documentation D0190, 2005 “*Utilisation de la chaleur du sol par des ouvrages de fondation et de soutènement en béton*” Swiss Society of Engineers and Architects.
- [10] Loveridge F., Powrie W., 2013 “*2D thermal resistance of pile heat exchangers*” Journal homepage: [www.elsevier.com/locate/geothermics](http://www.elsevier.com/locate/geothermics).
- [11] Hellstrom G., 1991. “*Ground Heat Storage: Thermal Analysis of duct Storage Systems*”. Ph.D Thesis. Department of Mathematical Physics, University of Lund, Lund.

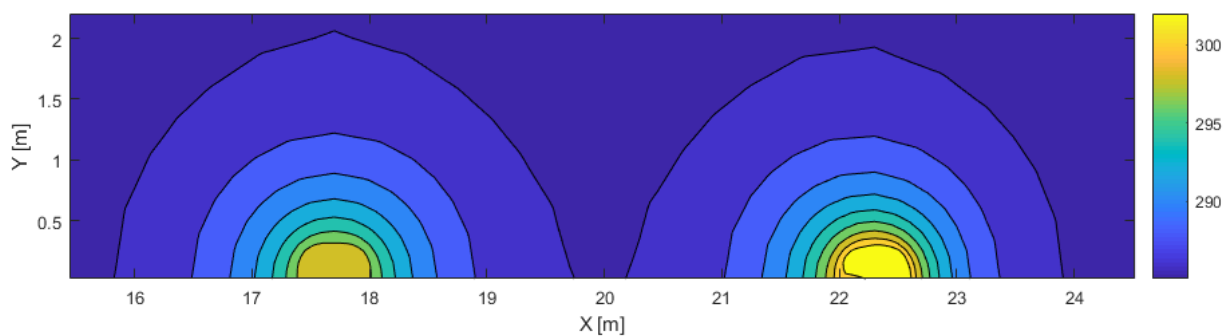
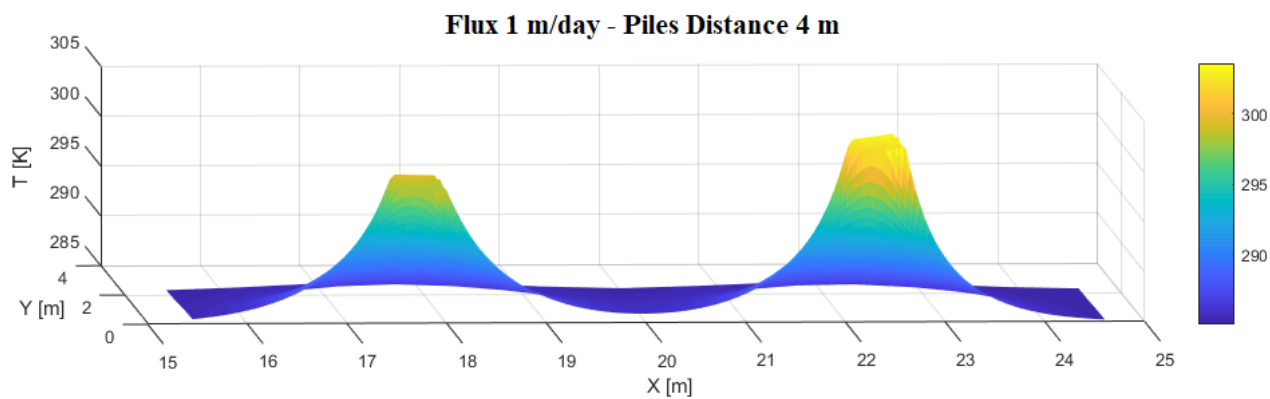
## References

- [12] Laloui L., Di Donna A., “*Energy geostructures – Innovation in Underground Engineering*” Editor Gilles Pijaudier-Cabot 2013.
- [13] Thermal Response Test - [https://en.wikipedia.org/wiki/Thermal\\_response\\_test](https://en.wikipedia.org/wiki/Thermal_response_test).
- [14] Cecinato F., Loveridge F.A. 2015 “*Influences on the thermal efficiency of energy piles*” Journal homepage: [www.elsevier.com/locate/geothermics](http://www.elsevier.com/locate/geothermics).
- [15] Charlier R., Radu J., Collin F. 2001 “*Numerical modelling of coupled transient phenomena*” *Revue Française de Génie Civil*, 5:6, 719-741, DOI.
- [16] Dupray F., Li C., Laloui L., 2014 “*Heat-exchanger piles for the de-icing of bridges*” Springer-Verlag Berlin Heidelberg.
- [17] Badinier T., de Sauvage J., Szymkiewicz F., Benitez B., 2020 “*Interactions between energy geostructures in the same aquifer*” European Geostructures Union (EGU) 2020.

# 9 APPENDICES

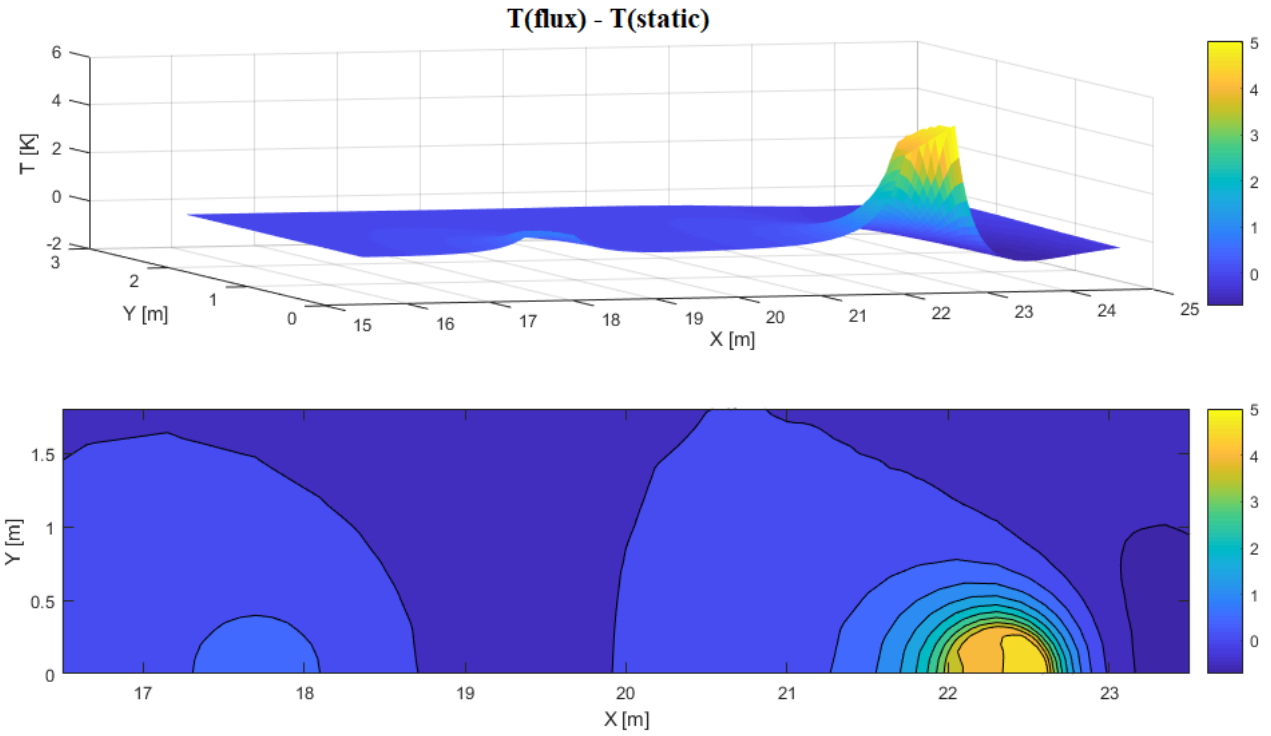


Appendix A 1: Temperature field of a 2xN piling in hydrostatic conditions. Piles distance of 4m.

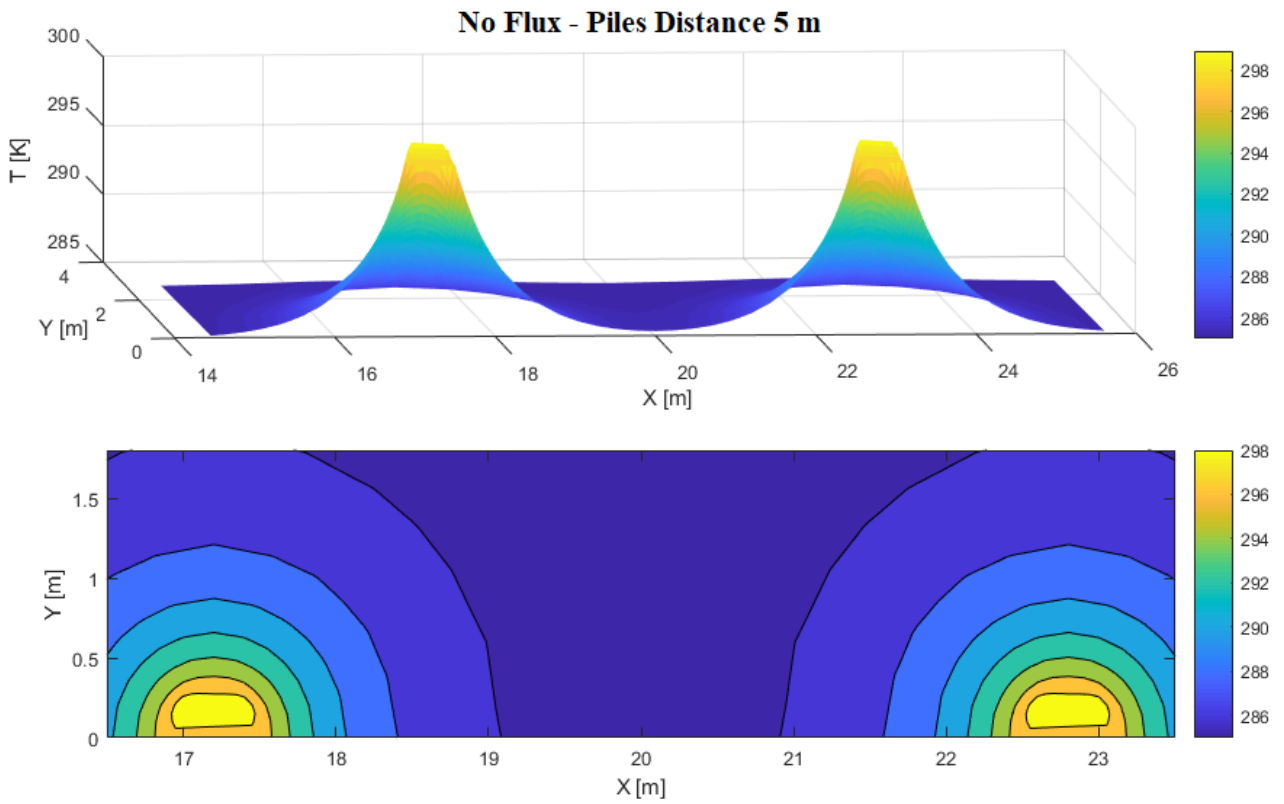


Appendix A 2: Temperature field of a 2xN piling with a groundwater flow applied. Piles distance of 4m.

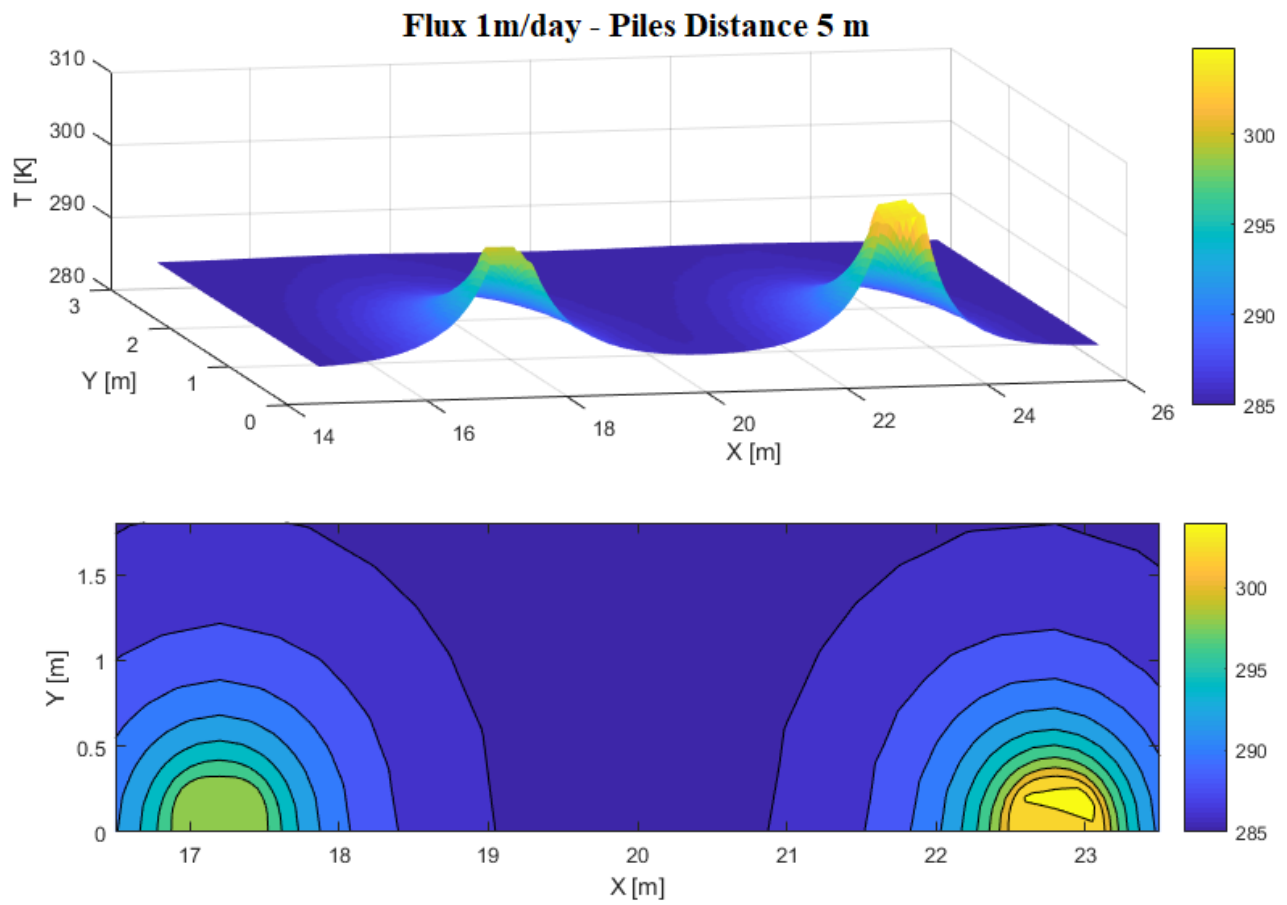
Appendices



Appendix A 4: Difference of the temperature field of 2xN piles, with and without a flow applied. Piles distance 4m.



Appendix A 3: Temperature field of a 2xN piling in hydrostatic conditions. Piles distance of 5m.



Appendix A 5: Temperature field of a 2xN piling with a groundwater flow applied. Piles distance of 5m.

## Silvestro MASSARO



12/27/1995 SAN GIOVANNI ROTONDO (FG)

ITALY Nationality: Italian

Via Zannotti 132 71016 - SAN SEVERO (FG) ITALY

3491495795

silvestro.massaro@studenti.polito.it

silvestro.massaro@epfl.ch

<https://www.linkedin.com/in/silvestro-massaro-6ba771160/>

### EDUCATION

- 03/29/2018 - up to present \* **Master's Degree in Civil Engineering**  
Politecnico di Torino  
*Numerical approaches for the design and optimization of energy geostructures: assessment of the thermal resistance of energy piles*  
average mark 27.4 - Credits 83 %
- 09/08/2014 - 03/27/2018 \* **Bachelor's Degree in Civil Engineering**  
Politecnico di Torino  
Thesis: Sistemi di trasporto innovativi: treni a levitazione magnetica  
*Vantaggi e svantaggi della tecnologia MagLev*  
Final grade 95/110
- 2014 **high school MATURITA' SCIENTIFICA**  
Final grade 89/100

### INTERNATIONAL EXPERIENCE

- 02/03/2020 - 06/19/2020 **Master Project at Laboratory of Soil Mechanics**  
École Polytechnique Fédérale de Lausanne - Lausanne - SWITZERLAND
- 09/01/2019 - 06/30/2020 \* **E+/EU PROGRAMME COUNTRIES**  
UNIVERSITE GRENOBLE ALPES (UGA) - GRENOBLE - FRANCE

### LANGUAGE SKILLS

Mother tongue Italian

Other languages

|           | UNDERSTANDING |         | SPEAKING           |                   | WRITING |
|-----------|---------------|---------|--------------------|-------------------|---------|
|           | Listening     | Reading | Spoken interaction | Spoken production |         |
| English * | B2            | B2      | B2                 | B2                | B2      |
| French *  | A2            | A2      | A2                 | A2                | A2      |

Levels: A1/2: Basic user - B1/2: Independent user - C1/2 Proficient user

[Common European Framework of Reference for Languages](https://didattica.polito.it/privacy/index_en.html)

## COMPUTER SKILLS

---

|                           |  |
|---------------------------|--|
| OPERATING SYSTEM          | Windows<br>good level  |
| PROGRAMMING LANGUAGE/CODE | C programming code, MATLAB<br>good level                                 |
| PROGRAM/SOFTWARE          | Software F.E.M. (Sap2000), ZSoil, LAGAMINE, STRATA<br>good level         |
| CAD                       | Software CAD (AutoCAD 2D - 3D)<br>good level                             |
| GRAPHICS                  | Geographic Information Systems (GIS), GIS Modeling<br>intermediate level |
| SPREADSHEET               | Microsoft Office<br>good level   |

## PERSONAL SKILLS/OTHER SKILLS

---

I have a great team spirit and organization acquired in group works and in university projects. Open-mindedness, empathy, interaction with other people are key words of my way of being.

## OTHER INFORMATION

---

Driving license  
Available to travel on business abroad  
Available to relocate abroad

## EXAMS \*

---

### Master's Degree in Civil Engineering

| conference date | Exam  | Credits | Final grade  |
|-----------------|---|---------|--------------|
| 06/25/2018      | Technology of construction materials                                | 6       | 27           |
| 07/17/2018      | Geomatics   | 6       | 30           |
| 01/30/2019      | Construction of Roads, Railways and Airports                        | 8       | 25           |
| 02/07/2019      | Hydrology   | 8       | 27           |
| 02/18/2019      | Foundations   | 8       | 27           |
| 06/19/2019      | Structural Mechanics II   | 8       | 24           |
| 06/27/2019      | Rock Mechanics  | 8       | 30 cum laude |
| 07/22/2019      | Theory and design of reinforced and prestressed concrete structures | 8       | 27           |
| 05/15/2020      | Numerical Methods in Geotechnical Engineering                       | 8       | 25           |
| 05/15/2020      | Slope stability/Geotechnical earthquake                             | 12      | 30 cum laude |
| 05/15/2020      | Earthquake Engineering  | 8       | 29           |
| 05/15/2020      | Professional Training   | 12      | passed       |

### Bachelor's Degree in Civil Engineering

| conference date | Exam                    | Credits |
|-----------------|-------------------------|---------|
| 01/28/2015      | Mathematical analysis I | 10      |
| 02/17/2015      | Chemistry               | 8       |
| 06/26/2015      | Geometry                | 10      |
| 07/03/2015      | History of energy       | 6       |

|            |   |    |
|------------|---|----|
| 09/15/2015 | Physics I   | 10 |
| 01/29/2016 | Drawing   | 6  |
| 02/22/2016 | Thermodynamics and Heat Transfer for Engineers    | 8  |
| 06/23/2016 | Science and technology of materials               | 6  |
| 07/01/2016 | Analytical Mechanics                              | 8  |
| 07/13/2016 | Geology/Safety and Civil Protection               | 12 |
| 09/05/2016 | Physics II  | 6  |
| 09/22/2016 | Topography  | 6  |
| 01/31/2017 | Hydraulics  | 10 |
| 02/08/2017 | Structural Mechanics                              | 10 |
| 04/08/2017 | English Language 1st level                        | 3  |
| 06/28/2017 | Seismic risk                                      | 6  |
| 07/06/2017 | Road infrastructures                              | 10 |
| 09/15/2017 | Structural Engineering                            | 10 |
| 02/01/2018 | Geotechnics                                       | 10 |
| 02/02/2018 | Computer science                                  | 8  |
| 02/02/2018 | Numerical and statistical methods for engineering | 8  |
| 02/06/2018 | Mathematical analysis II                          | 8  |
| 03/27/2018 | Final essay                                       | 3  |

\* Fields marked with an \* are certified by Politecnico di Torino, while the potential thesis description is added by the candidate.